



Soft Tissue Models for Enhancing Force Feedback in Teleoperation Systems

Lágyszövetmodellekkel támogatott erővisszacsatolt teleoperációs rendszerek

Árpád Takács

Ph.D. Thesis

Antal Bejczy Center for Intelligent Robotics
University Research and Innovation Center
Óbuda University

Supervisor: Dr. Tamás Haidegger

Doctoral School of Applied Informatics and Applied Mathematics

Budapest, 2017

Szigorlati bizottság:

Nyilvános védés teljes bizottsága:

Nyilvános védés időpontja:

ABSTRACT

In the past 20 years, research activities related to robotic surgery have gained much attention due to the rapid development of interventional systems. Advanced surgical devices present a fine example of Human–Machine Interfaces as well. While many surgical maneuvers have already been implemented with a degree of autonomy, most of these surgical robotic devices are still used as teleoperation systems. This means that a human surgeon is always required to be present in the control loop, as an operator. Parallel to the evolution of telesurgery, different model-based control methods have been developed, and experimentally tested. These enhance transparency and increase latency-tolerance, both in terms of long distance (space robotics, intercontinental operations) and short distance (local on-Earth scenarios) teleoperation. The effectiveness of traditional real-time control methods decreases significantly with the increase of time-delay, while time-varying latency introduces further challenges. A suitable controller can ensure high quality control signals and improved human sensory feedback. This can only be achieved by adequate models for all components of the telesurgical systems, including models of the human operator, the robot and the tool–tissue interaction. Using haptic controllers and accounting for the tissue dynamics, one can also address issues arising from communication latency. Stability and accuracy deterioration caused by latency and other external disturbances, such as contacting hard tissues or elastic tool deformation, can also be accounted for by using realistic soft tissue models. The integration of these models into model-based force control algorithms largely increase the robustness and reliability of robot-assisted interventions.

In telesurgery, cutting, indentation and grasping are just a few types of tissue manipulations that require high precision tools and techniques. The majority of modern telesurgical systems use only visual feedback, while the applicability of force or haptic feedback has been a lasting research topic in the field. An efficient implementation of force control incorporating haptic feedback can enhance the surgeon’s sensory capabilities during the operation. In order to achieve better performance for surgical robotics applications—in terms of stable control for teleoperation—it is crucial to understand the behavior of soft tissues through modeling their mechanical properties.

Creating an accurate tool–tissue interaction model would largely aid the design of model-based control methods. This way, force response of the manipulation is estimated using the model, and the required input force (control signal) can be derived. This allows the control of the tissue manipulator (in most cases, a surgical tool held by the robotic arm), in order to carry out the surgical manipulation tasks in an efficient, stable and accurate way.

The problem of distinguishing between soft tissues by testing their mechanical properties is often referred to as the cognitive role of haptic devices in simulation environments. It is a common view that today’s surgical simulators that are using haptic interfaces should rely on simple mechanical models of soft tissues, instead of complex, parameterized finite element models, thus

enhancing real-time operation and focusing on the most representative mechanical effects, such as creep (the phenomenon of permanent deformation due to mechanical stress), stress relaxation or residual stress.

This work presents a novel method for enhancing force feedback in teleoperation systems using a model-based approach. The aim is to address the design challenges of master–slave type telesurgical systems, which mostly arise from the system complexity, the communication delay and the integration of haptic feedback between the master and slave devices. This way, the most relevant qualitative and quantitative indicators of robotic systems can be improved, such as precision, performance and reliability. In order to achieve the control goals, modeling of the tool–tissue interaction during the procedures is crucial, which requires the formulation and verification of a generalized mechanical soft tissue model. This can be used for reliable reaction force estimation during a pre-defined surgical intervention.

Given an appropriate soft tissue model, its integration is possible into a user-defined model-based control method, which allows its direct implementation into modern surgical robotics systems. This work also gives a theoretical background on the methodology and verification of a proposed nonlinear soft tissue model. The verification is supported by a practical methodology on the integration into the da Vinci Surgical System, and the corresponding development environment, the da Vinci Research Kit. A polytopic model-based interaction controller is proposed, and control performance is investigated in order to address robustness against model uncertainties and time-delay.

Along with force control, the problem of haptic feedback in telesurgical systems is also addressed in this work. The da Vinci Surgical System currently lacks haptic feedback capabilities, limiting its usability in everyday surgical practice. This thesis proposes a validation method for tissue models and their polytopic representation by creating an experimental framework using the da Vinci Research Kit. Once allowing haptic feedback from the manipulated real tissue, this feature can be extended to surgical simulation using virtual tissue models, based on the proposed soft tissue modeling method.

The field of application of the proposed methods can be divided into three large groups. First, robotic surgical systems with haptic feedback capabilities can be improved by reflecting an estimated reaction force to the operator, based on the tissue mechanical properties and deformation data. Second, surgical simulators for training and education can be enhanced by implementing the tissue model, creating a realistic virtual environment for practical training and trials on specific interventions, such as prostatectomy, cholecystectomy or appendectomy. Third, the proposed model-based force control method can improve the performance of automated tissue manipulation tasks for fully or semi-automated surgical systems, including suturing, coagulation, cutting and grasping.

The integration of the proposed methods and models into clinical use is a question of availability of hardware and software components, too. The commercially available telesurgical systems were dominantly not designed to reflect force feedback to the operator, therefore a new stable slave compo-

ment is needed for reliable operation. Such systems are under development, but these are still awaiting commercialization and approval from national and global regulatory bodies. In the meanwhile, there is a wide range of components available for research and development uses, both in terms of hardware and software. Open-source repositories and global communities are actively working on the enhancement of prototypes and commercially available surgical systems, where methods and models, such as the ones presented in this work can be further developed, tested and validated.

KIVONAT

Az elmúlt 20 évben a robotsebészethez kapcsolódó kutatások jelentős eredményeket hoztak, különösen az ember–gép kölcsönhatások területén. Ma már számos, a műtőben gyakran alkalmazott mozdulatsor hajtható végre bizonyos fokú önállóság mellett a modern sebészeti berendezésekben, ugyanakkor ezek az eszközök továbbra is elsősorban mester–szolga alapú teleoperációs (távsebészeti) rendszerekként működnek. Ennek megfelelően a sebész továbbra is „integrális része” a szabályozási körnek, a döntéshozatal és a mozgásparancsok kiadása a sebész feladatkörébe tartoznak. A telerobotika fejlődésével párhuzamosan számos olyan modell-alapú szabályozási módszer látott napvilágot, mely lehetővé teszi az erővisszacsatolást a kezelő számára, és robusztusan kezeli az időkésltetésből adódó nem kívánt jelenségeket, mind nagyobb távolságok esetében (űrrobotika, kontinenseken átívelő teleoperáció), mind lokális környezetben. A hagyományos szabályozási módszerek hatékonyságát nagymértékben befolyásolja az időkésés mértéke, a késleltetés változó értéke pedig újabb kihívásokat jelent már a tervezési, rendszermeretezési szakaszban. Megfelelő tervezési eljárással javítható az szabályozás minősége, és stabilabb visszacsatolás valósítható meg a sebész felé. Ehhez minde nélkülött szükség van a távsebészeti rendszerek komponenseinek modelljére, így például a humán operátor, a szolga oldali robotkar és az ún. eszköz–szövet kölcsönhatás dinamikájának leírására. Az időkésésből és egyéb külső zavaró tényezőktől (pl. a sebészeszközök rugalmas deformációja, kemény szövetrel való ütközés) származó stabilitásvesztés és pontatlanság kezelhető megfelelő lágyszövetmodellek alkalmazásával, melyhez nagyban hozzájárulhat a lágyszövet dinamikájának vizsgálata és haptikus eszközök használata. Egy modellel támogatott erőszabályozási módszer jelentősen növelheti a robotokkal támogatott sebészeti beavatkozások robusztusságát és megbízhatóságát.

A vágás, tapintás és a szövetek megragadása néhány példa azokra a távsebészeti manipulációkra, melyek nagy pontosságú eszközöket és technikákat igényelnek. A modern távsebészeti rendszerek túlnyomórészt csak képi visszacsatolást tesznek lehetővé, bár az erő- és haptikus visszacsatolás alkalmazhatósága régóta foglalkoztatja a kutatókat. Egy olyan erőszabályozási módszer hatékony megvalósítása, mely tartalmazza a haptikus visszacsatolás fő elemeit, jelentősen növeli a sebész által érzékelhető információ mértékét a beavatkozás során. A modern sebészrobotikai rendszerek esetében a beavatkozások minőségének és megbízhatóságának növeléséhez kritikus tényező a lágyszövetek mechanikai tulajdonságainak ismerete, illetve a megfelelő eszköz–szövet kölcsönhatás modelljének felállítása. Ezáltal a manipuláció során jelentkező erőválasz becsülhető a modell segítségével, és a kívánt bemeneti szabályzójelek számíthatóak a robotkar irányításához.

Az egyes lágyszövetek megkülönböztetésének feladatát gyakran a haptikus eszközök kognitív szerepeként emlegetjük, melynek szimulációs környezetekben kiemelt jelentősége van. Általánosan elfogadott nézet, hogy a mai haptikus eszközökkel felszerelt sebészeti szimulátorok esetében egyszerűbb mechanikai modellekre van szükségünk a nehezen skálázható, végeelem-

módszer alapján felállított modellekkel szemben. Ez lehetőséget nyújt arra, hogy a valós idejű működés mellett a szöveteknek a sebészek számára ténylegesen fontos mechanikai viselkedését tudjuk leírni, szemben a gyakran elhanyagolható részleteket tárgyaló mikromechanikai megközelítéssel.

A kutatásom egyik közbenső célja egy olyan modell-alapú szabályozási módszer kifejlesztése volt, amely a napjainkban használt teleoperációs sebészrobotikai rendszerek struktúrájából és a haptikus visszacsatolásból eredő tervezési nehézségeket oldja fel, ezáltal javítva a robotikában fontos mutatókat, így például a pontosságot, teljesítményt és a megbízhatóságot. A kitűzött célok megvalósításához szükség van egy olyan mechanikai szövetmodell megalkotására és hitelesítésére, mely egy meghatározott sebészrobotikai beavatkozás esetén alkalmas arra, hogy az eszköz–szövet interakció során ébredő reakcióerőket megfelelő pontossággal becsülje. A kutatási célok között szerepelt a javasolt modell kiterjesztése a szövet felületének tetszőleges alakváltozásának esetére is. Sikeres verifikáció után a modell alkalmazható egy modell-alapú irányítási folyamatban, mely felépítéséből eredően beépíthető az Óbudai Egyetemen található da Vinci sebészrobot fejlesztőkörnyezetbe. Az erőszabályozás mellett szerepet kap a haptikus visszacsatolás, mellyel a da Vinci sebészrobotikai rendszer egy jelentős hiányossága pótolható, illetve a robusztusság vizsgálata az időkésleltetésből és a becsült modellparaméterek eltéréseiből adódó hibák esetére. A javasolt nemlineáris szövetmodell, annak kvázilineáris alakra hozása, transzformációja, a szabályozási struktúra megalkotása, végül pedig a módszer kísérleti igazolása képezték a munka gerincét.

A javasolt módszer alkalmazhatósági körét három fő terület foglalja össze. Elsőként azok a sebészrobotikai rendszerek, melyek rendelkeznek a haptikus visszacsatolás lehetőségével, a reakcióerő becsült értékének visszacsatolásával segíthetik a sebészek munkáját a bemutatott szövetmodell segítségével. Másodsorban a sebészeti szimulátorok és oktatóberendezések fejlesztéséhez járulhat hozzá egy olyan általános szövetmodell, mely például a prosztata- és epehólyag-eltávolítás vagy vakbélműtétek oktatására valóság-hű virtuális környezetet épít fel. Harmadrészt, a javasolt modell-alapú erőszabályozási módszer az egyes automatizált szövetmanipulációs feladatok elvégzését nagyobb biztonsággal és pontossággal tudja majd kivitelezni.

A bemutatott modellek és módszerek integrálhatósága mind az elérhető szoftveres, mind pedig a hardveres eszközöktől is függ. A napjainkban kereskedelmi forgalomban kapható teleoperációs rendszerek csak nagyon kis hányada alkalmas erővisszacsatolásra, ezért a megbízható működéshez jól megtervezett szolgál-oldali komponensekre van szükség. Ilyen rendszerek jelenleg is fejlesztés alatt állnak, azonban ezek egyelőre még nem alkalmazhatóak a klinikai gyakorlatban a szükséges engedélyek nélkül. Ugyanakkor számos komponens áll a kutatók és fejlesztők rendelkezésére, elsősorban nyílt forráskódú szoftveres könyvtárak és nemzetközi közösségek által, így a prototípusok és a már kereskedelmi forgalomban kapható sebészeti berendezések fejlesztése aktívan folytatódik majd az elkövetkező években. Ez lehetőséget nyújt az új módszerek és modellek – hasonlóan az ebben a doktori értekezésben bemutatottakhoz – tesztelésére, fejlesztésére és hitelesítésére.

DECLARATION

Undersigned, Árpád Takács, hereby I state that this Ph.D. thesis is my own work, wherein I only used the sources listed in the references. All parts taken from other works, either as word for word citation or rewritten keeping the original meaning, have been unambiguously marked, and reference to the source was included.

NYILATKOZAT

Alulírott Takács Árpád kijelentem, hogy ezt a doktori értekezést önállóan készítettem, és abban csak az irodalmi hivatkozások listájában szereplő forrásokat használtam fel. Minden olyan részt, amelyet szó szerint, vagy azonos tartalomban, de átfogalmazva más forrásból átvettem, egyértelműen, a forrás megadásával megjelöltem.

Budapest, September 20, 2017

.....
Árpád Takács

Contents

1	Introduction	16
1.1	A Brief History of Robotic Surgery	16
1.2	Modeling Teleoperation Systems	17
1.2.1	Components of Teleoperation Systems	18
1.2.2	Addressing Latency in Teleoperation Systems	25
1.3	Theoretical Tools Used in the Thesis	26
1.3.1	Heuristic Models in Soft Tissue Modeling	26
1.3.2	Tensor Product Model Transformation	29
2	Research Problem Statement	32
3	Methods	34
4	A Methodology for Soft Tissue Modeling	38
4.1	Experimental Verification of the Wiechert Model	39
4.1.1	Theoretical Verification of the Linear Wiechert Model	39
4.1.2	Model Verification for Non-Ideal Step-Input	41
4.1.3	Experimental Setup and Data Collection	42
4.2	Data Collection and Analysis	44
4.3	Introduction of Novel Nonlinear Soft Tissue Models	49
4.3.1	The Two-phase and Nonlinear Wiechert model	49
4.3.2	Verification of the Nonlinear Wiechert Model	49
4.3.3	Model Verification with Non-Uniform Surface Deformation	54
4.4	Summary of the Thesis	57
5	Polytopic Model-Based Interaction Control	59
5.1	Models of Soft Tissues in Force Control	60
5.2	Polytopic TP Model of the Nonlinear Wiechert Model	60
5.2.1	Model Construction	60
5.2.2	Model Verification	62
5.3	Polytopic TP Model for Force Control Applications	64
5.3.1	Controller Design	65
5.3.2	Simulation Results	68
5.4	Summary of the Thesis	70

6 Usability Assesment of the Proposed Soft Tissue Model	72
6.1 Haptic Feedback in Telesurgery	72
6.1.1 The Role of Haptic Feedback	72
6.1.2 Different approaches	74
6.2 Research Hardware Environment	74
6.2.1 The da Vinci Research Kit	75
6.2.2 Hardware Components	75
6.3 A Methodology for Model Evaluation and Usability	77
6.3.1 Experimental Methodology	78
6.3.2 Data Collection and Analysis	78
6.4 Results	79
6.4.1 Results for Phase I: User Matches	80
6.4.2 Results for Phase II: User Matches	82
6.4.3 Discussion of the Results	85
6.5 Summary of the Thesis	86
7 Conclusion	88
7.1 Summary of Contributions	88
7.2 New Scientific Results	90
7.3 Future Work	91
REFERENCES	93
OWN PUBLICATIONS RELATED TO THE THESIS	103
OWN PUBLICATIONS NOT RELATED TO THE THESIS	105

Acknowledgment

This thesis would not have been born without the help of the many people, who guided and continuously supported me through these years.

First of all, I am grateful to my supervisor, Tamás Haidegger. His enthusiasm and professional attitude have brought the best out of me, both in terms of *hard* and *soft* skills. I am proud to call him my mentor and friend. I am also grateful to Prof. Imre Rudas, my co-supervisor, who invited me to become a member of the Antal Bejczy Center for Intelligent Robotics, gave the opportunity to build my international professional network, and supported me in countless ways during my Ph.D. studies. I would like to thank Péter Galambos for his professional support in model-based controller design, and Gernot Kronreif for his valuable comments during my cooperation with the Austrian Center for Medical Innovation and Technology (ACMIT).

I am grateful for the endless help of the ABC-iRob team. Without their enthusiastic partaking in the experimental hardware setup and software support, this work would not be complete. I would also like to thank the ACMIT team in Weiner Neustadt and senior academics from Óbuda University for their valuable comments, and everyone, who contributed in any way to this work from the professional or administrative point of view.

I am beholden to my loving family, here and there. They gave me strength and motivation to carry on, and trusted me with their patience and understanding. I am also grateful for the continuous support and encouragement that I received from my friends and colleagues, selflessly helping me during my research in so many ways.

This research was partially supported by the Campus Hungary Scholarship of the Balassi Institute and the Conference Participation Support Grant of The Hungary Initiatives Foundation. I am thankful for these grants, as they allowed me to participate in international conferences and gave me the opportunity to present my work to the international scientific community. The generous Hungarian National Eötvös Scholarship of the Tempus Public Foundation is gratefully acknowledged, which made my 5-month visiting program possible to ACMIT. The research was also partially funded within the scope of the COMET (Competence Centers for Excellent Technologies) program of the Austrian Government.

Structure of the Thesis

The thesis is divided into seven chapters. Chapter 1 gives an overview on the components of teleoperation systems, emphasizing the role of modeling in modern surgical applications. A section of this chapter is dedicated for the discussion of the challenges arising due to communication latency, from the controller design point of view. Two important theoretical overviews are also presented: a brief summary is given on the most widely used rheological soft tissue models and their validity, and the most relevant definitions of Tensor Product Model Transformation are listed. Furthermore, this chapter introduces the frequently used keywords and concepts of the thesis.

Chapter 2 collects the challenges in the main topics of the thesis, highlighting why these problems require a solution utilizing novel approaches. The problems stated in this chapter are related, but not restricted to the model-based investigation of telesurgical applications. The aim of my work is to propose a solution to these challenges.

Chapter 3 explains the methods by which the research data and reference literature was collected, and which specific techniques or protocols were used to propose a solution for the research problems.

Chapters 4, 5 and 6 are covering the topics of the three major thesis groups, introducing the core research of my Ph.D. work. The chapters independently address the problems stated in chapter 2, guiding the reader through the major steps of solution development, methodology, theoretical background and experimental validation. The results and the evaluation of the findings are discussed at the end of each chapter.

Finally, chapter 7 gives a structured summary of the key results of my research, providing an outlook on the current and future efforts that can utilize the findings of this work.

Numbering of equations, tables and figures is following the structure of the chapters. The independent references are numbered as [1],[2],..., thesis-related own publications are denoted as [TA-1],[TA-2],..., while the own publications that are not related to this thesis are numbered as [TA-I],[TA-II],... The language of the thesis is English, following the U.S. English grammar and spelling rules.

Notations and Symbols

TABLE 1
COMMON ABBREVIATIONS AND NOTATIONS

ABC-iRob	Antal Bejczy Center for Intelligent Robotics
ACMIT	Austrian Center for Medical Innovation and Technology
CIS	Computer-Integrated Surgery
CISST	Computer Integrated Surgical Systems and Technology
CPS	Cyber-Physical Systems
DoF	Degree(s) of Freedom
DARPA	Defense Advanced Research Projects Agency
DVRK	da Vinci Research Kit
FE(A)	Finite Element (Analysis)
FEM	Finite Element Modeling
FPGA	Field-Programmable Gate Array
GUI	Graphical User Interface
HMI	Human–Machine Interface
HRI	Human–Robot Interaction
IEEE	Institute of Electrical and Electronics Engineers
JHU	Johns Hopkins University
LMI	Linear Matrix Inequality
LQ	Linear Quadratic
MIS	Minimally Invasive Surgery
MPC	Model Predictive Control
MTM(L/R)	Master Tool Manipulator (Left/Right)
MVS	Minimal Volume Simplex
NASA	National Aeronautics and Space Administration
NEEMO	NASA Extreme Environment Mission Operations
NN	Neural Network(s)
OR	Operating Room
PDC	Parallel Distributed Compensator
PSM	Patient Side Manipulator
(q)LPV	(quasi) Linear Parameter Varying
RMS(E)	Root Mean Square (Error)
ROS	Robot Operating System
SAGES	Society of American Gastrointestinal and Endoscopic Surgeons
SAW	Surgical Assistant Workstation
SLS	Standard Linear Solid
TP	Tensor Product

TABLE 2
COMMON VARIABLES AND SYMBOLS

A, A_0	Tissue surface area
b_i	Linear damper stiffness
c_i	Local stiffness parameters
δ	Linear validity range
ΔX	Deviation of X from the desired value
ϵ	Root mean square error
f_{sys}, F_{sys}	Force response of system <i>sys</i>
F_d	Desired force
$H(s)$	Transfer function (human behavior)
k_i, K_i	Linear spring stiffness
κ_i	Nonlinear spring stiffness
$\mathbf{p}, \mathbf{p}(t)$	Vector of parameters
ρ	Radius of affected surface
\mathcal{S}	Core tensor
s	Complex frequency
τ_x	General time constant
$\mathbf{S}(\mathbf{p}(t))$	System matrix
T_s	Sampling time
u_{eq}	Equilibrium state input
$u(t), \mathbf{u}(t), U(s)$	General input function
v	Compression rate
$w_i, \mathbf{w}^{(n)}$	Weighting function, vector of weighting functions
$\mathbf{w}(t)$	Disturbance input
W_{sys}	Transfer function (representing system <i>sys</i>)
\mathbf{x}	Vector of state variables
x_d	Desired state, indentation depth
$\dot{\mathbf{x}}$	First derivative of the state variables w.r.t. time
\mathbf{y}	System output function
$\mathbf{z}(t)$	Performance output

List of Figures

1.1	Structure of a general telesurgical system from the control point of view	19
1.2	The tool–tissue interaction model proposed by Leong <i>et al.</i>	23
1.3	Common models of viscoelastic materials	27
1.4	Two basic combinations of the mass–spring–damper viscoelastic models	28
4.1	Curve fitting on the experimental data by Leong <i>et al.</i>	40
4.2	Validation of the linear Wiechert model parameters	42
4.3	The proposed linear tool–tissue interaction model	43
4.4	Experimental setup for beef liver indentation tests	44
4.5	Flowchart of the steps of tissue palpation	45
4.6	Force response curves for step-input relaxation tests.	46
4.7	Force response curves for indentation tests at 20 mm/min	47
4.8	Force response curves for indentation tests at 100 mm/min	48
4.9	Verification of the results of the linear Wiechert model	48
4.10	Calculated 20 mm/s force response curves using parameter sets	50
4.11	Calculated relaxation force response curves using parameter sets	51
4.12	Force response validation curves for indentation tests at 100 mm/min	52
4.13	Compensated 20 mm/s force response curves using parameter sets	53
4.14	Compensated relaxation force response curves using parameter sets	53
4.15	Compensated force response validation curves for indentation tests	54
4.16	The schematic figure of the non-uniform indentation tests	55
4.17	Experimental setup for non-uniform surface deformation indentation tests	55
4.18	The final deformation surface at 6 mm indentation depth.	56
4.19	Measurement results and estimated response for non-uniform deformation	57
5.1	Weighting functions of the MVS polytopic TP model	62
5.2	The original model and the TP model in tissue relaxation	63
5.3	The original model and the TP model in constant compression rate	63
5.4	Weighting functions of the MVS polytopic TP model by Eq. (5.5)	65
5.5	Schematic block diagram of the controlled system	66
5.6	Weighting functions of the MVS polytopic TP model by Eq. (5.17)	67
5.7	Force tracking simulation results	69
5.8	Tracking error results for modeling tissue manipulation	69
5.9	Force tracking simulation results, for the robustness	69
5.10	Tracking error results, investigating the robustness of the proposed method	70
5.11	Tracking performance in the most critical point of the simulation	70

6.1	Schematic representation of the DVRK hardware structure	76
6.2	The da Vinci Surgical System and the da Vinci Research Kit	76
6.3	Indentation tests on a silicone artificial tissue sample	79
6.4	Relaxation force response curves for the specimens used during Phase I .	80
6.5	Force response curves for the specimens used during Phase I	81
6.6	Measured and average relaxation force response curves in Phase II	83
6.7	Measured and average force response curves in Phase II	84
6.8	Tissue characterization results from Phase II	86

List of Tables

1	Common abbreviations and notations	11
2	Common variables and symbols	12
4.1	Parameter estimation results from Leong’s relaxation tests	41
4.2	Corrected parameter estimation results from Leong’s relaxation tests	42
4.3	Initial linear parameter estimation from relaxation tests	46
4.4	Parameter estimation results from relaxation and compression tests	50
4.5	Corrected estimation results from relaxation and compression tests	53
4.6	Specific parameter values of the model verification	56
4.7	Verification cases for non-uniform surface deformation.	57
5.1	qLPV parameter domain values for creating the MVS polytopic TP model	61
6.1	Parameter estimation results from Phase I	80
6.2	Silicone–oil–grease volume ratio used for creating artificial tissue samples	83
6.3	Parameter estimation results in Phase II	85

Chapter 1

INTRODUCTION

1.1 A Brief History of Robotic Surgery

In recent years, a large number of surgical robotic systems and robotic surgery related research have been initiated and conducted. As a result, useful software and hardware tools appeared on the market, which accelerated the pursuit for new research results in modern robotic surgery and telesurgery. Computer-Integrated Surgery (CIS) and telemedicine are becoming popular in the world's developed countries, improving the quality of medical treatment and patient care. The development of these systems requires a strict and effective cooperation of surgeons, Information Technology (IT) experts, engineers and scientists from the various fields of natural and human sciences, creating the possibility of remote or even transcontinental surgery. The concept of these systems often originate from specific extreme applications, thus their testing also requires extreme environments, such as weightlessness or extremely high pressure.

There is no consensus about the title of “the first surgical robot”, since it is hard to define, what criteria should be used to claim such a robot's role fundamental. The first systems, which appeared in the 1970s were used for different purposes, primarily as assisting devices and supporting manipulators. The concept of telerobotics for surgery appeared in the early 1970s, initiated by the National Aeronautics and Space Administration (NASA). The goal of the original project was to provide medical assistance for the astronauts during their remote mission. For this purpose, remotely controlled robots would have been used, operated from the Earth. At that time, the proposal was not funded, and only limited documentation remained accessible. The idea was concluded in a short period of time, and another 15 years passed until the first prototypes appeared, mostly backed by US military grants. During the development phase, it became apparent that controlling telesurgical robots is very challenging, due to the effects of time-delay caused by the large distances. The attention from telesurgery in space shifted to shorter distance telesurgery solutions, leading to the introduction of the first surgical robots to the market by the 1990s.

The most successful robotic system for surgery, the da Vinci Surgical System (Intuitive Surgical, Sunnyvale, CA) grew out of the early results, successfully combining the advantages of various prototypes. In the past 20 years, technology continued to improve, and instead of the military applications, the private sector has become the driving force of the surgical robotics industry, which is now an estimated market of \$5 billion per year. Along with the constant improvement, other robotic devices appeared for enhancing sur-

gical capabilities, namely, in the fields of telesurgery, image-guided surgery and cooperatively controlled surgical robotics. In all of these fields, an important trend is that pre- and intra-operative information—in the form of imaging, physiological data collection, etc.—are playing an increasingly significant role during the procedure, and are enabling robotic systems to gain more autonomy. The field is rapidly changing thanks to the hundreds of research teams focusing on relevant projects. The computing capabilities of modern ICT devices allow the usage of more sophisticated systems, however, overarching regulations and standards in the field are still missing. Surgical robot specific standards (currently under development) will make it possible for the industrial players to better design their systems, to be able to prove their safety and accuracy to the authorities. As for today, most applications keep the human operator active in the control loop, enabling the robot only to enhance the surgeons' capabilities. Autonomous task execution on Earth and in space remains a research topic for the future.

1.2 Modeling Teleoperation Systems

Healthcare services that are performed, or supported by robots from long distances have opened new frontiers in diagnostics and surgery. The initial need of teleoperation first appeared in the early 1950s, while the idea telesurgery was born along the concept of space exploration, initiated by NASA in the 1970s. Although the concept of telesurgery in space has never been implemented in real clinical applications, several simulations and research projects have led to a breakthrough in 2001, when the first intercontinental telesurgical procedure, the *Lindberg operation* was carried out between the USA and France, based on ISDN communication [1]. The successful procedure proved that theoretically, in special cases, medical doctors, nurses and surgeons could contact and reach out for patients thousands of kilometers away. It is most likely that in the near-future, the research and development of telesurgical systems will focus on applications in remote, rural and dangerous areas, such as war zones or contaminated sectors. It is evident that the difference between surgical procedures on Earth and in space environments is huge. During the past decade, several remote surgery experiments were conducted by NASA on Earth, under extreme conditions. The trials took place in the world's only permanent undersea laboratory, NEEMO (NASA Extreme Environment Mission Operations), concluding their latest project on July 21, 2016.

Emerging issues in telesurgery include the modeling and control challenges of both the master and slave sides, while the communication with the surgical crew on Earth creates further issues to address, such as transmission data loss, signal latency (delayed information transmission) and lagging (delayed response). With the increase of the distance between the master and slave sides, these effects are magnified. Many disturbing effects can be reduced in a general teleoperation surgical robotic system by a well-chosen system architecture and proper control methods. A detailed review about the current capabilities in surgical robotics, primarily focusing on teleoperated systems was published by Hoeckelmann *et al.* [2], while available options and a proposed control and modeling framework for telesurgical applications was proposed by Jordán *et al.* [TA-16]. One of the major issues of currently available telesurgical systems is the lack of reliable haptic feedback, leaving surgeons to only rely on their visual sensing during procedures. This chapter gives

an overview of the concept of telesurgery, approaching the problem from the modeling point of view, addressing the effect of force control and the role of modeling.

Today, the da Vinci Surgical System is the best-known and most popular surgical robotic system, functioning as a teleoperated manipulator. As of September 30, 2016, there was an installed base of 3,803 units worldwide: 2,501 in the United States, 644 in Europe, 476 in Asia, and 182 in the rest of the world¹. In the case of the da Vinci, the system is not used routinely for long-distance procedures and interventions. Primarily, this is due to the limitations of the communication protocol, which is a custom-developed component of the system, and due to the missing complete legal framework underlying long-distance surgical robotic procedures [3]. However, there is a potential for using the da Vinci robot at a greater distance, which has been proved by some limited experiments. One of these includes the collaborative telerobotic surgery initiative by DARPA in 2005, when several modified da Vinci consoles were able to overtake the control from one another through the Internet [4]. In 2008, Canadian Surgical Technologies and Advances Robotics (CSTAR, London, ON) used the core network of Bell Canada for testing a modified, telesurgery-enabled version of the da Vinci. Altogether, six successful pyeloplasty procedures were performed on porcine kidneys using telesurgery, with the slave manipulator located in Halifax, Nova Scotia, 1,700 kilometers away from the controllers [5]. The Plugfest was one of the most notable experiments in the past years, allowing eight master devices of various surgical robots to connect with six slave machines [6]. Simulated interventions, such as peg transfer tasks (SAGES Fundamentals of Laparoscopic Surgery) were successfully supported globally for more than 24 hours, using the Interoperable Teleoperation Protocol (ITP) [7]. The recent advances in the reliability of the Internet network allows these high-level experiments to be executed safely, however, the Internet backbone infrastructure is becoming overloaded, with an immediate effect on the lag times. In order to protect the patients in the future, some of the security issues need to be addressed, in accordance with the IEC 80001-1:2010 (Application of risk management for IT-networks incorporating medical devices) [8]. When we discuss control over a delayed communication channel, numerous safety and performance issues arise. Furthermore, there is a need for surgical training in the use of latency-affected master console, helping the operators learn how to tolerate latencies and other disturbing effects [9].

1.2.1 Components of Teleoperation Systems

Just like every teleoperation system, master–slave surgical robotic systems in general consist of three major components from the control and modeling point of view: the slave device, the master device and the communication system. In the field of telesurgery, the slave-side modeling is extended with the phenomena of tool–tissue interaction, the contact problem addressing the behavior of the tool and the soft/hard tissue under manipulation. The modeling of the components is essential for building a valid simulator for the system as a whole, creating the possibility of observation and analysis of control attributes, properties and behaviors. The models are subject to validation, both individually and as a part of the assembly. The schematic illustration of the functional components of a general telesurgical system is shown in Fig. 1.1.

¹<http://www.intuitivesurgical.com/company/faqs.html>

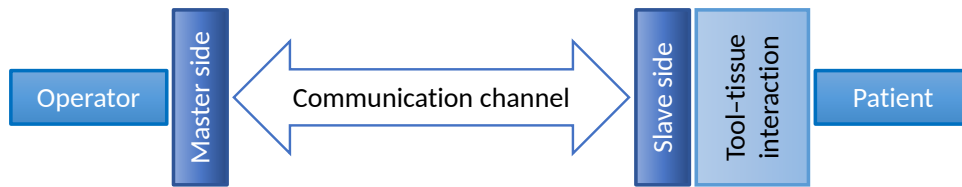


Fig. 1.1. Block diagram of a general telesurgical system from the control point of view.

Communication System

The communication system is the component responsible for data transfer, coding and decoding control signals and other tasks that make the communication between the master and slave devices possible. In general, the communication system includes a transmitter, a receiver and the communication medium. Signal quality and latency are both dependent from the subcomponents, individually. Besides quality issues, data loss is one of the most critical problems to be solved in telesurgical systems, which is, in general, the best handled by particular custom-designed protocols or the User Datagram Protocol (UDP).

Humans have limited adaptability to time-delay, it generally varies between 300–500 milliseconds. In 2001, during the first trans-Atlantic telesurgical intervention, the Zeus robot was in use, created by Computer Motion (Mountain View, CA). A mean signal delay of 155 ms was recorded [10]. According to the measurements, 85 ms of lag appeared in signal transmission, while it took 70 ms to encode and decode the video streaming from the slave side. It is important to note that currently all surgical robots employed routinely in clinical applications are only providing visual and audio feedback. Haptic feedback is yet to be perfected due to stability issues, and data encoding would also increase the lag in long-distance communication.

In order to achieve low dynamic distortion to the user, haptic devices have low intrinsic friction, however, the transparency of the system is largely affected by the computer interface. Digital control loops introduce non-idealities into to system through force/position data quantization, time-delay and time discretization [11]. All these effects introduce excess energy into the system (energy leaks), which may lead to an unstable control loop, if this energy is not dissipated through control or the mechanical friction of the devices [12].

Effects of time-delay can be reduced with various control methods designed for latency-tolerance, therefore, there is an opportunity to bridge larger distances with these technologies. In order to achieve this, the system components must be modeled in a robust way, including all three main components of the teleoperation system. From the communication system approach, the master includes a controller and/or a human operator (usually subject to latencies), which is interconnected with the slave model through a high-delay communication medium. Using appropriate predictive controllers, the time-delay can be partially alleviated in the deriving cascade setup, if the controller is well-tuned for both the master and slave systems [13].

Master Model

The master side is the component, where the human operator or a control device is located. In the past decades, several human models have been created to address the human behavior in the control loop. One of the most significant classical models is the crossover model, which was developed in the 1960s in order to model the behavior of fighter pilots during flight [14]. The crossover model is based on the time-dependent non-linear response of the human body, using a quasi-linear approximation. The complexity of the model highly depends on the precision of the task to be executed. However, there is a commonly used, reasonably good approximation:

$$H(s) = K_p \frac{\tau_L s + 1}{\tau_I s + 1} \frac{e^{-\tau s}}{\tau_N s + 1}, \quad (1.1)$$

where the term in the brackets stands for the human physiological limitations, including the delay of the human reaction time. The time constant τ_N refers to the neuromuscular system, where the delay occurs. K_p represents a static gain, while τ_I and τ_L express the time-delay section and the control time constant, respectively. The trade-off for the simplicity of this model is that it does not represent other, detailed human attributes, such as motivation, expertise and fatigue. Another popular model of human operators was created by Ornstein [15]. A significant development compared to the crossover model is that the Ornstein model can also be applied in tracking type tasks:

$$H(s) = \frac{a_1 s + a_0}{b_2 s^2 + b_1 s + b_0} e^{-\tau s}. \quad (1.2)$$

The a and b coefficient values are determined by taking some physical attributes into account, such as velocity or static gain, and are usually obtained from user trials, where the participants carry out a carefully designed task. Due to the relatively high number of parameters, this model can become rather sophisticated, allowing one to describe neuromuscular effects or other dynamic response characteristics [16]. Furthermore, a large variety of sensory input noise can be modeled using a general signal disturbance, creating the possibility to include vision modeling [17]. In practice, the most commonly used non-linear human operator model is the GM/UMTRI car driver representation, developed at General Motors. The basis of this model is a general, quasi-linear UMTRI driver model [18]. These models have been widely used for the representation of master–slave type telesurgical tasks, as numerous components of the driver model—including path observation and planning activities, speed control and sensory limitations—can be associated with components of a telesurgical system during tissue manipulation [19].

Slave Side Models

In telesurgical applications, functionality and safety requirements are higher than in other robotic applications. At the design stage, autonomous capabilities and proper mechanical modeling are important in satisfying these. In general, the kinematic model of a slave robot is described at a high level of precision, enabling its integration in dynamic and kinematic models [20, 21]. These models, along with the appropriate image guidance and modeling, can largely increase the accuracy and safety of surgical interventions [22]. In

robotic surgery, one of the most critical issues is the correct description of the model of the robot arm, the model of the manipulated tissue and the behavior of these elements during manipulation tasks on contact. This thesis primarily focuses on soft tissue manipulation problems, while the issues involving hard tissues are in the focus of machining technology studies, since drilling, milling and turning are affected by great vibration, and thus require stability issues. Most of the types of human soft tissues are inhomogeneous, viscoelastic, anisotropic and highly non-linear materials, therefore modeling is of high importance not only in robot control, but also in the use of surgical simulators.

Tool–Tissue Interaction Models

A comprehensive study about the existing soft tissue models used in most MIS applications and virtual surgical simulators was presented by Famaey and Sloten [23], introducing three major categories of deformation models: heuristic models, continuum-mechanics models and hybrid models. The complexity of each model mentioned above varies on a wide scale, although it is commonly accepted that approaches based on continuum-mechanics provide a more realistic response, but require significantly higher computational capacity. Analytical solution to the used mathematical models generally do not exist. On the contrary, heuristic models that consist of lumped, linear mass–spring–damper elements, which can be used for describing simple surgical tasks, like needle insertion. The derived equations can usually be solved analytically.

While the modeling of soft tissue behavior—the force and/or deformation response of the tissue due to its interaction with the surgical tools—has been in the focus of research for long, the challenging field of gaining information about the interactions of the robot arm and the tissue has only reached popularity recently. Among the arising issues, it is important to mention the problem of force feedback, the modeling of tools and the interaction with organs itself. A comprehensive review on current tool–tissue interaction models was carried out in [TA-14], providing a survey on research focusing on interactions described by models, following the principles of continuum mechanics and finite element methods. The focus of interest can also be extended to models of telesurgical applications, without strict boundaries of categories, giving an overview of model properties. In [24], a simple 1 Degree of Freedom (DoF) model of a rigid master and flexible slave connection was introduced. Here, the problem of tool flexibility is addressed as one of the greatest issues in the case of tool tissue interactions, since force sensing can only be applied at the fixed end of the tool, and its deflection can only be estimated. Besides tool flexibility, the compliant parameters of the models of the robotic arm and tissues are also important, and take significant parts of the tool tissue interaction system. Other extensions of the model exist for rigid slave, flexible joint and flexible master descriptions, the complexity of the model of the whole system can be extremely high. Great advantage of this approach is that not only the tool flexibility, but the whole transparency of the system is addressed. It is important to mention though that no detailed tissue modeling is provided, the use of rigid specimen model indicates that this approach is rather focusing on teleoperation. Basdogan *et al.* addressed the importance of tool–tissue interaction modeling in medical training through simulation in virtual reality, focusing on issues in haptics in MIS [25]. When working with soft tissues, the elastic behavior of the tool can usually be omitted, using rigid models of surgical accessories. In their work, they introduced two new approaches

to tissue modeling: the mesh-based Finite Element (FE) model, using modal analysis and the real-time meshless method of finite spheres. In the virtual environment, collision detection and perception of multiple tissue layers was created, accompanied with force and torque feedback to user's hand. This feature is supported by force and position sensors mounted on the tool, which is held by the user instead of a robotic arm. The complexity of the above mentioned methods is in connection with the required computational effort. In simple problems, the use of the method of finite spheres is suggested. Another approach to meshless methods was introduced by Bao *et al.*, where several layers were used as the model of the soft tissue, their interaction modeled with a heuristic Kelvin model [26]. Modeling of two important viscoelastic properties, the creep and relaxation is possible with this new three-parameter viscoelastic model, improving the performance of conventional mass–spring–damper approaches. Yamamoto suggested a method for the detection of lumps in organ tissues, such as kidney, liver and heart [27]. The importance of this work was a comprehensive comparison of seven different tissue models used in point-to-point palpation. The aim of the tests and model validations was to create a graphical overlay system that stores data on palpation results, creating a color scale overlay on the actual tissue, processing the acquired data using several tissue models, with a single 1 DoF force sensor at the fixed end of the tool. Yamamoto *et al.* also created an interpolable interface with haptic feedback and augmented visual feedback and performed palpation and surface detection tasks using vision-based forbidden-region virtual fixtures (control boundaries for safety that should not be crossed during an intervention) [28]. The tests were carried out on manufactured artificial tissues based on existing commercially available artificial prostate, using a complex, but—based on previous measurements—accurate Hunt–Crossley model. Position, velocity and force sensors were mounted on the slave manipulator and the visual feedback to the human user was generated with a stereo-vision system.

When dealing with viscoelastic materials interacting with tools, coupled problems arise, where additional mechanical models are required to describe the system response. A fine example to this issue is the task of needle insertion, where friction and the stick-slip phenomenon cause difficulties in assessing real tissue behavior in practice [29]. It is important to mention that even when the best-suited mathematical models are employed, material properties (Young-modulus, Poisson-ratio, etc.) can only be estimated. Validation of their values requires circumstantial physical experiments. When using heuristic, mechanical tissue models, the acquisition of explicit, but general material properties are omitted. Instead of using tables and possible ranges of these properties, spring and damping coefficients must be obtained from measurements, even when nothing else but the tool shape is changed. In their work, Leong *et al.* introduced and validated a mechanical model of liver tissue and its interaction with scalpel blade, creating a distributed model of mechanical viscoelastic elements [30]. With the serial connection of a Maxwell and Kelvin element, they introduced the Maxwell–Kelvin viscoelastic element. The primary aim of their work was to account for the tissue surface deformation due to the extensive shape of the tool, validating with the cutting experiment, where a 1 DoF force sensor was placed at the scalpel blade holder integrated with position measurement, as shown in Fig. 1.2. Besides many constitutive ideas, a great number of deficiencies can be found in the model that still needs to be improved, including mathematical errors in modeling, contradictions in the measurement result evaluation, inappropriate use of Laplace transformation and the overall pertinence of experimental results. Finding and correcting these deficiencies is a

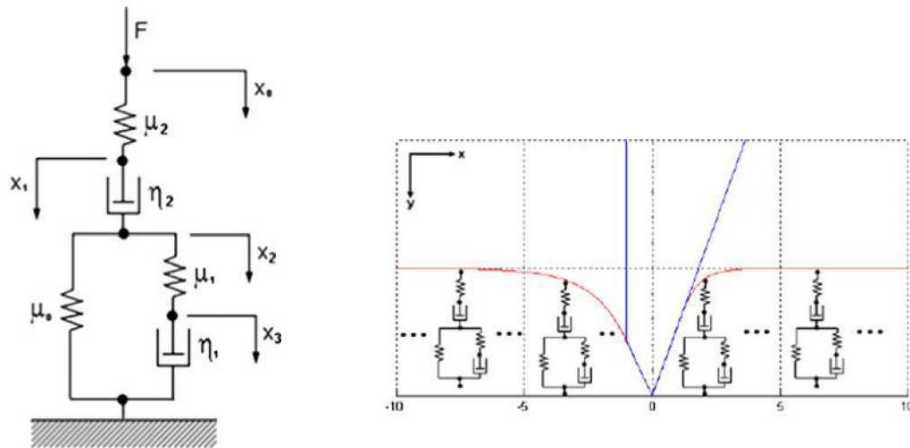


Fig. 1.2. The proposed Maxwell–Kelvin viscoelastic element (left) and the distributed tool–tissue interaction model (right), as it was published by Leong *et al.* [30].

part of this work, the proposed corrections to the methodology and mathematical formulations were published in [TA-6].

Liu *et al.* introduced a method for force control for robotic-assisted surgery on beating heart, thus applying motion compensation for the periodic motion of the organ [31]. By installing a force sensor at the end of the instrument, and tracking the 3D motion of the beating heart, they compared four different models from the viewpoint of tracking performance of the desired force. Besides the conventional viscoelastic models, a fourth, fractional derivative model of viscosity was examined. One of the relevant results of this experiment was to underline the importance of the right choice of tissue model.

In the past years, much focus has been drawn on needle insertion modeling. Due to the simplicity of the tool geometry, needle insertion problems were much discussed using Finite Element Modeling (FEM). Finite Element Analysis (FEA) is a widely used approach for tool tissue interaction modeling, where commercially available FEA software packages are used to aid and simulate the operation area. The great many built-in mechanical models can provide incredibly accurate and realistic solution for simulation. One of the largest drawbacks of this method is the sensitivity of computational time length with respect to the parameters used in FE simulations. These parameters are determined solely by the user, including spatial and time resolutions, thus many simulations need to be carried out on the same model to achieve the desired level of reliability. Goksel *et al.* introduced a novel technique to use real-time remeshing in the case of FEA modeling [32]. A mesh-based linear elastic model of both the needle and tissue was used, applying remeshing in order to compensate organ shift due to the invasiveness. The importance of the model is that both the tool and the tissue deformations were accounted for, although the motion models were the simplest possible in 3D. Continuum mechanics also provides numerous models that can be used for modeling organ and tissue deformations and kinetics.

Approaches using linear and nonlinear models of elasticity are widely used in practice. Linear models have limited usability despite the many advantages they carry (simplicity, easy-calculation and small requirements on computational capacity) due to inhomogeneous, anisotropic, non-linear characteristics of tissues and large relative deformations,

strains. However, nonlinear models in continuum mechanics lead to moderately complex models, even in simple surgical tasks. Misra *et al.* introduced a detailed complex mechanical model of continuum mechanics for the analytical modeling and experimental validation of needle bending at insertion into soft tissues [33]. A hyperelastic Neo–Hookean rupture model was used to describe the material properties and behavior of the soft tissue stimulant (gel), assuming linear elasticity in case of the needle. Experiments were carried out using different bevel-tipped needles and the needle bending curvature was validated using an unfiltered camera data. The importance of the work lays in the area of needle insertion path planning.

In the area of tool–tissue interaction research, one might be interested in rupture modeling. While most of the existing mechanical models assume reversible tissue deformation, even in the case of MIS, tissue rupture cannot be avoided. Mahvash and Dupon developed an analytical model of tissue rupture during needle insertion, focusing on the calculation of required insertion force [34]. The great advantage of this model is that despite the complex mechanical structure, the insertion events are divided into four different models, decomposing the process into moderately complex parts. Tissue modeling was aided with a modified Kelvin model, making the parameters of the linear components dependent of the deformation rate. The analytical model validated the experiments, showing that the required insertion force is inversely proportional to the insertion speed.

It is also important to mention models that are not directly describing insertion and cutting problems, but are rather used for investigating interaction of cable-driven manipulators controlled by human operators, acting on soft tissues. Kosari *et al.* introduced an adaptive parameter estimation and Model Predictive Control (MPC) method on cable-driven surgical manipulators, developing a 1 DoF mechanical model, concentrating on the problem of trajectory tracking [35]. Therefore, instead of the estimation of tissue reaction forces, focus was drawn to the response of the cable-driven manipulator in order to create a realistic force feedback to human user. The moderately complex model accounts for numerous mechanical properties and solves an optimal control problem for automating tissue compression.

Arguably, FEA-based solutions are still popular for modeling and predicting soft tissue behavior for specific use-cases. However, this approach is yet heavily supported by patient-specific information and requires an extensive pre-operative phase due to the complex boundary conditions. Due to the high computational performance required, real-time utilization in teleoperation systems is not achievable at a favorable resolution. Thus, as of today, this approach is not scaling well to various interventions, and therefore cannot be easily generalized. On the other hand, FEA dominantly relies on complex continuum-mechanics based models of the soft tissues, emphasizing their micromechanical behavior during the interventions, which is a useful property for modeling coupled problems (thermomechanics, fluid dynamics etc.). On the macro scale, where most of today’s telesurgical systems are operated, these effects are usually negligible, and thus the tissue behavior can be addressed with simplified models, concentrating on relevant mechanical properties.

The proper modeling of tool–tissue interactions is a relevant topic in standardization methods. With the help of initial calculations and simulations, efficient control methods can be chosen to avoid undesired pain and injury levels. Pain and injury onset levels for static contact force and peak pressure values has been deeply researched and standardized in the literature [36].

1.2.2 Addressing Latency in Teleoperation Systems

The general concept of teleoperation has long been used in various fields of robotics, including manufacturing, logistics and various service robotics scenarios [10]. Today, long-distance teleoperation is an actively discussed topic in space exploration [37] and intervention in hazardous environments [38]. Where traditional control algorithms might fail, latency-induced challenges can be addressed by novel ideas, including soft computing methods, neural control [39], supervisory control through Internet communication [40], passivity-based control [41] and various types of MPC for transparent teleoperation [42] and hybrid MPC solutions to Neural Network (NN) based control methods [43].

Current, commercially available telesurgical systems utilize the concept of unilateral teleoperation, where the position and/or force data from the master console is transmitted to the slave system, whereas the operator only receives visual feedback from the environment through the mounted camera system. However, in bilateral teleoperation, there is a communication of force and position data in both directions of the teleoperation system. This structure allows haptic feedback to the operator, therefore an extended virtual presence can be established in the physical surgical environment, increasing transparency [44]. There is a vast literature of control architectures addressing challenges and proposing solutions to bilateral teleoperation systems, emphasizing the effect of time-delay caused by the communication latency between the master and slave sides. A large percentage of these approaches are variations of position–position teleoperation [45], position–force [46] or force–force teleoperation [47]. Other approaches include a special group of linear controllers, robust H_{∞} control, system dynamics assessment and adaptive nonlinear controllers [48, 49, 50]. Obstacle avoidance, motion guidance and inertia scaling also play an important role in describing the dynamics of the specific teleoperation task, where passive decomposition [51] and time-domain passivity controllers [52] can enhance the performance of actions.

Depending on the nature of the applications, the latency in communication can range between milliseconds (Internet-based teleoperation in terrestrial conditions) to several minutes (space exploration). The magnitude of time-delay is determined by the distance between the master and slave devices and the medium of communication. It is a common view that in robotic systems, time-delay enforces a trade-off between the teleoperation stability and the control performance of the system. Local force feedback at the master side largely affects the performance and transparency of time-delayed teleoperation systems, which varies for different bilateral teleoperation architectures and the magnitude of the latency [53]. A common approach to increase robustness of delayed teleoperation is to apply additional damping on both the master and slave side of the system, however, this often leads to a slow response of the system [54], degrading its control performance. As the transparency of the system decreases, some methods can compensate the performance decay in bilateral teleoperation, by using scattering theory [55], wave-variable control [56] or passivity control [57]. Other approaches include the telemonitoring of force feedback under low latencies [58].

In the past decades, it has become a common view that large delays require accurate models of the operation environment based on prediction, creating a quasi real-time simulated response to the operator [59]. One of the most successful approaches to predictive control methods are utilizing the Smith predictor [60], while several approaches combine

the Smith predictor with Kalman filtering for achieving better performance results [61, 62]. The linear approximation of the effect of time-delay is also a common modeling approach in teleoperation control, utilizing the state-space representation of the system based on the first-order Taylor-expansion of the system [63, 64].

In order to summarize the challenges and current possibilities in teleoperation with time-delay in the range of a few seconds, a detailed report has been published by NASA in 2002 [65]. The report lists some of the most important tools and guidelines in teleoperation, highlighting the importance of predictive displays, where a realistic model of the environment is shown to the operator, which responds to the master console input real-time. This approach has proven to be very efficient if the latency is under 1 second, however, it requires a reliable model of the task environment, including the slave and slave–environment interaction models [66]. Another frequently discussed issue is related to the compliance of the slave side, as it can reduce the execution time and the overall forces acting on the environment during the manipulation [67]. From the haptics point of view, force reflection in bilateral teleoperation is critical in terms of stability. In real-life applications, direct force feedback can only be applied reliably with latencies under 2 seconds, however, in this range, high performance in completing teleoperation tasks can only be achieved with force feedback [68]. While this feedback can be achieved by numerous ways directly or indirectly, such as using visual feed on the force magnitude, or reflection of the force the hand of the operator that does not take part in the teleoperation, the best solution is considered to be when the interaction force is simulated and fed back to the operator based on the system model. Aiding this approach from the theoretical background, this thesis gives a proposal for modeling methodology of the interaction environment during teleoperation, more precisely, the modeling of tool–tissue interaction in the case of telesurgical manipulations on soft tissue.

1.3 Theoretical Tools Used in the Thesis

1.3.1 Heuristic Models in Soft Tissue Modeling

As it was discussed by Famaey and Sloten, the mass–spring–damper modeling approach is the simplest possible way of modeling the behavior of soft tissues [23]. Due to the unique material properties of soft tissues (anisotropy, viscoelasticity, inhomogeneity etc.), describing their behavior under manipulation tasks is very different from other materials that are used in industrial or other service robotic applications. The main idea of this approach is that linear or nonlinear spring and damper elements are combined together in a serial or parallel way, creating an assembly, which, when subjected to deformation, would present similar mechanical properties as the represented soft tissue. A detailed explanation of the structure of mass–spring–damper models was published by Wang and Hirai [69], investigating the behavior if serial and parallel models. They also discussed experimental results related to the rheological behavior of commercially available clay and Japanese sweets materials, using model parameter estimation.

In order to efficiently apply this model, the $u(t)$ deformation paths of the end points of the combined mechanical elements need to be known in time. Provided that this information is given, the force response can be described with a simple mathematical expression.

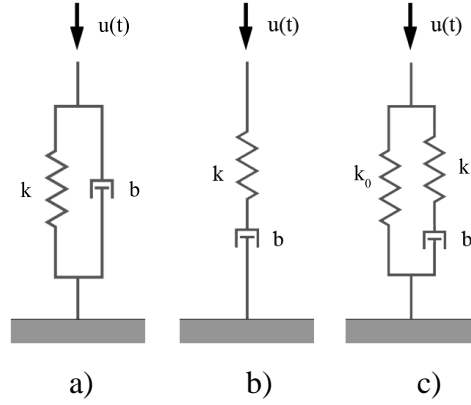


Fig. 1.3. Commonly used models for representing the mechanical behavior of viscoelastic materials: a) Kelvin–Voigt model, b) Maxwell model, c) Kelvin model.

The reaction force arising in the mechanical elements can be determined from basic mechanical properties. In the case of a spring element, this force (f_s) is calculated from the spring stiffness value (k), and the deformation of the spring in the longitudinal direction:

$$f_s = k(x_1 - x_2), \quad (1.3)$$

where x_1 and x_2 represent the end coordinates of the spring and damper elements. The reaction force (f_d) arising in the damper elements is calculated using the damping coefficient value (b) and the rate of deformation of the damper element:

$$f_d = b(\dot{x}_1 - \dot{x}_2), \quad (1.4)$$

where \dot{x}_1 and \dot{x}_2 refer to the speed that the end coordinates are moving the longitudinal direction. In heuristic soft tissue modeling, there are three basic models that are commonly used for describing tissue behavior in terms of viscoelasticity: the Kelvin–Voigt, the Maxwell and the Kelvin models, as shown in Fig. 1.3 [70]. In this section, only the behavior of linear models is discussed, but the general description applies to the nonlinear models, as well.

The Kelvin–Voigt model is the most commonly used heuristic model in analytical mechanics, capable of representing stress relaxation and reversible deformation. There exists an analytical solution to the force response in the form of an ordinary differential equation. This model is very popular in many fields of study due to its simplicity and easy interpretation. However, step-input response functions cannot be modeled using the Kelvin–Voigt model, as the reaction force arising as a result of a step-like deformation would be infinitely large due to the parallel connection of the damper element. In time domain, the force response function for the Kelvin–Voigt model is described by:

$$f_{KV}(t) = b\dot{u}(t) + ku(t), \quad (1.5)$$

where $u(t)$ is the deformation function. Similarly, the force response function in the frequency domain is as follows:

$$F_{KV}(s) = (bs + k)U(s). \quad (1.6)$$

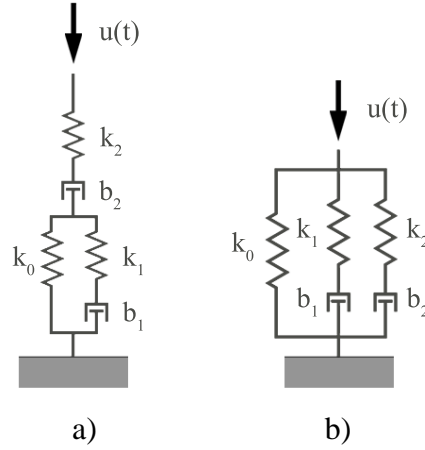


Fig. 1.4. Two basic combinations of the mass–spring–damper viscoelastic models: a) the Maxwell–Kelvin model and b) the Wiechert model.

The Maxwell model is the simplest approach to model *creep*. In this model, a damper and a spring element are connected serially, making the model usable for modeling stress relaxation. A major drawback of the Maxwell model is that the force response value (f_M) will asymptotically converge to 0 in the case of a constant deformation input. Therefore, this model is not capable of modeling residual stress. The actual deformation of the system cannot be expressed as the function of the acting forces, which is the result of the internal dynamics of this model, since the position of the virtual mass point connecting the spring and damper elements cannot be measured. On the other hand, in the frequency domain, the transfer function can be easily determined:

$$F_M(s) = \frac{kbs}{bs + k}U(s). \quad (1.7)$$

The Kelvin element is created by the parallel connection of a Maxwell-element and a single linear spring element. This combination is often referred to as the Standard Linear Solid model in viscoelasticity. In heuristic soft tissue behavior modeling, this is the most commonly used mass–spring–damper model, providing the simplest possible approach of representing residual stress, stress relaxation and elastic behavior in the case of step-inputs. In time domain, there exists a closed-form formulation, written as follows:

$$f_K(t) + \frac{b}{k_1}\dot{f}_K(t) = k_0 \left(u(t) + \frac{b}{k_0} \left(1 + \frac{k_0}{k_1}\dot{u}(t) \right) \right). \quad (1.8)$$

In the frequency domain, the transfer function of the Kelvin element is:

$$F_K(s) = \frac{b(k_0 + k_1)s + k_0k_1}{bs + k_1}U(s). \quad (1.9)$$

Due to the rapid development in the fields of robot control and surgical robotics, the creation of more sophisticated models has become essential in soft tissue behavior modeling. The accuracy requirements of advanced robotic surgical applications were not met anymore by the previously described simple models. In order to achieve better performance in these applications, new combinations of damper and spring elements were proposed. A new dynamic model is, where a Kelvin and a Maxwell element are connected

serially, creating a mass–spring–damper model consisting of five mechanical elements (Fig. 1.4). The major advantages of this model are that both the elastic behavior and stress relaxation of the tissue can be described in a significantly more effective and sophisticated manner, compared to the general Kelvin model. In the frequency domain, the transfer function is written as:

$$F_{MK}(s) = \frac{A_{2MK}s^2 + A_{1MK}s}{B_{2MK}s^2 + B_{1MK}s + B_{0MK}}U(s), \quad (1.10)$$

where A_{2MK} , A_{1MK} , B_{2MK} , B_{1MK} , B_{0MK} are linear combinations of parameters k_0 , k_1 , k_2 , b_1 and b_2 . It is important to note that increasing the complexity of a heuristic model does not necessary lead to better accuracy in terms of system behavior modeling. In the case of the Maxwell–Kelvin model, used in [30], the reaction force will converge to 0, similarly to the Maxwell model, therefore this model is clearly not the best choice for modeling long-term stress relaxation. It can easily be seen that if there is a damper element that is placed in the “cross-section” of the model (there is no spring element “bypassing” the flow of the force), the resulting reaction force would be 0 in the steady-state.

If a Kelvin element and several Maxwell elements are connected in a parallel way, the generalized Maxwell model is created. If there is only one Maxwell element integrated in the model, its simplest form, the Wiechert model is derived. With this approach, the modeling of the reaction force becomes smooth and significantly more accurate due to the possibility of finer “tuning” of mechanical parameters. A detailed comparison between the Standard Linear Solid and the Wiechert models have been provided by Wang *et al.* [71], highlighting the advantages of using the latter in liver and spleen organ force response modeling. Parameter estimation of the Wiechert model has also been done by Machiraju *et al.* [72], although the results were only based on tissue relaxation data, proposing its integration into finite element modeling softwares.

The transfer function of the Wiechert model is as follows:

$$F_W(s) = \frac{A_{2W}s^2 + A_{1W}s + A_{0W}}{B_{2W}s^2 + B_{1W}s + B_{0W}}U(s) = W_W(s)U(s), \quad (1.11)$$

where

$$\begin{aligned} A_{2W} &= b_1b_2(k_0 + k_1 + k_2), \\ A_{1W} &= (b_1k_2(k_0 + k_1) + b_2k_1(k_0 + k_2)), \\ A_{0W} &= k_0k_1k_2b_2, \\ B_{2W} &= b_1b_2, \\ B_{1W} &= b_1k_2 + b_2k_1 \text{ and} \\ B_{0W} &= k_1k_2. \end{aligned}$$

This transfer function plays a fundamental role in the investigation of the force response curves of the linear Wiechert model, a methodology discussed in details in chapter 4.

1.3.2 Tensor Product Model Transformation

Tensor Product Model Transformation (TP transformation for short) is a novel concept in quasi-Linear Parameter Varying (qLPV) model-based control, playing a central role pro-

viding valuable mean for connecting identification methods and polytopic systems theories. The basic idea behind TP Model Transformation is the transformation of an arbitrary function into polytopic TP form which is also capable of describing nonlinear dynamical systems for the purpose of controller design via linear matrix inequalities. The concept was introduced by Baranyi [73], and a practical guide for its applicability for qLPV control theory was published in [74].

In this section, some of the fundamental definitions of the TP Model Transformation are recalled.

Definition (LPV/qLPV model):

Consider the following LPV model:

$$\begin{bmatrix} \dot{\mathbf{x}}(t) \\ \mathbf{y}(t) \\ \mathbf{z}(t) \end{bmatrix} = \mathbf{S}(\mathbf{p}(t)) \begin{bmatrix} \mathbf{x}(t) \\ \mathbf{u}(t) \\ \mathbf{w}(t) \end{bmatrix}, \quad (1.12)$$

with state vector $\mathbf{x}(t)$, measured output $\mathbf{y}(t)$, performance output $\mathbf{z}(t)$, input $\mathbf{u}(t)$, and disturbance input $\mathbf{w}(t)$. The $\mathbf{S}(\mathbf{p}(t)) \in \mathbb{S}$ system matrix can be partitioned to $\mathbf{A}(\mathbf{p}(t))$, $\mathbf{B}(\mathbf{p}(t))$, $\mathbf{C}(\mathbf{p}(t))$ etc. system matrices, and it is defined over a hyper-rectangular parameter domain:

$$\mathbf{p}(t) \in \Omega = [a_1, b_1] \times [a_2, b_2] \times \dots \times [a_N, b_N] \subset \mathbb{R}^N. \quad (1.13)$$

If the parameters in $\mathbf{p}(t)$ are not independent from the $\mathbf{x}(t)$ state variables, it is called quasi-LPV (qLPV) model.

Definition (Finite element polytopic model):

The (1.12) LPV/qLPV model, where the system matrix is given as convex combinations of vertex system matrices:

$$\mathbf{S}(\mathbf{p}) = \sum_{r=1}^R w_r(\mathbf{p}) \mathbf{S}_r \quad \forall \mathbf{p} \in \Omega, \quad (1.14)$$

where for the \mathbf{p} parameter-dependent weighting functions w_r :

$$\sum_{r=1}^R w_r(\mathbf{p}) = 1, \quad w_r(\mathbf{p}) \geq 0 \quad \forall r, \mathbf{p} \in \Omega. \quad (1.15)$$

The term finite indicates that R is bounded.

Definition (Finite element polytopic TP model):

The (1.12) LPV/qLPV model, where the system matrix is given as convex combinations of vertex system matrices, and the weighting functions are decomposed to product of univariate functions:

$$\mathbf{S}(\mathbf{p}(t)) = \sum_{j_1=1}^{J_1} \sum_{j_2=1}^{J_2} \dots \sum_{j_N=1}^{J_N} \prod_{n=1}^N w_{j_n}^{(n)}(p_n(t)) \mathbf{S}_{j_1, j_2, \dots, j_N}. \quad (1.16)$$

Applying the compact notation based on tensor algebra (Lathauwer's work [75]) one has:

$$\mathbf{S}(\mathbf{p}(t)) = S \boxtimes_{n=1}^N \mathbf{w}^{(n)}(p_n(t)), \quad (1.17)$$

where the core tensor $\mathcal{S} \in \mathbb{S}^{J_1 \times J_2 \times \dots \times J_N}$ is constructed from the vertex system matrices $\mathbf{S}_{j_1, j_2, \dots, j_N} \in \mathbb{S}$, and the row vector $\mathbf{w}^{(n)}(p_n(t))$ contains scalar weighting functions $w_{j_n}^{(n)}(p_n(t))$, ($j_n = 1 \dots J_N$) that represent convex combinations as (1.15) for all n .

The polytopic TP model (1.17) is a special class of polytopic models, where the weighting functions are decomposed to the tensor product of univariate functions.

Definition (TP Model Transformation):

TP Model Transformation is a numerical method that transforms the LPV/qLPV models to polytopic TP model, so that the Linear Matrix Inequality (LMI) methods developed for polytopic model-based control can be applied to the resulting model [73].

The polytopic TP representation of an LPV/qLPV system can be obtained in various ways, of which the Minimal Volume Simplex (MVS) type polytopic model is used in this work, defined below:

Definition (MVS Polytopic TP model):

The (1.17) polytopic TP model, where the $\mathcal{S} \in \mathbb{S}^{J_1 \times \dots \times J_N}$ core tensor is constructed from the $\mathbf{S}_{j_1, \dots, j_N}$ matrices, in such a way that the $(\mathcal{S})_{j_n=j}$ n -mode subtensors construct the minimal volume enclosing simplex for the

$$\mathcal{S} \times_n \mathbf{w}_{j_n}^{(n)}(p_n) \quad (1.18)$$

trajectory for all $n = 1 \dots N$., where

$$(\mathcal{S} \times_n \mathbf{w})_{j_1, j_2, \dots, j_{n-1}, i_n, j_{n+1}, \dots, j_N} = \sum_{j_n} \mathcal{S}_{j_1, j_2, \dots, j_{n-1}, i_n, j_{n+1}, \dots, j_N} \mathbf{w}_{i_n, j_n}. \quad (1.19)$$

In the proposed structure, a TP-type polytopic controller is utilized, where the control signal is computed as:

$$\mathbf{u} = - \left(\mathcal{F} \boxtimes_{n=1}^N \mathbf{w}^{(n)}(p_n(t)) \right) \mathbf{x}. \quad (1.20)$$

Feedback gains $\mathbf{F}_{i_1, i_2, \dots, i_N}$ are stored in tensor \mathcal{F} .

It is important to note that the discussed model representations are also valid in discrete time domain, with no fundamental restrictions. Further reading about the TP Model Transformation, the MVS-type polytopic TP model generation and manipulation methods can be found in [76, 77, 78, 79].

Chapter 2

RESEARCH PROBLEM STATEMENT

Robots are gradually entering the operating room, aiding, or completely taking over different surgical maneuvers. The state-of-the-art is that these robotic systems are used as human-operated, telesurgical systems, where the human operator is an integral part of the control loop, while the robot is mimicking the gestures of the surgeon. The primary aim of telesurgical devices is to enhance the performance of the surgeon, applying hand tremor filtering, virtual guiding and motion scaling. From the engineering point of view, these teleoperation systems should provide a transparent, reliable and robust operation, which requires advanced approaches in terms of controller design and system modeling. In order to avoid stability loss and accuracy deterioration, the problems of signal latency due to the remote operation, elastic tool deformation and undesired hard tissue contact can be addressed by reliable soft tissue models. This way, various scenarios of the tool–tissue interaction can be approached from the modeling point of view.

Robot-assisted tissue manipulation requires high precision tools and techniques. Today's telesurgical systems dominantly rely on visual feedback, the commercially available systems do not provide haptic feedback to the surgeon. As the placement of force sensors into the surgical tools used in Minimally Invasive Surgery is very challenging, an alternative approach is needed for indirect reaction force estimation, in order to provide force sensation to the operator. Furthermore, automated surgical interventions also require an estimation of the behavior of the manipulated environment. The unique behavior of soft tissues as viscoelastic materials can only be described by sophisticated mathematical models, as the currently used models are only representing the predicted behavior locally. As the soft tissue is an integral part of the manipulation, the integration of its model at various level of engineering design is crucial.

- *Problem 1:* There is a need for a general soft tissue model that can represent soft tissue behavior during surgical interventions. The model should give a relation between tissue deformation and the reaction force, and should give a quantitative representation of the material, with adequate spatial and temporal resolution.

Teleoperation systems in general require sophisticated control approaches in order to assure transparency of the system and increase reliability. Modern telesurgical systems dominantly use traditional control approaches in order to increase robustness, which often means a trade-off for the accuracy requirements. An appropriate tool–tissue interaction model opens up the possibility for applying model-based control methods, allowing a

direct implementation to complete surgical robotics systems. Modern model-based controller design methods are limited by the mathematical representation of the system, therefore bringing the interaction models to a design-compatible form is essential.

- *Problem 2:* Control methods in telesurgical applications need to rely on sophisticated models of the tool–tissue interaction, requiring the models to be represented in predefined forms. In the meantime, the controller performance should be robust against time-delay and modeling uncertainties.

Haptic feedback in robot-assisted surgical systems offers the possibility to reflect the estimated or directly measured reaction force to the operator. Furthermore, surgical simulators with haptic feedback can introduce an important function for surgical training in education, where accurate soft tissue models can be used for creating virtual surgical scenarios. As different haptic devices provide different sensation and scaling of the reflected force, there is a need for a performance evaluation of the Human–Machine Interface for specific setups, addressing the validity of the utilized soft tissue models.

- *Problem 3:* A general methodology is needed for addressing the usability and validity range of tool–tissue interaction models in telesurgical scenarios, where haptic feedback is available. The methodology should be extended to both living and artificial tissues, and an appropriate framework is required for data acquisition, processing and evaluation.

Modeling of telesurgical systems is a complex task, where tool–tissue interaction and soft tissue modeling play an essential part. However, the appropriate models of the slave side (robotic arm), operator behavior and the communication system all have to improved simultaneously in order to achieve a superior performance in telesurgery. The problems stated in this chapter are focusing on an important part of model-based design and usability approaches, their discussion in this work proposes solutions that can aid the further research of the scientific community in the field.

Chapter 3

METHODS

During my doctoral research, I relied on specific methods in terms of experimental data collection, research protocols and techniques. Each of the research problems and statements of the hypotheses were relying on these methods. This chapter provides a detailed description of the research plan, step-by-step, focusing on its elaboration in the thesis groups.

The primary question in my research proposal was related to the state-of-the-art of the existing tool–tissue interaction models. It was my goal to investigate, to what extent this models could be used for improving the performance of telesurgical interventions, with special attention to the model description, its integrability into control methods in general, and finally, the validity of the specific interaction models in the wide range of telesurgical applications.

As of today, there is no general consensus on which tool–tissue interaction to chose for specific applications. An ambitious plan was formed to propose a general model that can be utilized in a wide range of intervention modeling, which required the investigation of the current tool–tissue interaction models, analyze them and find the best-fitting high level approach for my goals. I have created a structured list for my literature research, where I collected the properties of the investigated tool–tissue interaction models, available from the most extensive scientific paper libraries in the topic. I have collected the modeling approaches used in these works, focusing on soft tissue models, tool models, clinical use case, feedback type to the operator, applied sensors and model complexity. The literature research was covering the material of over 50 scientific papers in the topic of tool–tissue interaction, distinguished by their number of citation, publication date and relevance. Novel, well-cited papers with explicit focus on tool–tissue interaction received a higher preference, while older, less-cited ones were used as a reference in the comparison and assessment of modeling approaches.

After concluding the first phase of the literature research, I have collected 3 tool–tissue interaction models, which provided promising approaches for the improvement of telesurgical performance, tackling 3 independent challenges in modern surgical robotics design: the flexibility of cable-driven surgical tools; the problem of motion compensation in the case of moving organs; and the mechanical modeling of soft tissue behavior during the tool–tissue interaction. While there is a rich literature discussing methods for dealing with these challenges, I have decided to conduct a deeper investigation in the field of soft tissue modeling, proposing that a sufficiently accurate soft tissue model can be generalized

for a wide range of modeling surgical interventions. Such model could be directly utilized by various tool–tissue interaction approaches, e.g., modeling cable-driven interaction.

The behavior of soft tissues and viscoelastic materials have been the subject of research for long, not restricted for surgical robotics applications. However, a general soft tissue model has not been proposed yet, most of the approaches can be sorted into three large groups:

- rheological models,
- continuum-mechanics based models,
- hybrid models.

In search for a general solution, which could quantitatively represent the macroscopic mechanical properties of soft tissues, my literature research was focusing on rheological models and their use for specific tissue modeling and characterization applications. Based on the collection of research papers utilizing this approach, I created an overview of the existing model variations, addressing their advantages and disadvantages, finding that the Wiechert model provides the most general, yet simple description of tissue behavior.

As there is no generally accepted verification method for addressing the validity of soft tissue models, my aim was to propose a methodology that can aid the quantitative comparison of different viscoelastic materials using the Wiechert model. This part of the work was done in two phases. First, existing measurement data from the available literature was used for verifying the model. Second, experimental data was collected in a structured way, proposing a methodology to create a diverse set of measurement data. In these sets of measurements, reaction force data from tissue compression was recorded under known deformation profiles, and the soft tissue model verification was carried out by fitting the simulated tissue behavior on the measurement data, finding the best fitting set of mechanical parameters representing the Wiechert model. The curve fitting was utilizing the widely-used Root Mean Square Error (RMSE) minimization of the distance of measured and simulated data points. This method was later used in the same sparsity of data points for the performance evaluation of the model for different scenarios.

Taking the Wiechert model as a basic example, investigating the measurement data from the compression tests, I used an analytical method for improving the performance of the linear model. This included a proposal of introducing different types of nonlinearities into the structure, conducting further research on the limited literature available on nonlinear rheological models. Based on practical consideration, I have introduced the nonlinearities through the spring elements of the Wiechert model, and obtained the parameters of the investigated tissue models using curve fitting methods described. The model verification for uniform and non-uniform surface deformation was following this methodology as well.

The experimental data collection was carried out based on a carefully assembled measurement plan, and was documented for better reproducibility. The measurements required a palpation tool that was capable of maintaining a prescribed compression rate and recording the reaction force by the compressed tissue either by an in-built or mounted force transducer. The simultaneous recording of displacement and force allowed me to create a structured set of data for evaluation. This data collection method was used both for *ex vivo*

and artificial tissue samples, where the samples were cut or molded to a prescribed geometry and dimensions. This way, the method can be standardized, and the quantitative comparison of the tissue parameters can be validated.

Having verified the tissue model, I have conducted an extensive research on model-based control methods in robotic surgery, where soft tissue models were utilized to some extent. By investigating these approaches, I found that very few of them were relying on complex, nonlinear tissue models, requiring a controller design for linear or quasi-linear model representations. In order to achieve robustness and to design a controller system that is stable in the Lyapunov sense, LQ optimal control is a popular approach, where the controller is in the form of a Parallel Distributed Compensator (PDC). The method required a discretized representation of the nonlinear system and a control architecture. Polytopic Tensor Product (TP) modeling in an emerging field in the representation of nonlinear systems for such control problems. Based on this consideration, I created the Minimal Volume Simplex (MVS) polytopic TP form of the proposed nonlinear Wiechert model, and verified it by investigating its behavior on predefined deformation input functions, comparing the output to the one of the qLPV representation of the system.

The verification of the TP model was followed by the proposal of different control architectures, which were tested in the MATLAB Simulink (MathWorks, Inc, Natick, MA) simulation environment. As the conventional control architectures failed to solve the control problem in practice, I proposed a new modeling methodology in order to comply to the requirements of the controller design. The model was tested and verified on simulated tracking tasks, and was tested against robustness in the simulation environment as well.

The polytopic representation of the model allows its easy integration into the da Vinci surgical system, which was the first step towards proposing a tissue characterization methodology. Such representation allows one to use a large variety of control schemes for force control applications, allowing the reformulation of the highly nonlinear system to the interpolation of linear dynamic systems. The aim of this phase was to address the usability and validity range of the proposed soft tissue models, integrating it to a force-feedback palpation scenario, tested by a representative group of participants. The planning of the tissue characterization experiments were based on the findings of the literature research on trials with haptic devices, investigating different approaches to palpation scenarios, the average number and professional background of participants. The characterization trials were using the da Vinci Surgical System as the haptic interface, utilizing the da Vinci Research Kit (DVRK) and the Robot Operating System (ROS) platform. The palpation scenario was based on the guidelines from the automated tissue palpation experiments, but the compression rate was controlled by the participants during the trials. The participants were asked to carry out simultaneous palpation using both of the master tool manipulator arms of the da Vinci master console, controlling the palpation tool with their left hand, and palpating a virtual, polytopic representation of different tissue models. Then, they compared the real and virtual tissues, and looked for the match of the *ex vivo* sample from the different virtual ones. Their comments and final guesses on the matching tissue were recorded and evaluated both verbally and quantitatively. The collected data from the automatic tissue palpation for parameter estimation, and the characterization trials provide structured, aggregated data for further investigation of the proposed verification method, focusing on this special case of Human–Robot Interaction (HRI). The findings of this research provide valuable information to the research community, in order to better understand the oppor-

tunities and limitations of using haptic devices in telesurgical systems in real-life surgical scenarios.

Detailed description of the methods and evaluation can be found in chapters 4, 5 and 6, while the validity range of the methods is also addressed in the summary of these chapters.

Chapter 4

A METHODOLOGY FOR SOFT TISSUE MODELING

Cutting, indentation and grasping are the most common types of tissue manipulation that require high precision tools and techniques in robotic surgery. In order to achieve better performance for surgical robotics applications in terms of stable control for teleoperation, it is crucial to understand the behavior of soft tissues through their mechanical properties [10]. Creating an accurate tool–tissue interaction model would largely aid the design of model-based control methods. This way, force response of the manipulation is estimated using the model, and the required input force (control signal) can be calculated that would control the tissue holder (in most cases, the robotic arm) in order to carry out the surgical manipulation tasks in an efficient, stable and accurate way. A comprehensive study of the existing tool–tissue interaction models was presented by Famaey and Sloten in [23], collecting these into 3 major categories:

- *Continuum mechanics-based* models, which are mostly based on finite element analysis approaches;
- *Heuristic* models, which are built up from linear or nonlinear basic mechanical elements such as springs and dampers;
- *Hybrid* models, which usually represent a combination of the above mentioned approaches [80].

It is widely accepted that continuum mechanics-based models provide the most realistic response functions. However, a significant disadvantage of this approach is the vast computational requirement, limiting their usability in real-time simulations and applications. The heuristic models, which are also often referred to as the mass–spring–damper models or rheological models, are very popular in modeling surgical manipulation tasks, mainly indentation and grasping [70]. Using heuristic models, analytical solutions could be provided, making this a great advantage of using this approach in many modeling aspects of tool–tissue interaction [TA-15]. Several works provide measurement data for soft tissue indentation force response in both relaxation [81] and compression phases [26]. Heuristic models were comprehensively discussed by Yamamoto, comparing several simple models in point-to-point palpation for detecting hidden lumps in soft tissues [27]. Alkhouli *et al.* investigated the mechanical properties of human adipose tissues, although the linear viscoelastic model they used was only applied in the relaxation phase [82]. Troyer *et*

al. created a nonlinear viscoelastic model that was validated with relaxation tests, which is implementable in finite element algorithms in order to decrease computational requirements [83]. These models, along with the appropriate image guidance and modeling, can largely increase the accuracy and safety of surgical interventions [22]. Mechanical models can also be integrated with visual cues in order to improve the performance of haptic feedback devices. Such virtual models were used in pseudo-haptic feedback-based methods by Li *et al.*, using a silicone phantom tissue with embedded hard incisions [84]. A complex tissue model was presented by Leong *et al.*, where some of the soft tissue parameters were integrated, although, the correct acquisition of the parameters was not successful [85]. Some relevant measurement results were still published [30], despite the ill-formed mathematical description.

In their paper, the surface deformation shape was estimated to be exponential, although this assumption was not supported by any literature or experimental reference, and the relevant geometrical parameters were not published, either. The resulting transfer function was incorrectly derived for the proposed model, which resulted in an estimated force response with no physical meaning. Consequently, the published parameters were not fit to the experimental data, therefore the discussion of results was incomplete and incorrect. The paper was concluded by modifying the Dirac-delta function so that it would fit a single measurement point in the experimental results. To correct these shortcomings of the *a priori* research, this chapter follows the same basic idea as Leong *et al.*, then correctly deriving the mathematical formulae, and approximating tissue parameters and surface deformation shape, based on reproducible experimental data, which will be used for the verification of the proposed nonlinear soft tissue model.

4.1 Experimental Verification of the Wiechert Model

Chapter 1.3.1 introduced the most commonly used linear mass–spring–damper viscoelastic soft tissue models. Among these models, the Wiechert model (sometimes called the Maxwell–Wiechert model) is the simplest form of the generalized Maxwell model. In this approach, the previously explained Kelvin model is extended with a number of Maxwell elements, making this combination of elements capable of smooth modeling of the reaction force of the soft tissue. The transfer function of the Wiechert model is given in Eq. (1.11).

4.1.1 Theoretical Verification of the Linear Wiechert Model

In order to address the validity of the currently used linear mass–spring–damper models, an *a priori* verification of these approaches was carried out in the first phase of this work. The verification was relying on a sufficiently documented experimental data by Leong *et al.* [30]. In their work, 30 pieces of coagulated liver tissue samples were examined by indentation. The cylinder-shaped specimens were 10 mm in height and their diameter was also 10 mm. The tissue specimens were compressed at a compression rate of 10 mm/s until the strain of 0.7 was reached, then the relaxation response was measured in terms of the axial force, for a total of 20 minutes of experimental time. In order to acquire the measurement data for the purpose of this work, the data points were determined by

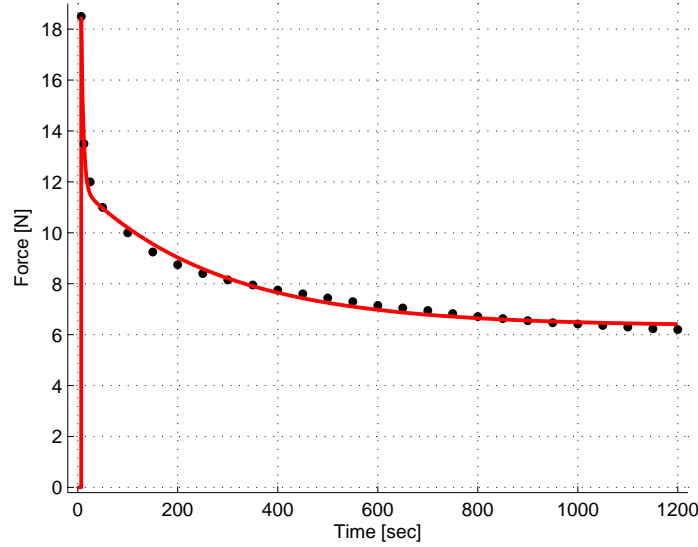


Fig. 4.1. Curve fitting using MATLAB *cfTool* toolbox. The red curve represents the fitted force response, the black dots are the original experimental data points. $A = 5.4$ [N], $B = 6.737$ [N], $C = 6.34$ [N], $X = 0.003606$ [1/s], $Y = 0.2248$, [1/s].

using traditional image viewer software, recording pixel coordinate information from the published force response curves. The curve fitting procedure was then applied on this set of points.

In order to simplify the calculations, and to be able to create an analytical solution for the force response, the deformation input function was modeled as a step-input, which is a very good approximation of the original combination of the ramp and constant deformation functions due to the long experimental time. Therefore, the force response function is given as the inverse Laplace transform of Eq. (1.11), where the transfer function $W_W(s)$ is multiplied by the Laplace transform of the step-input.

$$f_W(t) = \mathcal{L}^{-1} \left\{ W_W(s) \frac{y_d}{s} \right\}, \quad (4.1)$$

where $y_d = 7$ mm is the indentation depth at the maximum deformation. The inverse Laplace transform can be obtained easily using partial fraction decomposition, then applying the transformation on each of the elements. Thus, using the Wiechert model for describing the tissue behavior, the general form of the force response function is given by:

$$f_W(t) = Ae^{-Xt} + Be^{-Yt} + C, \quad (4.2)$$

where A, B, C, X and Y are unknown parameters that can be obtained from the curve fitting procedure. The actual model parameters are calculated by solving the following set of algebraic expressions:

$$A + B + C = k_0 + k_1 + k_2, \quad (4.3)$$

$$X(B + C) + Y(A + C) = \frac{k_2}{b_2}(k_0 + k_1) + \frac{k_1}{b_1}(k_0 + k_2), \quad (4.4)$$

TABLE 4.1

PARAMETER ESTIMATION RESULTS FROM FORCE RELAXATION TESTS BASED ON THE EXPERIMENTAL DATA BY LEONG *et al.*, REPRESENTED BY EQ. (1.11).

Model type	k_0 [N/m]	k_1 [N/m]	k_2 [N/m]	b_1 [Ns/m]	b_2 [Ns/m]	RMSE
Linear Wiechert	906	962	771	4281	21393	0.0329

$$CXY = \frac{k_0 k_1 k_2}{b_1 b_2}, \quad (4.5)$$

$$X + Y = \frac{k_1}{b_1} + \frac{k_2}{b_2}, \quad (4.6)$$

$$XY = \frac{k_1 k_2}{b_1 b_2}. \quad (4.7)$$

The curve fitting procedure was carried out by using the MATLAB *cftool* toolbox. The values of the unknown model parameters are listed in Table 4.1.

Note that these values correspond to the cylindrical tissue sample, with the previously listed geometrical parameters. The model parameters, however, can be converted to represent quasi-specific stiffness and damping coefficient values, projected on a unit surface, expressed in the dimensions of N/(m·m²) and N/(ms·m²).

The fitted curve to the given set of data points is shown in Fig. 4.1. The mean square error of the fitting is $\epsilon_s = 0.0329$ N, where the subscript s stands for the step-input. It is clear that the Wiechert model describes the tissue behavior in a significantly more accurate manner than the widely used Kelvin model or other, lower order approaches. This difference is more significant if the stress relaxation is investigated in a long time-span.

4.1.2 Model Verification for Non-Ideal Step-Input

As it was discussed in the previous section, the deformation input function was modeled as an ideal step-input on the transfer function Eq. (1.11). In order to verify the model, the original deformation function by Leong *et al.* was applied on the transfer function, where the maximum deformation of 7 mm was reached by a constant deformation rate of 1 mm/s. This yielded a different force response curve due to the relaxation phenomenon already undergoing during the compression phase. The crucial point is the peak force that is reached at the time of 7 seconds. As it can be observed in Fig. 4.2, in the case of the original input function, the largest difference between the fitted curve and the model response appears around this crucial point, corresponding the mean square error value of $\epsilon_r = 0.5022$ N, where r stands for the non-ideal step-input. This error is one order of magnitude higher than that of the ideal step-input response. In order to address the error of this approximation in terms of physical parameters, a correction was carried out by modifying the parameter values one of the branches of the Wiechert model, thus correcting the parameters of the serially connected elements k_1 and b_1 . A new pair of these parameters was found by post-optimization, where the mean square error of the response curve was considered as the cost function. The new model parameters are listed in Table 4.2, where

TABLE 4.2
CORRECTED PARAMETER ESTIMATION RESULTS FROM FORCE RELAXATION TESTS BASED ON THE
EXPERIMENTAL DATA BY LEONG *et al.*, REPRESENTED BY EQ. (1.11).

Model type	k_0 [N/m]	$k_1^* = c_1 k_1$ [N/m]	k_2 [N/m]	$b_1^* = c_2 b_1$ [Ns/m]	b_2 [Ns/m]	RMSE
Linear Wiechert	906	962	771	4281	21393	0.0322

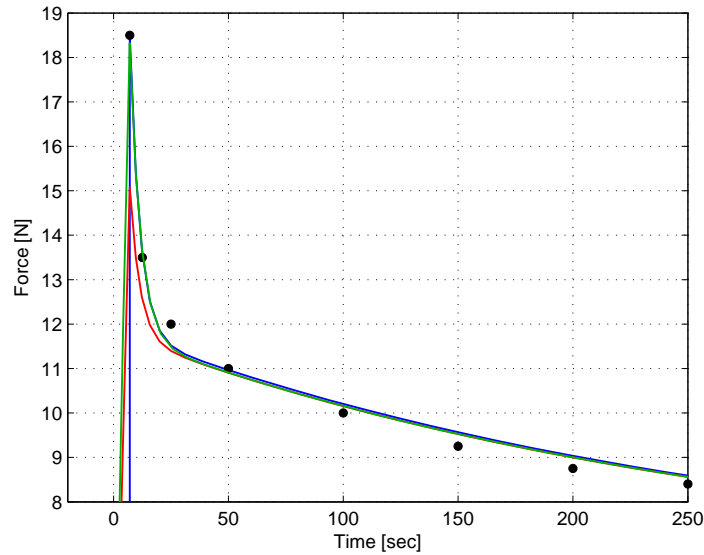


Fig. 4.2. Validation of model parameters. Green: ideal step-input response curve with the uncompensated model parameters; blue: the response of the model with the original input function with the uncompensated model parameters; red: the response curve on the original input function with the compensated parameters k_1^* and b_1^* .

$c_1 = 2$ and $c_2 = 1.9$ are the constants and represent the magnitude of required correction of the parameters due to the non-ideal step-input.

The simulated force response functions using the corrected parameter values are also shown in Fig. 4.2. The mean square error of the response curve of the corrected system is $\epsilon_c = 0.0322$ N, which is 5.5% lower than in ideal the step-input case (the subscript c stands for the corrected model). In order to highlight the differences between the response curves, the simulation data is only displayed until the time of 250 seconds. The resulting curves after 250 seconds were not significantly different.

4.1.3 Experimental Setup and Data Collection

Experimental Setup

While the results of Section 4.1.2 showed that the linear Wiechert-model gives a fairly good estimation of the tissue behavior in the tissue relaxation phase induced by step-input, this method does not allow one to address the tissue behavior in the case of dynamic deformation, such as constant compression rate indentation. There exists no relevant measurement data for force response values in the case of soft tissue indentation at different

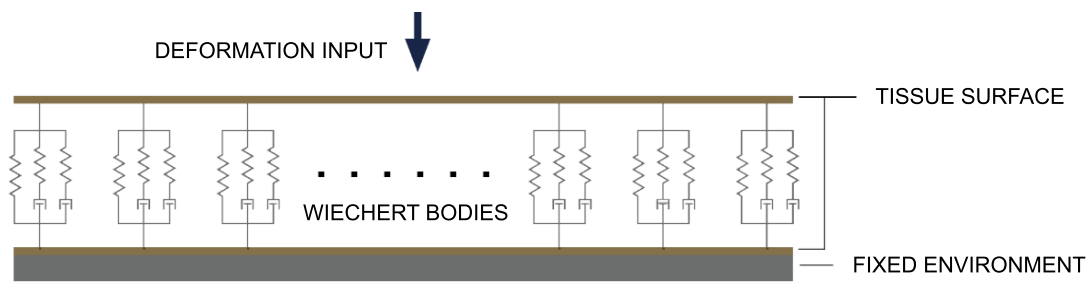


Fig. 4.3. The proposed linear tool–tissue interaction model, where the Wiechert elements are distributed along the tissue surface.

constant compression rate values. Therefore, a new set of experimental tissue compression tests were carried out and documented in order to have a better insight into the tissue behavior by various manipulations.

Let us consider a tool–tissue interaction model, where mass–spring–damper elements are distributed under the deformed tissue surface, represented by the Wiechert model (Fig. 4.3). Similar to Section 4.1.2, the model parameters can be obtained by applying a uniform deformation input on the surface during the following experiment. 6 pieces of cubic-shaped fresh beef liver samples were investigated, with the edge length of 20 ± 2 mm. The size of each specimen was measured before and after the experiments. Each of the specimens were compressed at three different compression rates: a slow rate of 20 mm/min, a medium rate of 100 mm/min and a near-step input at 750 mm/min (maximum compression rate provided by the system). The indentation tests were carried out at the Austrian Center for Medical Innovation and Technology (ACMIT), Wiener Neustadt, on a Thümler GmbH TH 2730 tensile testing machine connected to an Intel Core i5-4570 CPU with 4GB RAM, using the ZPM 251 (v4.5) software. The force response data was collected with an ATI Industrial Automation Nano 17 titanium six-axis Force/Torque transducer, using the 9105-IFPS-1 DAQ Interface and power supply at 62.5 Hz sampling time. An Intel Core i7-2700 CPU with 8 GB RAM hardware and the ATICombinedDAQFT .NET software interface was used for data visualization and storage. In the case of each specimen (marked by letters A–F), at first, the low and medium speed indentation tests were carried out, reaching 4 mm of indentation depth. The deformation input function was also recorded for validation purposes. A custom made 3D-printed indenter head with a flat surface larger than the specimen surface size was mounted on the force transducer, in order to achieve a uniform surface deformation at all points of the tissue on the plane perpendicular to the indentation axis. The movement of the head started 1 mm above the specimen surface, and in the evaluation, only the first 3.6 mm of indentation data was used in order to filter out any nonlinearity in the ramp-input function. In the first two cases, data was recorded only during the head movement, while each specimen was subjected to indentation 12 times. The force response curves showed no systematic deviation from the first responses, which allows one to assume that no substantial tissue damage was caused during the initial experiments. The final, near-step input was applied several times on each specimen, although it was found that the force response magnitude in the relaxation phase (1 minute) decreased significantly during the second and third experiments on the same tissue, supposedly from the severe damage to the internal structure. Therefore, in the case

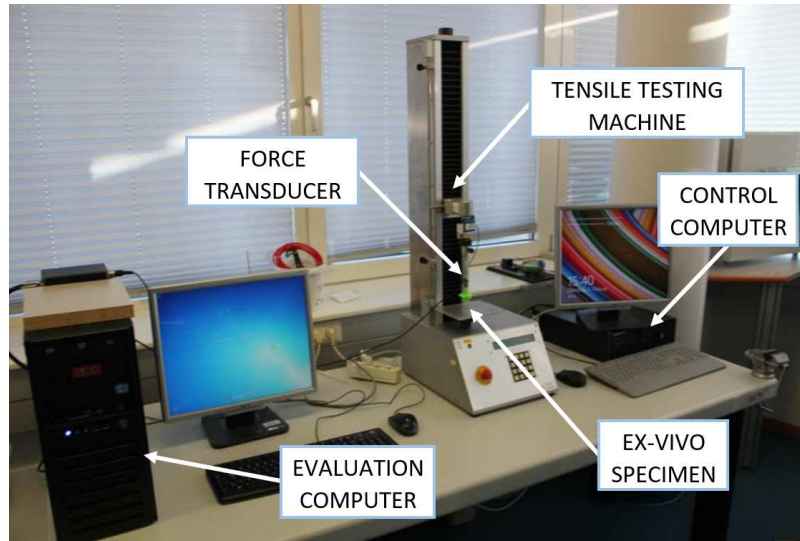


Fig. 4.4. Experimental setup for beef liver indentation tests at the Austrian Center for Medical Innovation and Technology.

of each specimen, only the very first set of measured data points was used for the parameter estimation from the force response relaxation data. A photography of the experimental setup is shown in Fig. 4.4, and the detailed flowchart of the steps of the experiment is shown in Fig. 4.5.

4.2 Data Collection and Analysis

Relaxation Tests

In order to have an initial estimation on the soft tissue parameters, the force response data from relaxation tests was evaluated. The indentation speed of 750 mm/min was approximated with a step-input. An analytical expression for the force response of the soft tissue can be easily calculated by obtaining the inverse Laplace transform of Eq. (1.11), using partial fraction decomposition, where the transfer function $W_W(s)$ is multiplied by the Laplace transform of the step-input function.

$$f_{W_r}(t) = \mathcal{L}^{-1} \left\{ W_W(s) \frac{x_d}{s} \right\} = x_d \left(k_0 + k_1 \left(1 - e^{-\frac{k_1}{b_1}t} \right) + k_2 \left(1 - e^{-\frac{k_2}{b_2}t} \right) \right), \quad (4.8)$$

where $f_{W_r}(t)$ is the force magnitude during the relaxation tests and $x_d = 4$ mm is the depth of the compression at the maximum deformation. The relaxation data for all six specimens is displayed in Fig. 4.6. For better visual representation, the average response curves are also shown in Fig. 4.6, which was obtained by taking the average values of the response data from each specimen, weighted with respect to its surface size and normalized to 20×20 mm. It is important to note that an unexpected break in the curves was observed in all cases, which is most likely the effect of the deceleration of the indenter, as it reaches the prescribed depth. This break does not effect the force response results significantly, because the most relevant sections of the response curves are the initial relaxation slopes (force relaxation) and the steady-state values (residual stress). As the closed-form

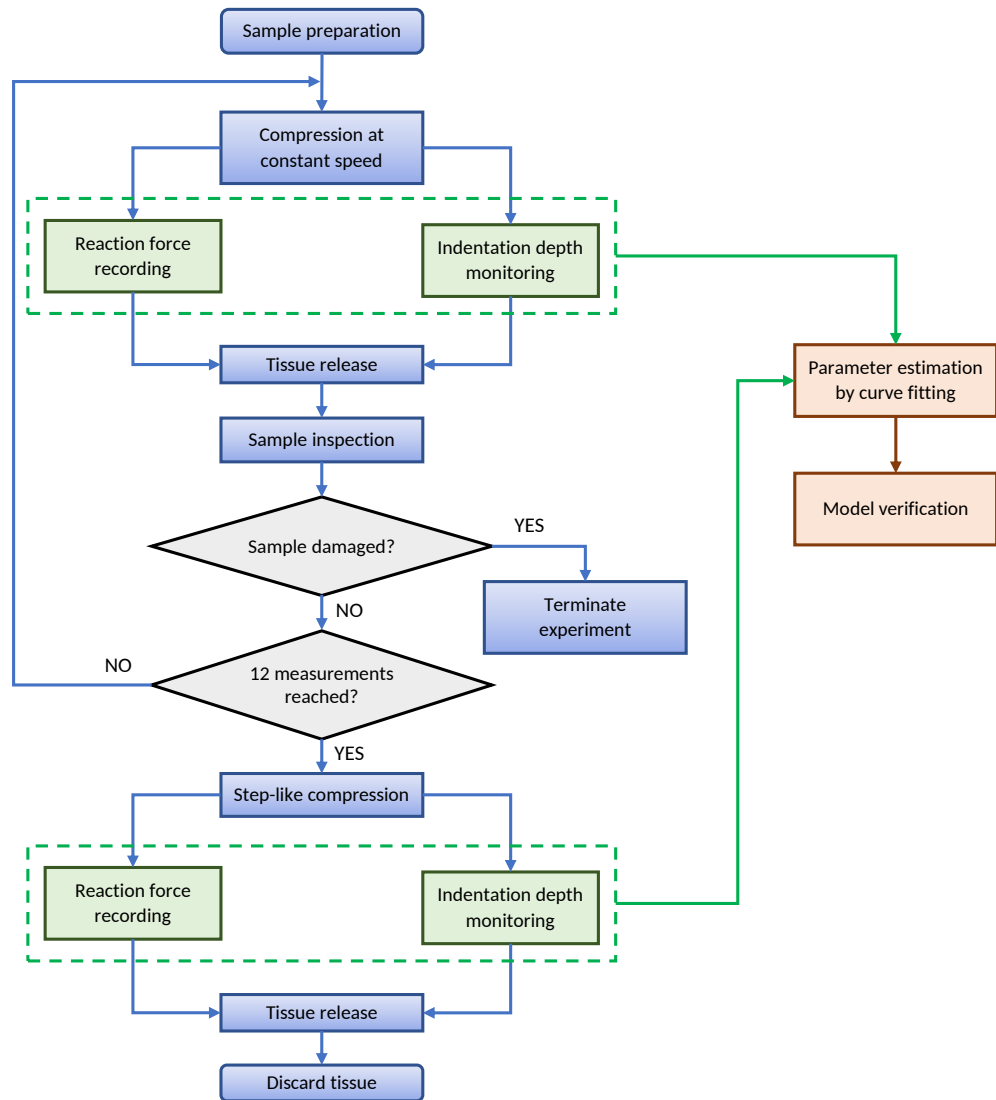


Fig. 4.5. Flowchart of the steps of soft tissue palpation during data collection experiments.

solution to the step-input was given, curve fitting on the original measurement data was applied. For this procedure, the MATLAB *cftool* toolbox was used. The parameters were independently obtained for each of the six specimens and were compensated by the tissue surface magnitude, resulting in six sets of parameters of stiffness and damping values:

$$k_i^c = k_i \frac{A_0}{A}, i = 1, 2, 3, \quad (4.9)$$

$$b_j^c = b_j \frac{A_0}{A}, j = 1, 2, \quad (4.10)$$

where A is the surface area of each specimen and $A_0 = 400 \text{ mm}^2$ is the reference surface size. The results of the soft tissue parameter estimation from force relaxation tests

TABLE 4.3

INITIAL PARAMETER ESTIMATION FROM RELAXATION TESTS, USING THE LINEAR WIECHERT-MODEL, REPRESENTED BY EQ. (1.11).

Specimen	k_0^c [N/m]	k_1^c [N/m]	k_2^c [N/m]	b_1^c [Ns/m]	b_2^c [Ns/m]	Surface size
A	119.6	110.1	78.9	36.2	1210	20×20 mm ²
B	80.2	90.6	74.8	30.2	860	20×20 mm ²
C	57.9	167.8	101.4	90.1	1154	19×19 mm ²
D	82.8	138.9	109.5	58.5	1249	21×21 mm ²
E	67.9	95.8	53.9	118.1	1312	19×19 mm ²
F	81.1	256.2	132.9	105.8	1661	22×22 mm ²
Average	81.6	143.2	91.9	73.2	1241	407.83 mm ²

are shown in Table 4.3. It can be observed that the individual parameter values are in the same order of magnitude for all specimens, in some cases a moderate deviation can be found from the average value. This can be considered as a result of the non-identical deformation input from the tensile machine, the imperfect cubical shape of the specimens, and the varying internal fiber structure of the liver. This deviation from the average can be observed in the verification phase and at additional experiments on *ex vivo* tissues, presented in chapter 6, and are less significant in the case of artificial tissue samples. The effect on the validity range of the model in tissue characterization is also discussed in chapter 6, utilizing further experimental results and relying on the quantitative representation of different tissue samples, while the effect of incorrect parameter estimation on the force control performance is addressed in chapter 5.

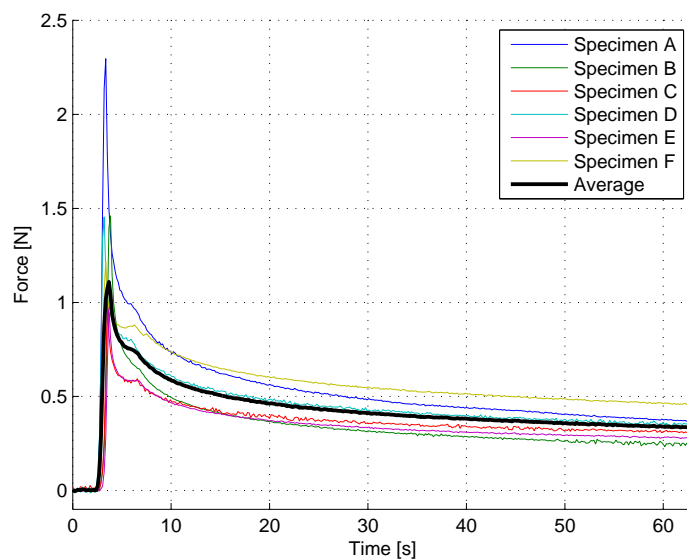


Fig. 4.6. Force response curves for step-input relaxation tests.

Constant Compression Rate Indentation Tests

As it was shown previously (Sections 4.1.2 and 4.2), the Wiechert model gives a very good approximation of the soft tissue behavior in the force relaxation phase, verified on the experimental data. Theoretically, using this model, force response curves in the case of other known displacement functions can be estimated. To validate the results, two more sets of indentation tests with constant compression rates were carried out on each of the specimens. The average force response curves for each specimen for the cases of 20 mm/min and 100 mm/min are displayed in Fig. 4.7 and Fig. 4.8, respectively, along with the global weighted average response curve. Note that for better visualization, the curves are displayed in an indentation depth–force graph instead of the previously used time–force diagram. The indentation depth was 4 mm. The figures only show the first 3.6 mm of deformation for previously discussed reasons. Utilizing the same method for obtaining the analytical force response as it was used in the step-input case, the following analytical expression was obtained for the force response:

$$f_{W_c}(t) = \mathcal{L}^{-1} \left\{ W_W(s) \frac{v}{s^2} \right\} = v \left(k_0 t + b_1 \left(1 - e^{-\frac{k_1}{b_1} t} \right) + b_2 \left(1 - e^{-\frac{k_2}{b_2} t} \right) \right), \quad (4.11)$$

where v denotes the compression rate (20 mm/min or 100 mm/min) and f_{W_c} stands for the force response magnitude. Ideally, by substituting the model parameters into Eq. (4.11), the force response data should predict the measurement data. Considering that the 750 mm/min indentation was approximated as a step-input, a minor compensation of the previously obtained parameters would still be needed. However, the constant compression rate indentation results showed that the shape of the analytical response curve largely differs from that of the measured response, clearly questioning the validity of the linear Wiechert model in this indentation phase. From the haptics application point of view, tissue behavior under constant compression rate is significantly more relevant than under relaxation. The average measurement data and the predicted response curves at the com-

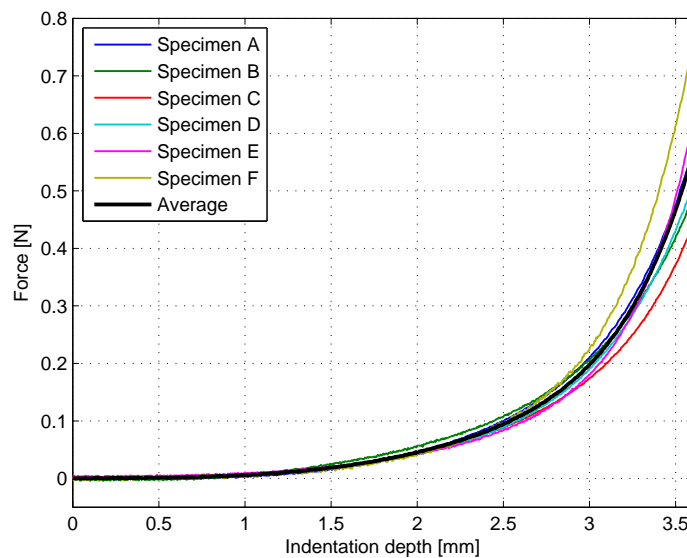


Fig. 4.7. Force response curves for constant compression rate indentation tests at 20 mm/min.

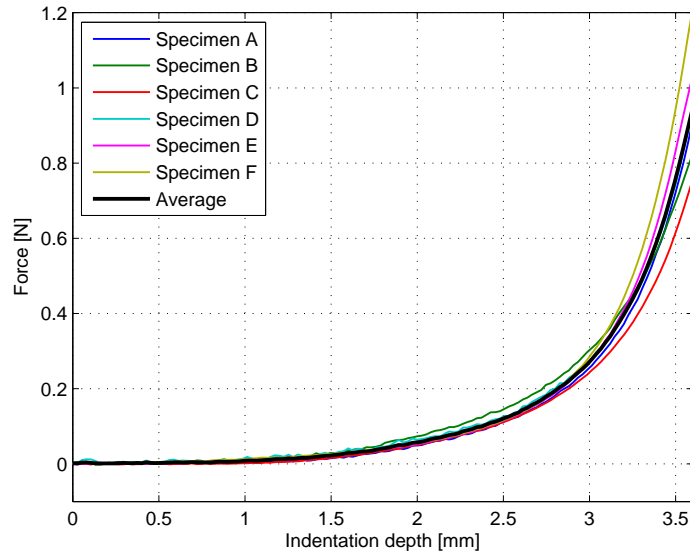


Fig. 4.8. Force response curves for constant compression rate indentation tests at 100 mm/min.

pression rate of 100 mm/min are shown in Fig. 4.9. The best fitting curve, assuming positive mechanical parameter values is also displayed in Fig. 4.9. The measurement data and its major deviation from the estimated response implies that the reaction force magnitude under constant compression rates represent progressive stiffness characteristics instead of a linear one. This phenomenon may be caused by the complex mechanical structure of the

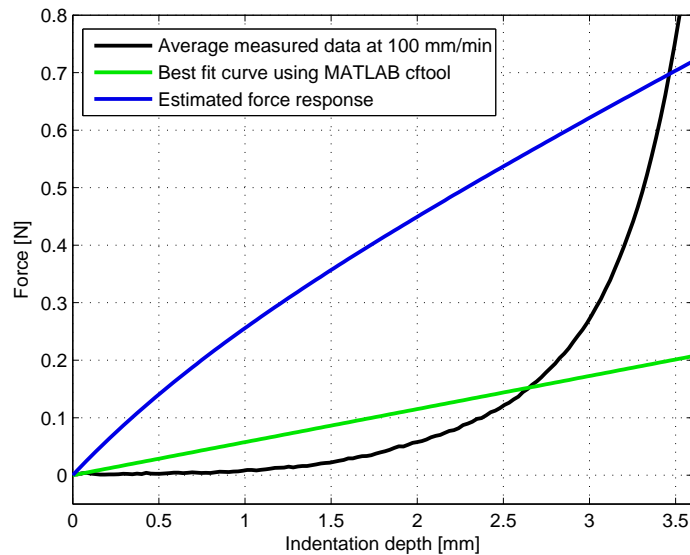


Fig. 4.9. Verification of the results of the linear Wiechert model at the compression rate of 100 mm/min. The blue curve shows the predicted force response from the parameter data acquired from relaxation tests, while the measured force response is represented by the black curve. The green curve corresponds to the best fit using reasonable mechanical parameters, clearly indicating that the model is not capable of predicting the reaction force in the case of constant compression rates.

liver tissue, which cannot be observed during step-response relaxation tests. According to the Wiechert model, one would expect a superposition of reaction forces of a linearly elastic element (k_0) and two Maxwell elements that introduce damping (stress relaxation) into the system, which is well-represented by the analytical solution. However, the shape of the measured response curves does not show any nature of relaxation at a first glance, indicating that tissue behavior might be more complex, as discussed in the next section.

4.3 Introduction of Novel Nonlinear Soft Tissue Models

4.3.1 The Two-phase and Nonlinear Wiechert model

In general, the damping parameters of a dynamic system are rather difficult to estimate. In most cases, the behavior of a viscous damper element is approximated using trivial methods, such as modal damping [86]. Therefore, it is more convenient to introduce nonlinearity to a given model through the stiffness elements. In the proposed two-phase Wiechert model, the mechanical behavior is anticipated as follows. Although liver is a largely homogeneous and isotropic soft tissue, significant level of porosity can be found in its structure. This two-phase structure delays the viscoelastic behavior during the compression phase until a certain indentation depth δ is reached. The single spring element k_0 becomes nonlinear (with exponential characteristics), while the remaining two elements, serially connected to the damping elements, will behave as delayed stiffness in the system:

$$k_0(x) = K_0 e^{\kappa_0 x}, \quad (4.12)$$

$$k_j(x) = \begin{cases} 0, & \text{if } x < \delta \\ K_j, & \text{if } x \geq \delta \end{cases}, \quad (4.13)$$

for all $x > 0$ and $j = 1, 2$. If $\kappa_0 = 0$, $k_0(x)$ is a linear stiffness, while also setting $\delta = 0$ would yield the previously introduced linear Wiechert model.

While the previous variation introduces two new parameters κ_0 and δ to the linear system, in this third approach, the complexity of the model is increased by adding yet another parameter, upon the assumption that there should be no discontinuities in the mathematical description of the model, and the progressive stiffness characteristics should be coupled with the phenomenon of relaxation as well. In this nonlinear case, all of the three spring elements have the same behavior, with the following stiffness values defined:

$$k_j(x) = K_j e^{\kappa_j x} \quad (4.14)$$

for $j = 1, 2, 3$. This representation yields a total of 8 unknown parameters for the curve fitting, creating a model that could be used both in compression and relaxation phases for reaction force estimation.

4.3.2 Verification of the Nonlinear Wiechert Model

Table 4.4 shows the values of the individual mechanical parameters and combined RMSE values obtained by the best-fit curves in all three cases discussed above. As the curve fitting

TABLE 4.4

PARAMETER ESTIMATION RESULTS FROM FORCE RELAXATION AND CONSTANT COMPRESSION RATE TESTS, REPRESENTED BY EQS. (1.11), (4.12), (4.13) AND (4.14).

Model type	K_0 [N/m]	K_1 [N/m]	K_2 [N/m]	b_1 [Ns/m]	b_2 [Ns/m]	κ_0 [m ⁻¹]	κ_1 [m ⁻¹]	κ_2 [m ⁻¹]	δ [mm]	RMSE <i>comb.</i>
Linear	4.86	57.81	53.32	9987	10464	-	-	-	-	1.1941
Two-phase	8.25	90.88	3.49	800.9	0.093	601.1	-	-	1.8	0.2804
Nonlinear	2.03	0.438	0.102	5073	39.24	909.9	1522	81.18	-	0.1319

procedure was running simultaneously on both datasets, the RMSE value was computed as the sum of the individual errors for both curves. The calculated force response curves using the listed parameters are shown in Fig. 4.10 and Fig. 4.11. Clearly, the purely linear

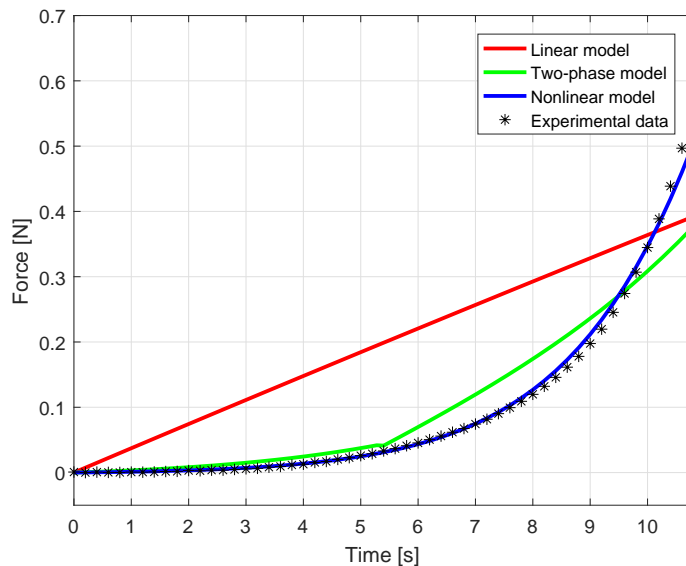


Fig. 4.10. Calculated force response curves using the parameter sets from Table 4.4, in the case of tissue indentation at constant compression rate of 20 mm/s.

model (red curve) is not capable of modeling soft tissue behavior in both the cases of stress relaxation and constant compression rate force response. The mechanical explanation of this phenomenon is that a system with linear spring and damper elements attached to each other as in the Wiechert model, cannot represent a progressive rise in the reaction force under constant compression rates. Because of the presence of the damping elements, the slope of the force response curve must decrease by the laws of physics. Therefore, the linear Wiechert model will never fit the presented experimental data either qualitatively or quantitatively. The two-phase model (green curve) introduces the progressive stiffness characteristics using a single spring element, while the effect of damping is delayed by δ . As shown in Fig. 4.10 and Fig. 4.11, the curve fitting is more effective than in the linear case. However, the sudden change in the stiffness characteristics upon reaching δ impairs the smoothness of the response function. This issue can be eliminated by using the non-linear Wiechert model (blue curve) with three spring elements with progressive stiffness

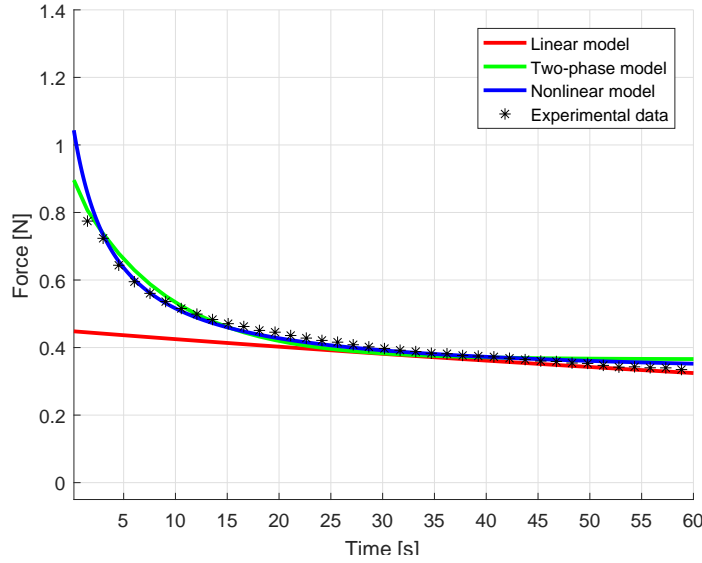


Fig. 4.11. Calculated force response curves using the parameter sets from Table 4.4, in the case of tissue indentation with a step-input, recording the stress relaxation data.

characteristics. The figures show that the fitted curves are representing the model behavior very well, with a largest relative error of 12%. Table 4.4 shows that the level of nonlinearity of the spring elements is higher than in the previous two models, as K_0 , K_1 and K_2 values are in average one order of magnitude lower than in the linear or in the two-phase case. This indicates that the general behavior of the system is mainly determined by the nonlinear characteristics of the spring elements.

Due to the nonlinear form of the model, no analytical expression for the force response can be obtained. Instead of using the MATLAB *cftool*, the *fminsearch* function was applied to find the optimal set of parameters [TA-8]. The values of the individual mechanical parameters and combined root mean square error values are shown in Table 4.4. The curve fitting was carried out simultaneously on both datasets of 20 mm/min and 750 mm/min responses, and the combined error values were obtained as the sum of the individual errors for each curve, serving as the cost function for *fminsearch*. The estimated force responses, utilizing the parameters from Table 4.4, are shown in Fig. 4.10 and Fig. 4.11.

In order to verify the parameters independently, a simulation was run on the nonlinear model with the obtained parameters, with the constant compression indentation rate of 100 mm/s. The nonlinear system can be represented by the following system of differential equations:

$$\begin{aligned}
 \dot{x}_0 &= v(t), \\
 \dot{x}_1 &= \frac{1}{b_1} K_1 (x_0 - x_1) e^{\kappa_1 (x_0 - x_1)}, \\
 \dot{x}_2 &= \frac{1}{b_2} K_2 (x_0 - x_2) e^{\kappa_2 (x_0 - x_2)},
 \end{aligned} \tag{4.15}$$

where $v(t)$ is the surface deformation rate, x_0 denotes the position of an arbitrary point at the surface, while x_1 and x_2 represent two virtual points, connecting k_1 - b_1 and

k_2 - b_2 elements, respectively. The system output is the reaction force, $F(t)$, calculated by

$$F(t) = K_0 x_0 e^{\kappa_0 x_0} + K_1 (x_0 - x_1) e^{\kappa_1 (x_0 - x_1)} + K_2 (x_0 - x_2) e^{\kappa_2 (x_0 - x_2)}. \quad (4.16)$$

The simulation results were mapped on the experimental data, shown in Fig. 4.12. The average RMSE, calculated separately with respect to each specimen, yielded $\epsilon_{RMSE} = 0.1748$ N, with an average relative error of 30%, which indicates that the model represents the investigated manipulation tasks very well. It was expected that the simulated curve gave lower force values than those of the measured, as the parameters were obtained partly by fitting the curve on the step-response. In the simulation, ideal step-input was assumed, while, during the experiments, the maximum indentation speed was 750 mm/min. This lower-than-desired indentation speed yielded lower stiffness values due to the rapid relaxation during the compression phase. The effect can be observed in both Fig. 4.10 and Fig. 4.12.

The exact deformation input function of the tensile machine is not known, therefore an approximation was employed for the non-ideal step-input function to verify the above mentioned phenomenon. The simulated non-ideal deformation was chosen as 375 mm/min constant ramp input, considering the nominal 750 mm/min deformation rate and the deceleration of the indenter head at the maximum indentation depth. The results of curve fitting for the nonlinear Wiechert model, accounting for non-ideal step input, and the corresponding parameter values are displayed in Fig. 4.13, Fig. 4.14 and Table 4.5, respectively.

Significant difference between the compensated and uncompensated parameter values can only be observed in the κ values, which corresponds to the nonlinearity of the spring elements. The RMSE value for the new curves is nearly one order of magnitude lower, while the largest relative error is 25%, similarly to the case of ideal step-input simulation.

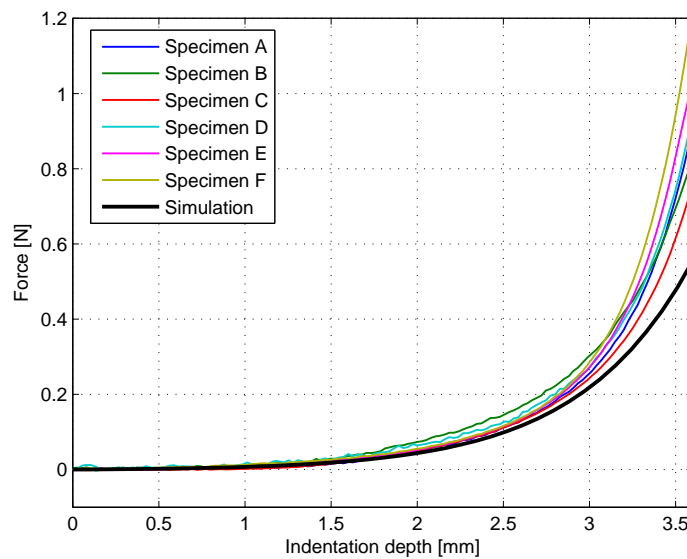


Fig. 4.12. Force response curves for constant compression rate indentation tests at 100 mm/min, showing the simulated response of the nonlinear model, using the parameters listed in Table 4.4.

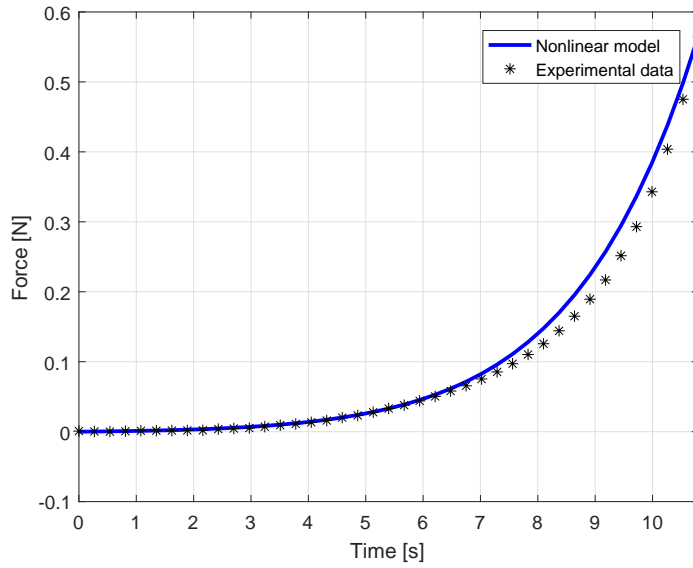


Fig. 4.13. Compensated force response curves, accounting for non-ideal step-input, using the parameter sets from Table 4.5, in the case of tissue indentation at constant compression rate of 20 mm/s.

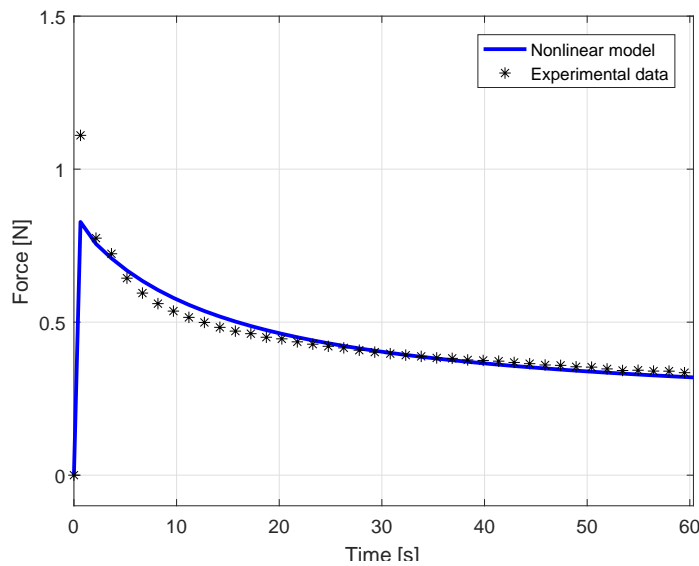


Fig. 4.14. Compensated force response curves, accounting for non-ideal step-input, using the parameter sets from Table 4.5, in the case of tissue indentation with a step-input, recording the stress relaxation data.

TABLE 4.5

PARAMETER ESTIMATION RESULTS FROM FORCE RELAXATION AND CONSTANT COMPRESSION RATE TESTS, ACCOUNTING FOR THE NON-IDEAL STEP-INPUT, REPRESENTED BY EQ (4.14).

Model type	K_0 [N/m]	K_1 [N/m]	K_2 [N/m]	b_1 [Ns/m]	b_2 [Ns/m]	κ_0 [m ⁻¹]	κ_1 [m ⁻¹]	κ_2 [m ⁻¹]	RMSE <i>comb.</i>
Nonlinear	0.483	1.501	0.102	13448	12.91	1231	1.231	31.79	0.0295

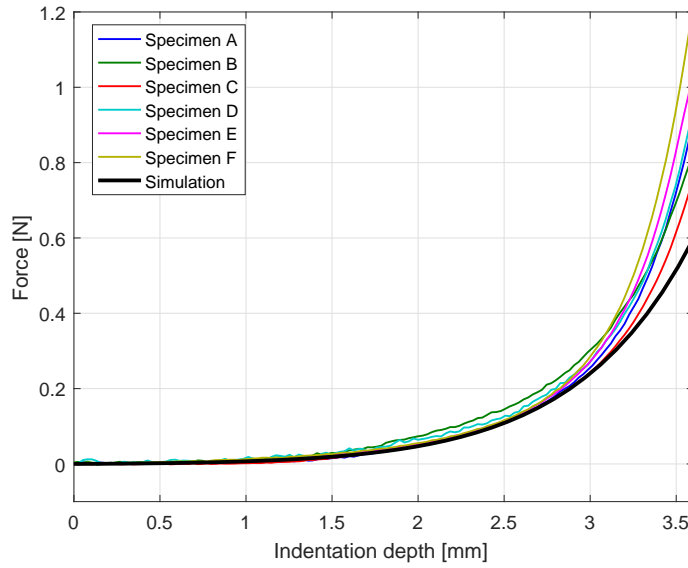


Fig. 4.15. Force response curves for constant compression rate indentation tests at 100 mm/min, showing the simulated response of the nonlinear model, using the compensated parameters listed in Table 4.5.

Mapping the simulation results to the experiment at 100 mm/min constant deformation rate, the average RMSE yielded $\epsilon_{RMSE} = 0.1898$ N, with the average relative error of 25%, 5% lower than in the uncompensated case. This indicates that the non-ideal step-input needs to be accounted for, as tissue relaxation takes place in a very short time, even during rapid compression phase. The validation curves for the 100 mm/min indentation tests with the compensated parameters is shown in Fig. 4.15.

4.3.3 Model Verification with Non-Uniform Surface Deformation

In order to verify the approach proposed in Fig. 5.5, extended to the case of non-uniform surface deformation, additional palpation tests were carried out. Three specimens with the dimensions of $25 \times 25 \times 200$ mm from the same beef liver were palpated with a sharp instrument, though not physically damaging the surface. Constant rate indentations were carried out at four different indentation rates (5 mm/s, 10 mm/s, 20 mm/s and 40 mm/s) at different points of the surface of each specimens, reaching 6 mm of indentation depth. The indenter used for the experiments was a 3D-printed piece that was mounted on the flat instrument used in the experiments at uniform deformation. At the tip, the indenter had the sharpness of 30° , its length was 30 mm. It was assumed that the indenter created a line-like deformation input on the surface of the specimens, perpendicular to their longest dimension. The schematic figure of the non-uniform indentation is shown in Fig. 4.16, a photo of the experiment is presented in Fig. 4.17 In order to estimate the reaction force, a few assumptions have been made prior to the verification:

- only uniaxial deformation is considered, therefore all non-vertical forces are neglected in the calculations,
- it is assumed that the indentation only affects the liver structure in a certain ρ distance from the indentation point,

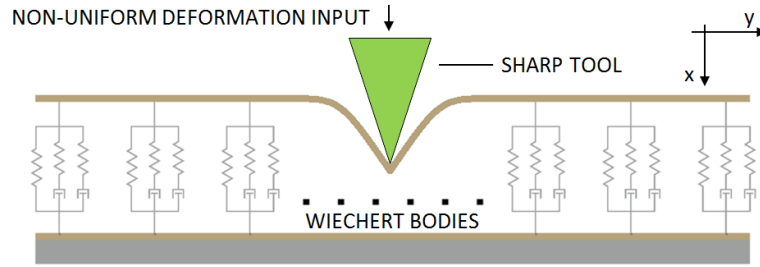


Fig. 4.16. The schematic figure of the non-uniform indentation tests.

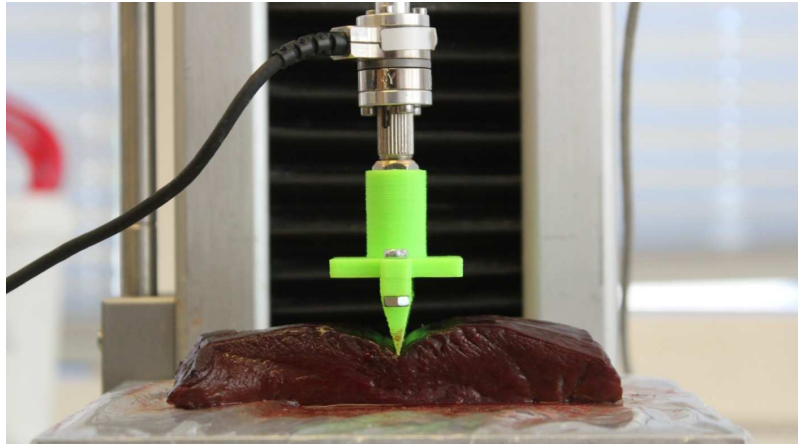


Fig. 4.17. Experimental setup for non-uniform surface deformation indentation tests.

- the surface deformation shape is approximated as a quadratic function and is uniform along the width of the specimen.

The reaction force is assumed to be the sum of the reactions of infinitely small elements on the tissue surface:

$$F(t) = \iint_{y,z} f(y, z, t) dy dz, \quad (4.17)$$

where $f(y, z, t)$ is the force response of a single infinitely small element at the surface point (y, z) at a given time t . $f(y, z, t)$ can be calculated by solving Eq. (4.16) for each surface element, using the unique deformation rate $v_{x,y}(t)$ of the element, and utilizing *specific* stiffness and damping values shown in Table 4.6. These specific values were obtained by normalizing the appropriate parameters to the surface size of 1 m^2 . In the next step, the tissue surface was discretized using square-shaped elements $A_i = A_{y_i, z_i}$ with the edge length of 0.1 mm . The corresponding deformation rate profiles, $v_i(t)$, were obtained as follows. The indentation tests were recorded by a video camera, fixed along the z -axis. Movements of 7 surface points were tracked by analyzing 12 video files frame-by-frame, at the time intervals of 1 sec. The resolution of the picture was 1980×1080 pixels, the recordings were taken at 25 frames per second. An average deformation profile was calculated by processing the data manually. It was found, that a reasonably good approximation to the final deformation surface (after reaching the $x_d = 6 \text{ mm}$ indentation

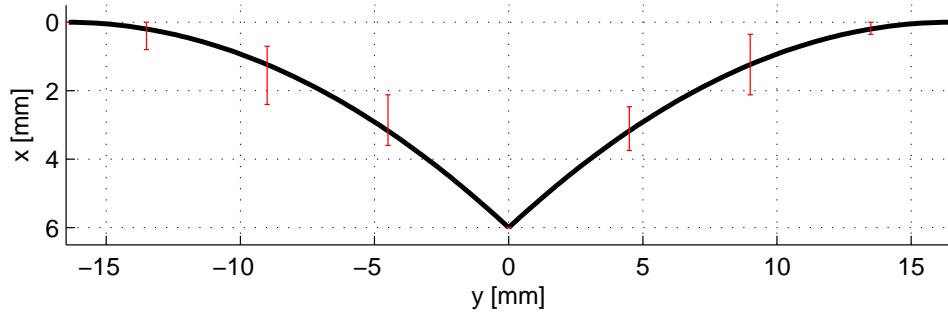


Fig. 4.18. The final deformation surface at 6 mm indentation depth. The red bars indicate the deviation of the measured position data of the examined surface points. $\rho = 16$ mm.

depth) was:

$$x(y) = \frac{x_d}{\rho^2}(|y| - \rho)^2, \quad (4.18)$$

which assumes that the deformation surface is symmetrical to the axis of indentation. Furthermore, it is assumed that

$$\left. \frac{dx}{dy} \right|_{y=\rho} = 0, \quad (4.19)$$

neglecting the doming effects during the indentation (surface deformation in the negative axis direction). These effects are more relevant at the regions far from the indentation point, and due to the progressive spring characteristics in the model, these regions contribute very little to the overall force response. The final surface deformation shape is shown in Fig. 4.18, along with the error bars, which show the deviation of the investigated surface points from the proposed surface function.

Utilizing the assumptions above, the deformation rate profile $v_i(t)$ can be obtained at each surface point A_i , provided by the following equation:

$$v(y, t) = \frac{v_{in}}{\rho^2}(|y| - \rho)^2, \quad (4.20)$$

indicating that in the case of constant indentation rate, each surface point is moving at a constant speed. Eq. (4.17) was solved for each element and the force response was obtained and summed according to Eq. (4.18). Simulation results and the estimated force response for the 3rd specimen at 10 mm/min indentation rate are shown in Fig. 4.19. As it is shown in Fig. 4.19, the measured force response curves initially follow the estimated curve reasonably well, both qualitatively and quantitatively. It can be observed that at the

TABLE 4.6

SPECIFIC PARAMETER VALUES FOR THE USE OF NON-UNIFORM SURFACE DEFORMATION MODEL VERIFICATION, REPRESENTED BY EQ. (4.15).

K_0^s [N/m ³]	K_1^s [N/m ³]	K_2^s [N/m ³]	b_1^s [Ns/m ³]
5075	1095	255	$127 \cdot 10^6$
b_2^s [Ns/m ³]	κ_0 [m ⁻¹]	κ_1 [m ⁻¹]	κ_2 [m ⁻¹]
$1.1 \cdot 10^6$	909.9	1522	81.189

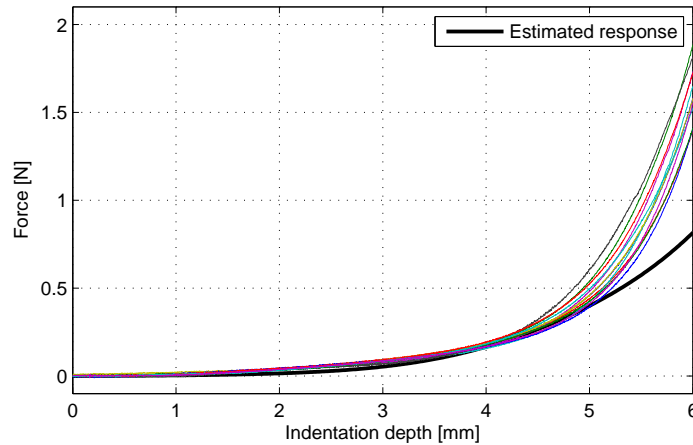


Fig. 4.19. Measurement results and estimated force response for the case of 10 mm/min indentation for non-uniform surface deformation.

TABLE 4.7

VERIFICATION CASES FOR NON-UNIFORM SURFACE DEFORMATION AND THE OBTAINED ROOT MEAN SQUARE ERROR (RMSE) VALUES.

Sp. No.	Indentation speed	RMSE
1	5 mm/min	1.384
2	5 mm/min	2.015
3	10 mm/min	1.4682
3	20 mm/min	1.9002
3	40 mm/min	2.8214

indentation depth of 4 mm, the slope of the measured curves increases rapidly, which is assumed to be due to the tension forces normal to the indentation axis. This is an expected behavior, indicating that at higher deformation levels, the 1 DoF approach of the problem should be handled with caution. The validity range of the proposed method is determined in 20% relative deformation, measured on *ex vivo* liver samples with the thickness of 2 cm. The RMSE values for each verification case are shown in Table 4.7, the largest relative error is 35% below 20% of relative deformation. The proposed soft tissue model can also be extended to more complex surface deformation functions. If that is the case, given that the boundary conditions are well-defined, one would find finite element modeling methods a useful tool for determining the surface deformation shape function [87].

4.4 Summary of the Thesis

Mass–spring–damper models play a significant role in soft tissue modeling, as the simplicity of the approach reduces computational requirements compared to finite element-based methods, offering a tool for real-time tissue behavior simulation and reaction force estimation. This chapter presented a method for reaction force estimation in the case when the surface deformation shape is known. A novel nonlinear model was created and veri-

fied on liver tissue samples. It was shown that in the case of uniform surface deformation, the estimated force response gave a very good match on the measurement data. It was also shown that in the case of non-uniform surface deformation, the idea of distributed mass–spring–damper models led to a reasonably good estimation of reaction forces.

The primary limitation of this approach appears when the describing function of the surface deformation shape takes steep slopes and sudden changes, amplifying the effect of lateral tension forces. These effects can be compensated by taking the elongation of the tissue surface into account, which is part of my future work.

Despite its limitations, the model could be a useful tool for modeling and reaction force estimation when carrying out surgical manipulations with blunt instruments, providing model data for model-based haptic feedback control methods and virtual surgical simulators. Based on the results discussed in this chapter, my further future work includes the extension of the model to more complex surface deformations, real-time prediction of the reaction force based on on-line deformation shape measurement and the integration of the model into virtual simulators for modeling specific surgical interventions.

Chapter 5

POLYTOPIC MODEL-BASED INTERACTION CONTROL

Surgical robots, as Cyber-Physical Systems (CPS), are one of the finest examples of advanced Human–Machine Interfaces (HMI). Many types of surgical manipulations have a certain degree of autonomy, however, the human operator (surgeon) is still present as an integral part of the control loop. Thus, cognitive skills are exploited during the interventions, although the teleoperation systems dominantly use visual feedback over force/haptic feedback [TA-16]. Haptic feedback-based force control is actively studied in master–slave teleoperation structures, since the sensory capabilities of the human operators can be increased with a successful and reliable implementation. Long distance telesurgery also carries the difficulties originating from time-delay, which can induce instability in force-controlled systems, especially in the case of contact with hard surfaces [TA-7]. To overcome these issues, several approaches have been studied in recent years.

One of the most successful approaches is the model-based control method. Providing a reliable mechanical model of the human body (especially for soft tissue, such as organs or skin) can enhance the available force controllers [TA-14].

This chapter extends the usability of the proposed nonlinear Wiechert model for force control applications. The approach fits to the concept of the quasi Linear Parameter Varying modeling, the polytopic model representations and the Linear Matrix Inequality based control design methods. The main goal of this work is to integrate the nonlinear mathematical model of the process of tool–tissue interaction into the modern modeling approach of qLPV/LMI-based control theory. The systematic derivation of the model and the illustrative numerical example will guide the reader through the transformation of the nonlinear system equations into a polytopic TP representation.

It is important to note that the presented soft tissue model was created based on physical considerations, as it was presented before [TA-8]. TP Model Transformation can be considered as a gateway between the traditional model representations and the polytopic modeling. It can be proven that mathematically correct stability analysis can be achieved when LMI-based control design is taken into consideration. In the particular case of this study, the derived model can be utilized on the slave side of the teleoperation system, integrated in a cascade controller assembly [88]. This cascade structure supports the realization of force control in extreme scenarios, such as inter-continental or inter-planetary teleoperation [1].

5.1 Models of Soft Tissues in Force Control

The challenge of reaction force estimation and force control in surgical robotics can be approached from various directions. No general ideal solution exists due to the complexity of the instruments, wide range of required control methods and limitations in the final applications (such as sterilization or restrictions on sensor placement and mounting). One of the first architectures of such control was developed for ROBODOC, the first robotic system to perform complete hip replacement [89]. The control algorithm provided an intuitive HMI allowing the surgeon to guide the robot in a collaborative manner, while force feedback was used to modify the feed rate for cutting, achieving a force controlled velocity input. Lee *et al.* presented a sensorless method for estimating reaction forces acting on a typical surgical robotic instrument, using a state observer. In their approach, they used a sliding mode control with sliding perturbation observer (SMCSPO) for the instrument manipulation [90]. Yuen *et al.* showed that a force control method using feed-forward motion terms can largely improve the force tracking performance in the case of contact with soft tissues, which is a crucial problem for manipulating loosely attached or moving organs e.g., during beating heart surgery [91]. Another relevant work in the topic of force tracking in beating heart surgery was published by Liu *et al.*, utilizing the Kelvin–Boltzmann viscoelastic model [31]. Moreira *et al.* introduced a method for soft tissue force control using active observers and a viscoelastic interaction model, confirming that using a realistic tissue model can increase the performance of the force control [92]. Force control has also been an emerging field of interest in robotic catheter cardiac ablation [93] and in minimally invasive surgery [94]

In the following sections, the proposed nonlinear Wiechert soft tissue model is transformed to a polytopic qLPV model, representing the tissue dynamics that is—regarding its mathematical formalism—suitable for direct use of LMI-based control design methods. As a next step, a model-based force control scheme is presented, utilizing this off-the-shelf tool–tissue interaction model. The discussed structure involves a model-based controller, where the required states for the state-feedback controller are acquired using a reference dynamic model of the system, derived using the nonlinear model. The discussed approach utilizes the Tensor Product Model Transformation [95] as a systematic methodology capable of transforming analytical nonlinear qLPV state-space representations into polytopic form, which can be directly used in LMI-based multi-objective controller synthesis.

5.2 Polytopic TP Model of the Nonlinear Wiechert Model

5.2.1 Model Construction

In order to create an appropriate qLPV model that can be used for LMI-based controller design, first of all, a goal for the control effort has to be defined. Let us consider the case, where the position of the instrument tip is controlled by tracking the desired value $x_d(t)$, which in mathematical sense could be written as $x_0(t) = x_d(t)$, where $x_0(t)$ denotes the value of tissue surface deformation.

The corresponding control design methods address the regulation of the qLPV model's state to 0 by state feedback or output feedback. That is, the qLPV model should be formu-

lated to represent the error dynamics. This way, the state vector of the qLPV model must be chosen as error according to the actual desired states, and the output must also represent the error. For these reasons, the following state variables, $\Delta x_0(t) = x_0(t) - x_d(t)$, $\Delta x_1(t) = x_0(t) - x_1(t)$ and $\Delta x_2(t) = x_0(t) - x_2(t)$ are used in the qLPV model, and its output similarly, as $\Delta y(t) = y(t) - y_d(t)$, where $y_d(t)$ stands for the desired force output

$$y_d(t) = K_0 x_d(t) e^{\kappa_0 x_d(t)}. \quad (5.1)$$

Then, the following qLPV model can be constructed:

$$\begin{bmatrix} \Delta \dot{\mathbf{x}}(t) \\ \Delta y(t) \end{bmatrix} = \begin{bmatrix} \mathbf{A}(\mathbf{p}(t)) & \mathbf{B}_u & \mathbf{B}_w \\ \mathbf{C}(\mathbf{p}(t)) & 0 & 0 \end{bmatrix} \begin{bmatrix} \Delta \mathbf{x}(t) \\ u(t) \\ w(t) \end{bmatrix}, \quad (5.2)$$

where

$$\begin{aligned} \mathbf{p}(t) &= \begin{bmatrix} e^{\kappa_1 \Delta x_1(t)} & e^{\kappa_2 \Delta x_2(t)} & \frac{x_0(t)e^{\kappa_0 x_0(t)} - x_d(t)e^{\kappa_0 x_d(t)}}{x_0(t) - x_d(t)} \end{bmatrix}, \\ \mathbf{A}(\mathbf{p}) &= \begin{bmatrix} 0 & 0 & 0 \\ 0 & -\frac{K_1}{b_1} p_1 & 0 \\ 0 & 0 & -\frac{K_2}{b_2} p_2 \end{bmatrix}, \mathbf{B}_u = \begin{bmatrix} 1 \\ 1 \\ 1 \end{bmatrix}, \mathbf{B}_w = \begin{bmatrix} 1 \\ 0 \\ 0 \end{bmatrix}, \\ \mathbf{C}(\mathbf{p}) &= [K_0 p_3 \quad K_1 p_1 \quad K_2 p_2], \quad w(t) = \dot{x}_d(t). \end{aligned}$$

The fact that the desired state appears in the system matrix shows well the nonlinear property of the system: its settling behavior changes with the $x_d(t)$ desired state. Because the $\Delta x_0(t)$ error variable changes with the desired state, the $\dot{x}_d(t)$ signal appears in the qLPV model and it is considered as disturbance.

Using the qLPV model Eq. (5.2), the MVS polytopic TP model can be obtained for the parameter dependent system matrix:

$$\mathbf{S}(\mathbf{p}) = \begin{bmatrix} \mathbf{A}(\mathbf{p}) & \mathbf{B}_u & \mathbf{B}_w \\ \mathbf{C}(\mathbf{p}) & 0 & 0 \end{bmatrix}, \quad (5.3)$$

considering the nonlinear parameter values from Table 4.4 and qLPV parameter and domain values from Table 5.1, which were obtained by substituting the boundary values of the variables Δx_0 , Δx_1 and Δx_2 into \mathbf{p} .

The transformation yields to an exact polytopic TP model form, where

$$\begin{aligned} \mathbf{S}(\mathbf{p}) &= \mathcal{S} \boxtimes_{n=1}^3 \mathbf{w}^{(n)}(p_n(t)) = \\ &= \mathcal{S} \times_1 \mathbf{w}^{(1)}(p_1(t)) \times_2 \mathbf{w}^{(2)}(p_2(t)) \times_3 \mathbf{w}^{(3)}(p_3(t)) = \\ &= \sum_{j_1=1}^2 \sum_{j_2=1}^2 \sum_{j_3=1}^2 w_{j_1}^{(1)}(p_1) w_{j_2}^{(2)}(p_2) w_{j_3}^{(3)}(p_3) \mathbf{S}_{j_1, j_2, j_3}, \quad (5.4) \end{aligned}$$

TABLE 5.1

QLPV PARAMETER DOMAIN VALUES FOR CREATING THE MVS POLYTOPIC TP MODEL.

p_1	p_2	p_3	c_0
[-]	[-]	[-]	[N/m]
0.9–213482	0.9–2.10592	0.9–1594.8	1.9792–11000

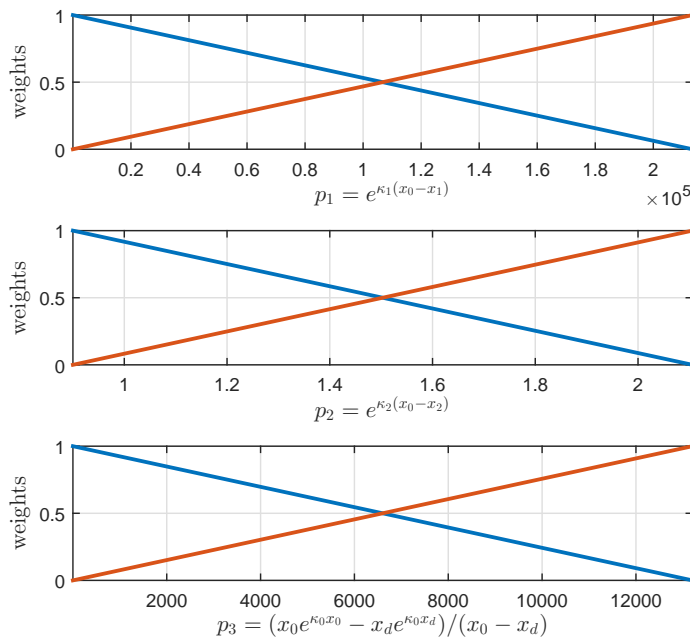


Fig. 5.1. Weighting functions $w^{(1)}$, $w^{(2)}$ and $w^{(3)}$ of the MVS polytopic TP model for the members of the parameter vector $\mathbf{p}(t)$.

the core tensor \mathcal{S} contains the $2 \times 2 \times 2$ vertex systems, and the corresponding weighting functions are shown in Fig. 5.1.

5.2.2 Model Verification

In order to verify the polytopic TP model, numerical simulations were carried out to compare the force response functions to the original nonlinear differential equations. Simulations results in both the tissue relaxation and constant compression rate phases are shown in Fig. 5.2 and Fig. 5.3, respectively. As expected, the simulations indicate identical dynamic behavior for both cases, as the polytopic TP model is capable of representing the analytic qLPV model.

The presented polytopic qLPV modeling methodology opens up new possibilities for addressing the dynamic and stability-related behavior of complex, nonlinear and parameter-dependent systems, such as the physical interaction of robots with biological tissues. Through LMI-based optimization, control synthesis can be performed according to pre-defined closed loop performance requirements. The polytopic TP model representation that is derived in this study, allows for addressing force control problems in robotic surgical devices. The control goal formulated in Section 5.2 can be handled using static and dynamic output feedback or state feedback control schemes as well. The criteria for optimal and/or robust control in LMI-based design can be addressed over a given parameter domain that is relevant to the application.

Using TP Model Transformation, the presented nonlinear soft tissue model can be transformed into a representation that directly fits to LMI-based controller design. As

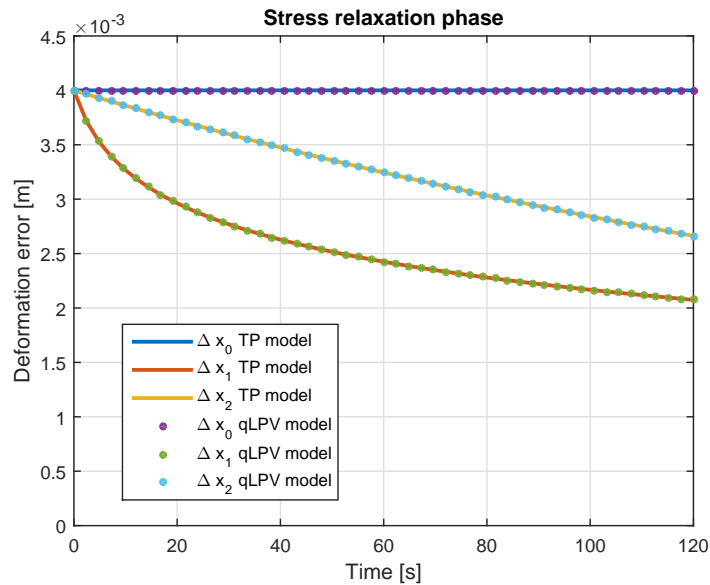


Fig. 5.2. Comparison of the original nonlinear model and the TP model in the tissue relaxation phase. $u(t) = 0$, $\mathbf{x}(t=0) = [0.004 \ 0 \ 0]^T$.

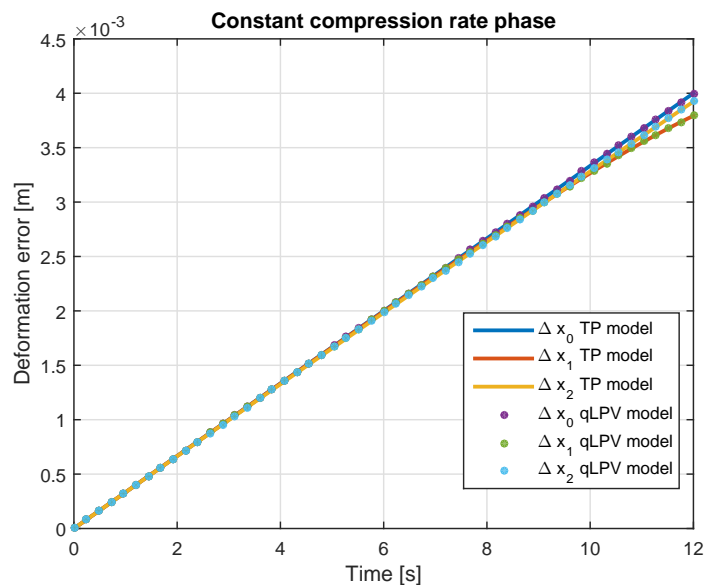


Fig. 5.3. Comparison of the original nonlinear model and the TP model in the constant compression rate deformation phase. $u(t) = 20$ mm/min, $\mathbf{x}(t=0) = [0 \ 0 \ 0]^T$.

it was shown, the model can represent the behavior of soft tissues in the case of compression tests, which is an important step towards its implementation into model-based position/force control problems. The qLPV model defined in Eq. (5.2) is written in an appropriate form for such controller design, where the way of defining the desired state is part of the modeling. For simplification reasons, $x_d(t) = 0$ mm was assumed in the open-loop simulation.

In Section 5.3, the reformulation of the above presented system model is discussed

in order to determine a representation that will serve as a basis for the design of closed loop control. The structure of the derived qLPV model and the corresponding polytopic form allows for applying well known control schemes and specifying meaningful objective functions for the purpose of LMI-based optimization. Investigation of the viable closed loop structures and the actual control design is also addressed in the next section.

5.3 Polytopic TP Model for Force Control Applications

Regarding the Polytopic TP Model of the nonlinear system described in Eq. (4.15) and Eq. (4.16), the detailed derivation of the model was given in Section 5.2, rearranged in a way that considers the so-called error dynamics. The proposed qLPV model assumes that the control goal is the force control of the surgical instrument at the tissue surface contact.

In most engineering applications, it is more plausible to use discrete time domain instead of continuous representations, due to the sampled nature of modern control systems. By introducing the discrete notation, at any time step t , one can rewrite Eq. (5.2) as:

$$\begin{bmatrix} \mathbf{x}_{t+1} \\ y_t \end{bmatrix} = \mathbf{S}(\mathbf{p}) \begin{bmatrix} \mathbf{x}_t \\ u_t \end{bmatrix}, \quad (5.5)$$

where the discretized system matrix, according to the zero order hold (ZOH) principle [96], can be written as:

$$\mathbf{S}(\mathbf{p}) = \begin{bmatrix} T_S \cdot \mathbf{A}(\mathbf{p}) + \mathbf{I} & T_S \cdot \mathbf{B} \\ \mathbf{C}(\mathbf{p}) & 0 \end{bmatrix}, \quad (5.6)$$

and

$$\begin{aligned} \mathbf{p}(t) &= [e^{\kappa_1 x_1(t)} \quad e^{\kappa_2 x_2(t)} \quad e^{\kappa_0 x_0(t)}], \\ \mathbf{A}(\mathbf{p}) &= \begin{bmatrix} 0 & 0 & 0 \\ \frac{K_1}{b_1} p_1 & -\frac{K_1}{b_1} p_1 & 0 \\ \frac{K_2}{b_2} p_2 & 0 & -\frac{K_2}{b_2} p_2 \end{bmatrix}, \quad \mathbf{B} = \begin{bmatrix} 1 \\ 0 \\ 0 \end{bmatrix}, \\ \mathbf{C}(\mathbf{p}) &= [K_0 p_3 + K_1 p_1 + K_2 p_2 \quad -K_1 p_1 \quad -K_2 p_2]. \end{aligned}$$

It is important to note that this is only an approximation of the original, continuous-time system, however, from the controller design point of view, more relevant for its better representation of digitally controlled robotic systems. $T_S = 1$ ms denotes the discrete time-step. This value was selected based on practical considerations, being a suitable processing time for current surgical systems [97]. The domains were obtained by creating a rough estimate for the lower and upper limits of x_i , $i = 1, 2, 3$ during manipulations. The minimal volume simplex (MVS) polytopic TP model form is written as:

$$\begin{aligned} \mathbf{S}(\mathbf{p}) &= \mathcal{S} \boxtimes_{n=1}^3 \mathbf{w}^{(n)}(p_{n,t}) = \\ &= \mathcal{S} \times_1 \mathbf{w}^{(1)}(p_{1,t}) \times_2 \mathbf{w}^{(2)}(p_{2,t}) \times_3 \mathbf{w}^{(3)}(p_{3,t}) = \\ &= \sum_{j_1=1}^2 \sum_{j_2=1}^2 \sum_{j_3=1}^2 w_{j_1}^{(1)}(p_1) w_{j_2}^{(2)}(p_2) w_{j_3}^{(3)}(p_3) \mathbf{S}_{j_1, j_2, j_3}, \quad (5.7) \end{aligned}$$

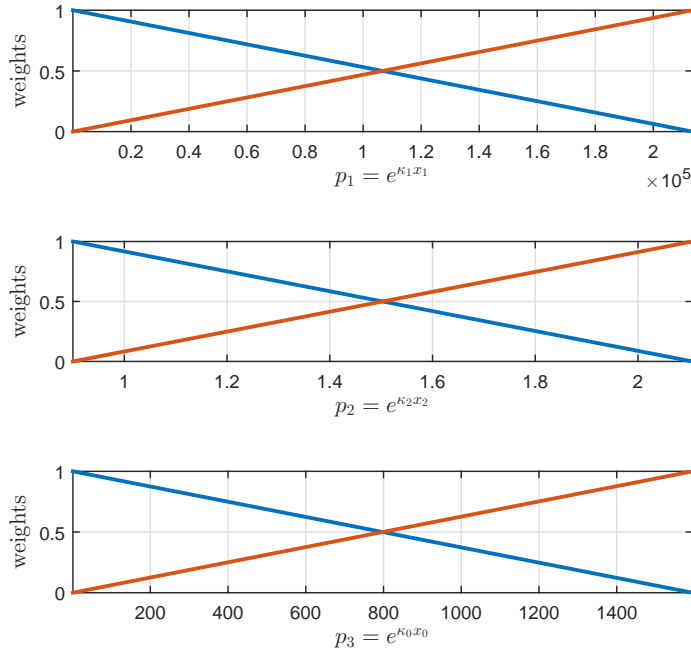


Fig. 5.4. Weighting functions $\mathbf{w}^{(1)}$, $\mathbf{w}^{(2)}$ and $\mathbf{w}^{(3)}$ of the MVS polytopic TP model represented by Eq. (5.5) for the members of the parameter vector $\mathbf{p}(t)$.

where the core tensor \mathcal{S} contains the $2 \times 2 \times 2$ vertexes and the corresponding univariate linear weighting functions, as shown in Fig. 5.4.

5.3.1 Controller Design

While Eq. (5.5) is mathematically suitable for stable state-feedback controller design, its practical realization is challenging due to the fact that the states x_1 and x_2 cannot be controlled directly, therefore their convergence to the desired $x_i = 0$ state is very slow. On the other hand, x_0 can be affected directly through speed control—assuming an ideal input controller, this holds for the position of x_0 as well—, not taking the system dynamics into consideration, which subordinates the behavior to the dynamics of the relaxation poles. Therefore, achieving $x_0 = 0$ too soon would mean that the output of the system will only depend on the slowly converging states, which would not allow one to realize the desired force control performance in surgical robotics, in terms of speed and precision. To overcome these limitations, this chapter proposes an alternative approach to the control problem, avoiding the setting of x_0 to a stationary state before the desired time. Let us consider the force output described in Eq. (4.16) the state of the system to be controlled. The derivative of expression Eq. (4.16) takes the form:

$$\dot{F} = \dot{x}_0 c_0(x_0, x_1, x_2) + \dot{x}_1 c_1(x_0, x_1, x_2) + \dot{x}_2 c_2(x_0, x_1, x_2), \quad (5.8)$$

where

$$c_0 = K_0 e^{\kappa_0 x_0} (1 + \kappa_0 x_0) + K_1 e^{\kappa_1 (x_0 - x_1)} (1 + \kappa_1 (x_0 - x_1)) + \quad (5.9)$$

$$+ K_2 e^{\kappa_2 (x_0 - x_2)} (1 + \kappa_2 (x_0 - x_2)), \quad (5.10)$$

$$c_1 = -K_1 e^{\kappa_1 (x_0 - x_1)} (1 + \kappa_1 K_1 (x_0 - x_1)), \quad (5.11)$$

$$c_2 = -K_2 e^{\kappa_2 (x_0 - x_2)} (1 + \kappa_2 K_2 (x_0 - x_2)). \quad (5.12)$$

Let us consider

$$\Delta F = F - F_d, \quad (5.13)$$

the new single state variable of the qLPV system, where F_d is the desired reaction force to be achieved. The input of the system is $u = \dot{x}_0$, and the derivative of ΔF can be written as

$$\frac{d}{dt} \Delta F = \dot{x}_0 c_0 + \dot{x}_1 c_1 + \dot{x}_2 c_2 - \dot{F}_d. \quad (5.14)$$

In the equilibrium state, $\frac{d}{dt} \Delta F = 0$, therefore:

$$u_{eq} c_0 + \dot{x}_1 c_1 + \dot{x}_2 c_2 - \dot{F}_d = 0, \quad (5.15)$$

where u_{eq} stands for the input at the equilibrium state. Following the idea on the error dynamics presented in Section 5.2, the input of the second qLPV model can be introduced as:

$$\Delta u = u - u_{eq}, \quad (5.16)$$

where

$$u_{eq} = \frac{1}{c_0} (\dot{x}_1 c_1 + \dot{x}_2 c_2 - \dot{F}_d).$$

This approach allows us to collect all system variables and parameters in a single qLPV model parameter c_0 , resulting in a very simple form. The schematic block diagram of the controlled system is shown in Fig. 5.5. Introducing the time-discretization as discussed above, we can write:

$$\Delta F_{t+1} = \Delta F_t + T s \cdot c_0 \Delta u_t. \quad (5.17)$$

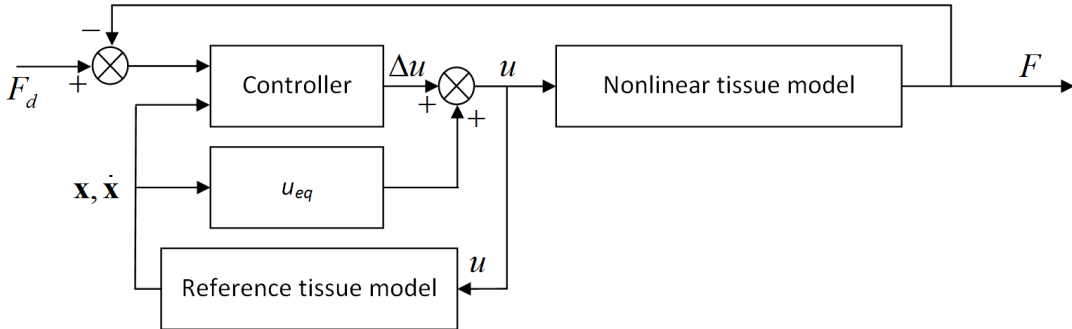


Fig. 5.5. Schematic block diagram of the controlled system.

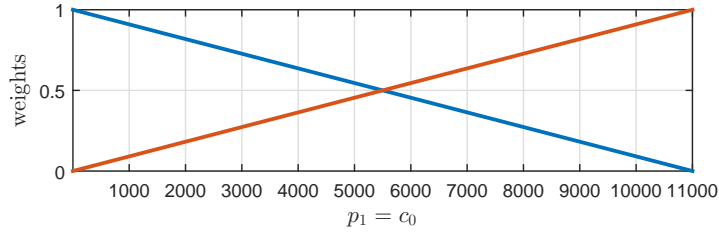


Fig. 5.6. Weighting function w' of the MVS polytopic TP model represented by Eq. (5.17).

The system matrix can be written in the form of:

$$\mathbf{S}'(c_0) = \begin{bmatrix} 1 & T_S \cdot c_0 \\ 1 & 0 \end{bmatrix}. \quad (5.18)$$

The core tensor \mathcal{S}' contains 2 vertexes:

$$\mathcal{S}'_{(1)} = \begin{bmatrix} 1 & 0.009 \\ 1 & 0 \end{bmatrix}, \quad \mathcal{S}'_{(2)} = \begin{bmatrix} 1 & 11 \\ 1 & 0 \end{bmatrix}, \quad (5.19)$$

the corresponding weighting functions are w' , as shown in Fig. 5.6. The parameter domain for c_0 was determined numerically, and was refined due to experimental considerations. The numerical values are listed in Table 5.1.

The controller of the system is determined in the following form:

$$\mathbf{u} = -\mathbf{F}(\mathbf{p})\mathbf{x}, \quad (5.20)$$

where in this particular case:

$$\mathbf{F}(\mathbf{p}) = \mathcal{F} \boxtimes_{n=1}^1 \mathbf{w}' = \sum_{i=1}^2 \mathcal{F}_i w'_i(c_0), \quad (5.21)$$

requiring a stable system in the Lyapunov sense.

Systems that can be described by a model in the form of interpolation of linear dynamic systems, such as the presented polytopic model, can be stabilized by a Parallel Distributed Compensator (PDC), as follows [98].

Let be

$$\mathbf{S}_r = \begin{bmatrix} \mathbf{A}_r & \mathbf{B}_r \\ \mathbf{C}_r & \mathbf{D}_r \end{bmatrix} = \mathbf{S}_{i_1, i_2, \dots, i_N},$$

where $r = \text{ordering}(i_1, i_2, \dots, i_N)$ ($r = 1 \dots R = \prod_n I_n$). The function *ordering* yields a linear index, equivalent of an N-dimensional array's index i_1, i_2, \dots, i_N , the array size is $I_1 \times I_2 \times \dots \times I_N$. The weighting functions can be reformulated as

$$w_r(\mathbf{p}(t)) = \prod_n w_{n, i_n}(p_n(t)).$$

Theorem (Global and asymptotic stabilization of the convex TP model):

Find $\mathbf{X} > 0$ and \mathbf{M}_i satisfying equation

$$-\mathbf{X}\mathbf{A}_r^T - \mathbf{A}_r\mathbf{X} + \mathbf{M}_r^T\mathbf{B}_r^T + \mathbf{B}_r\mathbf{M}_r > 0 \quad (5.22)$$

for all r and

$$-\mathbf{X}\mathbf{A}_r^T - \mathbf{A}_r\mathbf{X} - \mathbf{X}\mathbf{A}_s^T - \mathbf{A}_s\mathbf{X} + \mathbf{M}_s^T\mathbf{B}_r^T + \mathbf{B}_r\mathbf{M}_s + \mathbf{M}_r^T\mathbf{B}_s^T + \mathbf{B}_s\mathbf{M}_r > 0, \quad (5.23)$$

for $r < s \leq R$, except for the pairs (r, s) , such that $w_r(\mathbf{p}(t))w_s(\mathbf{p}(t)) = 0$ for all $\mathbf{p}(t)$.

The above conditions can be considered as LMIs with respect to \mathbf{X} and \mathbf{M}_r , positive definite matrices \mathbf{X} and \mathbf{M}_r can be found or show that no such matrices exist. Such representations imply that the dynamic linear systems are in continuous or discrete time normal state space form, or linear input-output difference equation form. If the system consists of subsystems described by normal form state equations, the controller system's consequents are linear state feedback laws. Thus, the PDC results in nonlinear state regulation, which is guaranteed if the feedback law satisfies the series of LMIs [99]. The feedback gains are obtained by utilizing the solutions for \mathbf{X} and \mathbf{M}_r , such as:

$$\mathbf{F}_r = \mathbf{M}_r\mathbf{X}^{-1}, \quad (5.24)$$

using the ordering function to determine the components of tensor \mathcal{F} . An illustrative example of an LMI-based PDC controller design for the TORA system can be found in [98]. Kuti *et al.* published an extensive literature on the generalization of the TP model transformation for control design, showing that the separated structure of parameter dependencies within the polytopic TP model can be exploited during the controller design. Corresponding application examples with numerical calculations on further mechanical systems were published for a dual-excenter vibration actuator [77], an inverted pendulum [100], and fluid volume control in blood purification therapies [101]. The reader is encouraged to explore these examples for a deeper and general understanding of the modeling and controller design techniques employed in this thesis.

The final PDC (Parallel Distributed Compensator) controller for the system described by Eq. (5.18) was found solving the LQ optimal control problem using convex optimization algorithm provided by the MATLAB *tptool* toolbox and the *YALMIP* interface, a toolbox for optimization and modeling for MATLAB [102, 103]. The resulting core tensor yields:

$$\mathcal{F} = \begin{bmatrix} 0.36347 \\ 0.08747 \end{bmatrix}. \quad (5.25)$$

5.3.2 Simulation Results

The proposed closed-loop controller solution was tested and simulated on a typical gesture of a surgical interventions, grasping. The process of grasping, holding and releasing of the tissue was investigated by setting F_d to a desired trajectory, followed by the derivation of control performance and robustness. Three specific cases were investigated in the latter case: first, the real tissue parameters were ill-estimated, i.e., the reference tissue model parameters were 20% lower than the parameters used for controller design. Second, the simulation of a badly calibrated observer was done by linearly reducing the reference tissue model output by 20%. Third, a time-delay term of $\tau = 2$ ms was added to the reference tissue state output, modeling a slow observer behavior. Simulation results and the force tracking error for all cases are shown in Fig. 5.7, 5.8, 5.9 and 5.10.

Fig. 5.7 shows that the proposed control scheme is suitable for realizing force control in a stable and precise manner, utilizing the selected soft tissue model. The tracking error

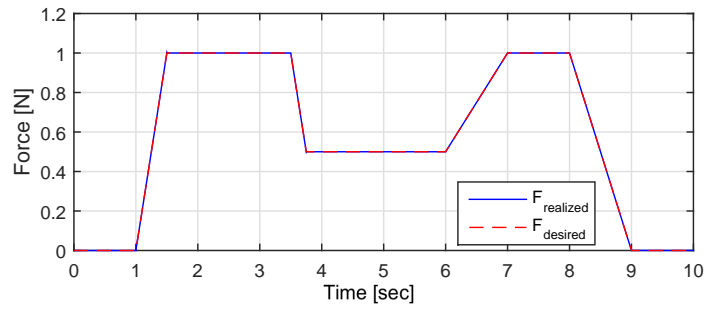


Fig. 5.7. Force tracking simulation results for modeling the grasping, holding and release of tissue. The simulation was carried out on the discrete time systems with the time-step of 1 ms.

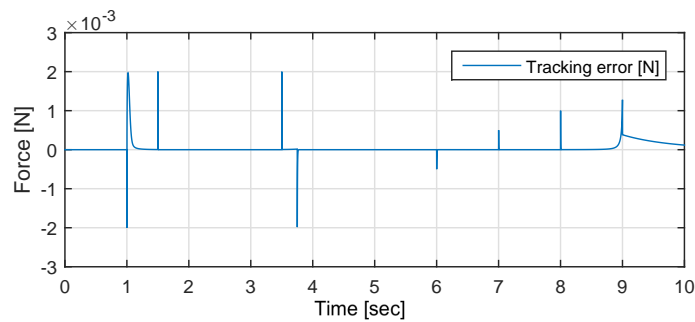


Fig. 5.8. Tracking error results for modeling the grasping, holding and release of tissue.

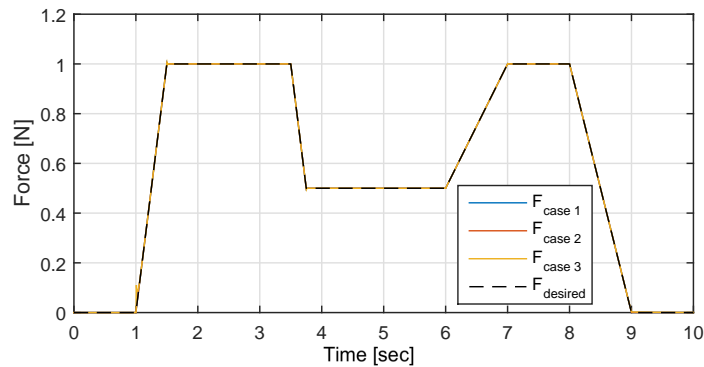


Fig. 5.9. Force tracking simulation results for modeling the grasping, holding and release of tissue, investigating the robustness of the proposed method. Case 1: incorrect estimation of the tissue parameters in the reference tissue model. Case 2: incorrectly calibrated observation, state output reduced by 20%. Case 3: slow observation, state feedback is delayed by 2 ms.

for the presented gesture did not exceed 5 mN, which is a favorably low value for surgical interventions. The needle-like peaks in the tracking error represent short transients, which arise from the sudden change in the time derivative of the desired force. In practice, these transients may be extended due to the physical limitations of actuators and the phenomenon of saturation. The results were achieved using the discrete sampling rate of 1 ms, which is a realizable processing time for modern surgical systems, in terms of arithmetic performance. The proposed controller was tested for robustness in the case of three different approaches, including ill-conditioned parameter estimation and observer design,

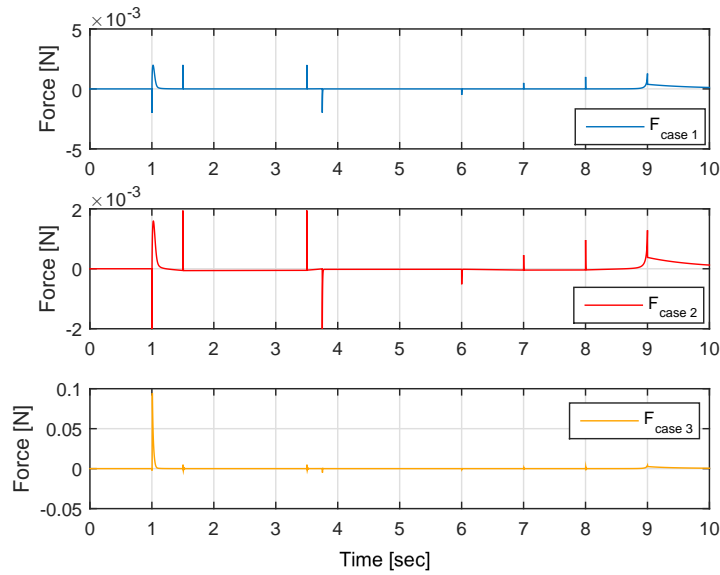


Fig. 5.10. Tracking error results for modeling the grasping, holding and release of tissue, investigating the robustness of the proposed method.

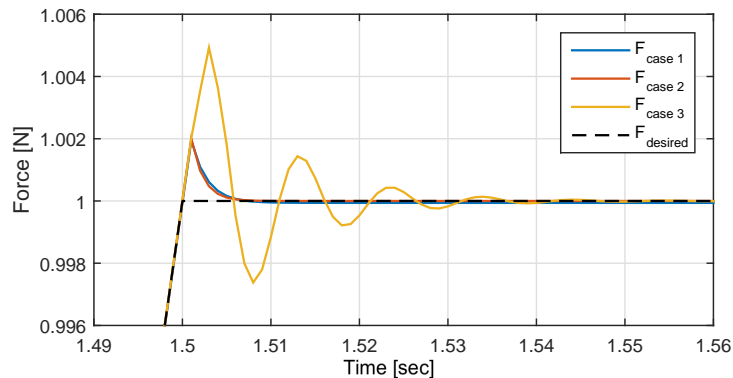


Fig. 5.11. Tracking performance in close-up view in the most critical point of the simulation according to the tracking error results.

and time-delay. The different behavior of these three cases is shown in Fig. 5.11, indicating that there is no significant decrease in the tracking performance under the mentioned disturbances. Minor oscillation can be observed in the case of delayed feedback, which, when the delay time is increased, ultimately leads to stability loss. Further investigation of the phenomena and implementation of delay-based control schemes are part of my future work.

5.4 Summary of the Thesis

In this chapter, a control scheme and the corresponding control design methodology were presented for regulating interaction force during autonomous manipulation of soft biological tissues. The proposed approach utilizes recent results of polytopic model-based

control through the framework of Tensor Product Model Transformation. The goal of the presented approach is the control of reaction force during the robotic interaction with soft tissues e.g., grasp–hold–release cycles. Since biological tissues typically have highly nonlinear dynamic behavior (progressive stiffness characteristics, stress relaxation etc.), time invariant linear controllers cannot provide ideal performance across the whole operation domain.

Based on my previously published nonlinear tissue model, the parameter-dependent error dynamics was derived and the resulted system was reformulated in order to avoid the error rendered by the slow dynamics of one state variable. The reformulated system allows for concentrating the three original parameter dependencies into a single parameter, and construct a feed forward term for the equilibrial input. An additional state feedback controller was utilized that handled the unmodeled dynamics and further disturbances. Since the state variables cannot be measured in the real process, a reference tissue model was used. The state feedback controller was designed by LMI-based synthesis providing the variable gains as parameter dependent polytopic TP functions. The overall system was evaluated via numerical simulations, with very promising results. The implementation of the proposed method into supervised telemanipulation/telesurgical equipments would enhance the performance of these systems, allowing haptic sensing to the operator. Future work includes the experimental validation of the system in both virtual and *ex vivo* environments, extending the model with a discrete-time PDC state observer.

Chapter 6

USABILITY ASSESSMENT OF THE PROPOSED SOFT TISSUE MODEL

6.1 Haptic Feedback in Telesurgery

6.1.1 The Role of Haptic Feedback

The number of Minimally Invasive Surgical procedures is continuously increasing. MIS allows shorter patient recovery time and the decrease of surgical trauma. However, due to the long, rigid design of the MIS tools, the limited vision and confined operation space, several ergonomic difficulties and limitations have arose that are yet to be solved. These include the deprivation of dexterity, loss of depth perception due to the two-dimensional video image feedback, distributed hand–eye coordination and special tool manipulation, and most importantly, the loss of tactile feedback [104]. While most of these limitations were addressed and partially solved with the introduction of robot-assisted MIS and telesurgery, by using stereo visual feedback, tremor filtering and ergonomic Human–Machine Interfaces, the lack of force feedback limits the ability of the surgeon during organ palpation, tumor localization and the identification of other anatomical structures during surgery [105].

The role of haptic feedback in telesurgery is twofold. First, restoring tactile information is essential for assessing the surface textural properties of the investigated organs. This feature is generally useful for artery and lump detection, therefore the lack of tactile feedback leads to a more difficult localization of palpable anomalies, such as kidney stones or tumors. Second, haptics may provide a realistic force feedback to the robot operator (the surgeon), providing information about the mechanical characteristics of the tissue. Haptic feedback improves the quality of basic surgical maneuvers (grasping, palpation, cutting), and allows collision detection. Further safety functions can also be implemented, such as the application of virtual fixtures both in the case of intra-operative scenarios and surgical simulators [106]. Tissue characterization requires complex perception of the operating environment, where beside tissue stiffness (hardness), relaxation properties and other viscoelastic phenomena can also be investigated and accounted for, when using haptic feedback. It was also shown that for tissue characterization tasks, utilizing force feedback leads to better results than only visual feedback, while, with the combination of the two, superior results can be achieved [107].

While the lack of haptic feedback proves to be a limitation to modern robot-assisted MIS procedures, today's telesurgical systems provide no, or limited solutions that are commercially available. Increased cost, sterilization difficulties and the sizing limitations of force sensors at the end effector are key issues in introducing haptic feedback to these systems through direct force sensing at the tool tip. To address these, several approaches were investigated for indirect force estimation, e.g. accounting for joint flexibility [24], the dynamics of cable-driven manipulators [35] or force estimation through soft tissue modeling [TA-6].

There is no general consensus among laparoscopic surgeons, if, and at what level would haptic feedback improve the outcome of procedures. According to many surgeons, having higher quality visual feedback alone provides adequate information about the tissue palpation force for safe and reliable operation, however, the lack of haptic feedback is often considered as a major limitation in robot-assisted MIS procedures [108]. Clearly, an experienced surgeon finds the lack of haptic feedback less disturbing, than a novice. However, in haptic guidance, learning spatiotemporal trajectories, contrary motion compensation and strategy planning, the presence of haptic feedback and/or surgical simulators can greatly enhance force skill learning for trainees [109].

Providing a complex and reliable perception for the operators, haptic devices can not only enhance intra-operative performance, but also become an essential tool in surgical training and pre-operative planning. In recent years, the use of surgical simulators have largely increased, offering different training scenarios, anatomical variations and conditions in the operating environment [110]. Using haptic devices, a new dimension opened up in performance evaluation during procedures. Moreover, due to the complex mechanical behavior of soft tissues, augmented simulations require reference data from real surgical scenarios, and should be tested by human operators in order to validate the usability of the virtual models [111].

The problem of distinguishing between soft tissues by testing their mechanical properties is often referred to as the cognitive role of haptic devices in simulation environments [112]. It is a common view that today's surgical simulators that are using haptic interfaces should rely on simple mechanical models of soft tissues, instead of complex, parameterized finite element models, thus enhancing real-time operation, and focusing on the most representative mechanical effects. By using bilateral haptic devices and accounting for the tissue dynamics, one can also solve issues arising from communication latency and high computational requirements by investigating hand/master and slave/environment interactions [113]. Stability and accuracy deterioration caused by latency and other external disturbances, such as contacting hard tissues or elastic tool deformation, can also be addressed using realistic soft tissue models, their integration into model-based force control algorithms largely increase the robustness and reliability of robot-assisted interventions [TA-13].

This chapter presents a novel methodology for testing the usability of soft tissue models in robot-assisted MIS setups, focusing on the modeled mechanical properties of soft tissues and their integration into surgical simulators with haptic capabilities.

6.1.2 Different approaches

The integration of soft tissue properties to robot-assisted and virtual reality based MIS procedures is an actively researched topic within the field of surgical robotics. Methods for acquiring useful measurement data use a combined experimental procedure of measuring tissue relaxation force under step-like tissue compression and force measurement during constant compression rate indentation input. Samur *et al.* proposed a method for tissue parameter estimation using a custom indenter during laparoscopic surgery, employing inverse finite element solution to estimate optimum values of nonlinear hyperelastic and elastic properties [114]. Beccani *et al.* developed a tool for intra-operative wireless tissue palpation, using a cylindrical palpation probe, estimating local volumetric stiffness values, assuming linear elastic behavior of the tissue [115].

A deformable model-based on nonlinear elasticity and finite element method for haptic surgical simulators was proposed in [116], validated on real-time simulations of laparoscopic surgical gestures on virtual liver models. Trejos *et al.* suggested an augmented hybrid impedance control scheme to perform force control, providing model-based control background for tactile sensing instrument in intra-operative tissue palpation [117]. Endoscopically guided, minimally invasive cannulation tasks were investigated by Wagner *et al.*, testing the hypothesis that force feedback can improve surgical performance, finding that applied forces by the surgeons can be decreased for those with adequate training background [118]. Tholey *et al.* developed an automated laparoscopic grasper with force feedback capability, in order to aid the surgeons in differentiating tissue stiffness through the PHANTOM (Sensable Technologies, Woburn, MA) haptic device [104]. Participants were asked to differentiate between tissues, having provided visual and/or haptic feedback to complete the task. Luboz *et al.* published an extensive patient-specific data for facial tissue characterization, relying on linear elastic models [119], while a FEA-based characterization method and soft tissue deformation model was proposed by Zou *et al.* in [120].

Alternative approaches are also popular in general force feedback for laparoscopic training and procedures. Horeman *et al.* developed a training system that provided visual haptic feedback of the interaction forces during procedure [121]. They found that providing haptic feedback through visual representation considerably improved the quality of the solved tasks. A detailed feasibility study of lung tumor detection using kinesthetic feedback was published by McCreery *et al.*, creating an *ex vivo* experimental environment, modeling various tissue stiffness values, injecting agar into healthy tissues, substituting haptic feedback with recorded force data [122].

The viscoelastic tissue model used in this work is taken from chapter 4, implemented as a parameter-dependent, discretized virtual model-based on the Tensor Product model transformation, as derived in chapter 5. The aim of this phase of the research is to provide a general methodology for addressing the usability and validity range of the proposed tool-tissue interaction model in telesurgical scenarios, where haptic feedback is available.

6.2 Research Hardware Environment

On closed systems, it is fairly difficult to conduct fundamental research, for obvious reasons. Therefore, in order to achieve technological development, some of the manufacturers

grant partial accessibility to their closed systems. In the case of the da Vinci, there exists a real-time stream of kinematic and user event data from the robot that can be read, provided by the da Vinci API. It is important to mention that the total replacement of certain components, such as the controller body, can transform the da Vinci system into an open-source platform. Raven II is one of the most successful open-source robotic platforms. Developed at the University of Washington and supported by DARPA¹, the Raven II became the greatest competitor of the da Vinci system. Furthermore, with the help of the National Institutes of Health² (NIH), 8 robots have been created and distributed to European and North-American locations. Currently, the Raven II research platform can be purchased from Applied Dexterity Inc.³ The platform operates based on the Robot Operating System architecture.

6.2.1 The da Vinci Research Kit

The da Vinci Research Kit is one of the most capable research platforms in surgical robotics. In fact, the kit is a collection of retired, first-generation da Vinci robot components and tools, provided with additional open-source control electronics and software. As the platform serves as the primary hardware in the experiments conducted in this chapter, a short description of its components and capabilities is discussed in the next subsections.

6.2.2 Hardware Components

The DVRK contains the components listed below:

- Two da Vinci Master Tool Manipulators (MTMs),
- Two da Vinci Patient Side Manipulators (PSMs),
- A stereo viewer,
- A foot pedal tray,
- Manipulator Interface Boards (dMIBs),
- Basic accessory kit.

The research kit contains the original, unmodified mechanical components therefore it is possible to transform a da Vinci Classic system into a research kit, although some of the components are not available for researchers due to their commercial use. In the DVRK hardware set, the Endoscopic Camera Manipulator (ECM) is not included along with several other components from the original system, but the lack of these elements is not a major issue from the development point of view. In general, for research purposes, the control electronics and control software are the most essential parts of the system. Recently, a novel, open controller platform was created by JHU, Worcester Polytechnic Institute (WPI) and their partners [123]. The source files of the control electronics were also published online. The research platform is equipped with an IEEE 1394a Firewire interface, capable of maintaining a communication speed of 400 Mbit/sec. In order to achieve

¹<http://www.darpa.mil>

²<http://www.nih.gov/>

³<http://applieddexterity.com/>

a satisfactory degree of security and reliability, it is crucial to create real-time communication between the devices in the system. The control box includes two FPGA modules and two Quad Linear Amplifiers (QLA), as shown in Fig. 6.1.

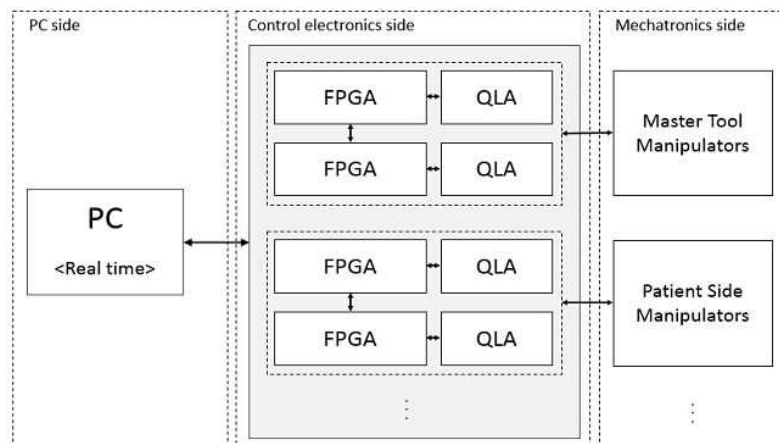


Fig. 6.1. Schematic representation of the DVRK hardware structure.

The assembly described above is capable of driving and controlling a single robotic tool. Two da Vinci Master Tool Manipulators and two da Vinci Patient Side Manipulators can be controlled using four sets of control electronics, requiring a total of 8 pieces of FPGAs and QLAs. The integration of the DVRK to a retired, fully operational da Vinci robot is shown in Fig. 6.2.



Fig. 6.2. The da Vinci Surgical System and the da Vinci Research Kit. System components: Patient Side Manipulators (left), the DVRK controller (middle) and the Master Tool Manipulators (right).

The da Vinci Research Kit is based on the centralized computation and distributed I/O architecture [124]. The main advantage of this structure is that there is only one control electronics that maintains contact with the peripheral inputs and outputs, allowing the

central computer unit to perform the calculations, located at the control units. In general, the central unit is a Linux-based computer with some real-time component expansion.

Low Level Software Architecture

The FPGA module firmware is available online⁴, and published under a BSD license, therefore it can be freely modified. The RT-FireWire is one of the best approaches to solve the real-time communication between the subsystems over Firewire, while the communication implementation is achieved through standard Linux C++ libraries [125]. The PC-side operating system is preferably Linux-based, as there exists a real-time extension (RTLlinux), a Linux OS that runs under the supervision of a hard real-time microkernel [126]. The software architecture, as a whole, can be divided into five functional layers (I-V) and three development layers (A-C) [123]. The functional layers, implemented on the PC side, are stratified by the complexity of their function, while the development layers are sorted by the programming language complexity they use. The open-source property is extensively supported by the previously described SAW and CISST libraries, allowing the system to be used as a completely open research platform.

6.3 A Methodology for Model Evaluation and Usability

Direct haptic sensation during open surgical procedures is an important guide for surgeons for the assessment of the types and health of different anatomical structures. However, in the case of MIS and robot assisted surgical procedures, numerous tasks require a new approach in the interpretation of haptic information, such as tissue characterization, classification, lump detection and localization [127]. The human sensing of soft tissue characteristics through robot-assisted palpation is a complex process from mechanical and neurophysiological points of view. Due to the tissue compliance and its highly nonlinear behavior, and the indirect transfer of haptic information, efficient tool–tissue interaction modeling requires an understanding the limits of human perception, when the palpation is carried out using a teleoperation system [128]. This way, not only the quality of robot-assisted haptic feedback can be assessed, but one can also address the validity of the soft tissue models used for the enhancement of model-based control methods for telesurgical applications. The purpose of this work is to provide a general methodology for the evaluation of such soft tissue models through understanding the human perception of reaction force during the remote palpation of *ex vivo* and artificial soft tissues, and during the palpation of virtual tissue models.

Tissue samples with different mechanical properties were investigated during the experiments, which were completed in two phases: Phase I and Phase II. During Phase I, the artificial tissue samples were selected from a wide range of stiffness, being compared to two very different *ex vivo* soft tissue samples: chicken liver and chicken breast. After the evaluation of Phase I, new artificial tissues samples were created, aiming to match the mechanical properties of the selected *ex vivo* tissue sample, based on their estimated behavior. In Phase II, 2 *ex vivo* samples and 3 artificial tissue phantoms were prepared for this task. In Phase II, a refined set of 14 artificial tissue phantoms were compared to a single

⁴<https://github.com/jhu-cisst/mechatronics-firmware/wiki/FPGA-Program>

ex vivo chicken breast sample, as explained in Section 6.3.1. Experiments were carried out using the da Vinci Research Kit, integrated in the Computer Integrated Surgical Systems and Technology (CISST) toolkit [TA-12]. Force sensing was achieved using an OptoForce (OptoForce Ltd., Budapest, Hungary). The instruments were integrated using the Robot Operating System Indigo version under a 64 bit Ubuntu 14.04 LTS operating system. The ROS packages were based on the 08/2016 release of the Johns Hopkins University sawIntuitiveResearchKit distribution⁵.

6.3.1 Experimental Methodology

In both phases of the experiments, the first step was to determine the mechanical properties of the samples, using curve fitting on the nonlinear mass–spring–damper Wiechert model, following the experimental setup published in [TA-6]. After the acquisition of the parameters, participants were asked to carry out remote 1 DoF, axial palpation on each of the samples, using the da Vinci Master Tool Manipulator (MTM) as the master device. The physical palpation of the tissues was done with the da Vinci Patient Side Manipulator (PSM) equipped with an OptoForce 3 DoF sensor, as shown in Fig. 6.3. The applied force was fed back to the operator through the MTM, serving as a haptic device, which was allowed by a custom software implementation for the DVRK. The theoretical resolution of the OptoForce sensor was 0.0025 N, while the resolution of the PSM force feedback values was 0.1 N, which was taken into consideration in force upscaling during the trials, as explained later. The nominal load capacity of the OptoForce sensor was 40 N for 1 mm single axis deformation at 2% nonlinearity. Having verified the maximum reaction force values measured, it was assumed that the relative deformation of the elastic sensor surface was less than 5% with respect to the tissue deformation, which was negligible compared to the uncertainties originated from the non-rigidity of the PSM arms. After the teleoperated palpation, participants were asked to carry out similar maneuvers using the da Vinci MTM, palpating the virtual models of the selected tissue samples. Participants were allowed to compare the sense of touch during teleoperation and virtual palpation using the da Vinci device at any time, and were asked to pair up the real tissues with the virtual ones. The usability study was validated by evaluating the correct answers both qualitatively and quantitatively.

6.3.2 Data Collection and Analysis

Data collection was done by recording the reaction force of the palpated tissues during their controlled deformation. The thickness of the investigated artificial tissue samples was identically 20 mm, the *ex vivo* tissue samples had a deviation of ± 5 mm from that dimension. Palpation test on the *ex vivo* tissues were carried out at different points of the surface, indicating that this deviation does not have any significant effect on the measured reaction force data. The indentation depth of all measurements was 4 mm, and regardless of the non-uniform surface deformation, each of the samples were modeled as a single nonlinear Wiechert element. These assumptions are valid within the investigated range of deformation, and the tissue parameter values can be generalized to specific stiffness and

⁵<https://github.com/jhu-dvrk/sawIntuitiveResearchKit/wiki>

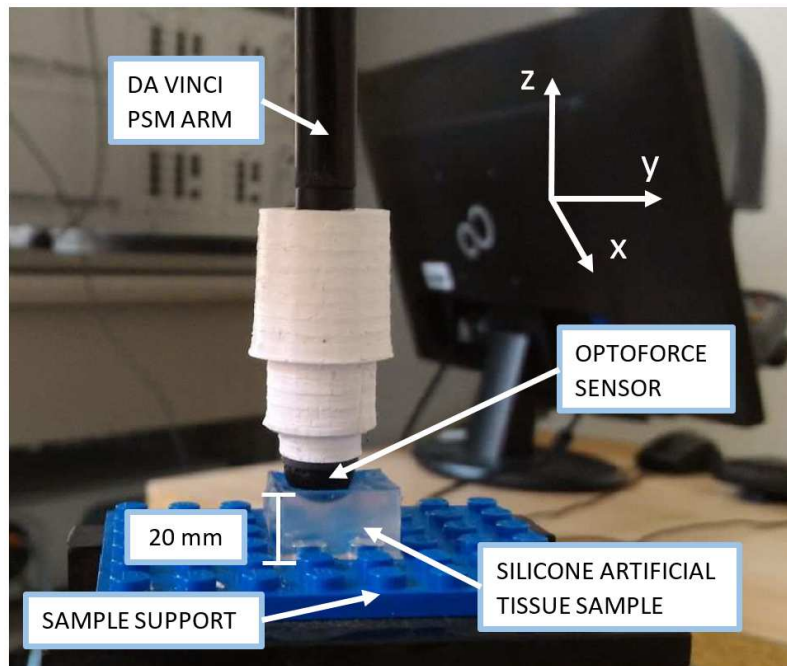


Fig. 6.3. Indentation tests on a silicone artificial tissue sample, using the da Vinci PSM arm with an OptoForce 3 DoF force sensor.

damping parameters using the method developed in-house [TA-6]. Each of the samples were subjected to a step-like deformation, where the compression rate was 50 mm/s, and the relaxation response was measured for 30 seconds. After the relaxation tests, the samples were compressed at a constant compression rate of 0.5 mm/s, and the force response during the compression was recorded. As each sample was tested 5 times for both types deformation tests, the results were averaged and processed for tissue parameter acquisition by fitting the force response data to the theoretical response [TA-8]. Data collection was done at the sampling rate of 50 Hz, taking into consideration that the da Vinci Research Kit supports 60 Hz at maximum, while the OptoForce device can easily handle 200–300 Hz sampling rate as well.

6.4 Results

The results section is divided into two parts: automatic data collection for tissue parameter estimation; and tissue characterization/comparison trials. Tissue comparison was done both in Phase I and Phase II with different groups of volunteers. Their task was to find the matching virtual tissue model to the actually palpated one, the answers were recorded and evaluated. Typical palpation movements and reaction forces were recorded as well, as presented in Sections 6.4.1 and 6.4.2.

6.4.1 Results for Phase I: User Matches

Data Collection

During Phase I, three silicone artificial tissue samples were molded using Silorub ds f-TG silicone, and were softened using Rubosil methyl-silicone oil. Samples A, B and C contained 0, 15% and 30% silicone oil, respectively. The *ex vivo* chicken breast sample was marked as specimen D, while the *ex vivo* chicken liver sample was marked as specimen E. The *ex vivo* samples were covered with fresh-keeping film in order to keep the silicone surface of the OptoForce sensor intact. Typical force relaxation response curves and the results of constant compression rate indentation are shown in Fig. 6.4 and Fig. 6.5, respectively.

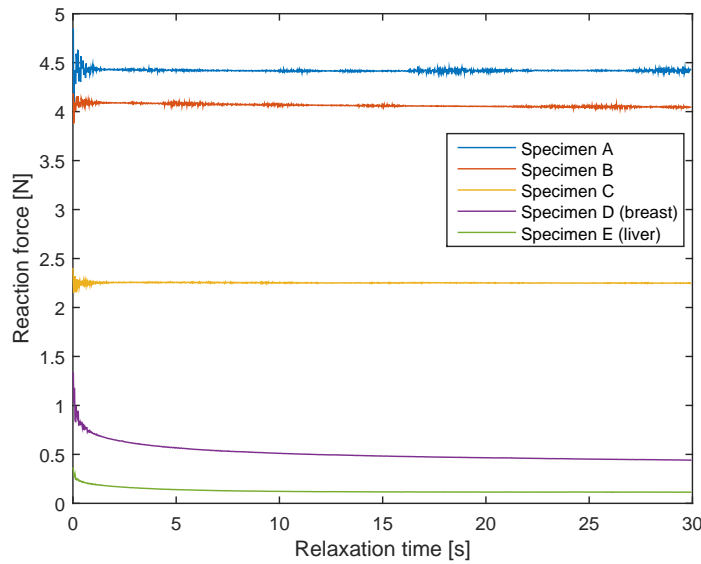


Fig. 6.4. Typical relaxation force response curves for the specimens used during Phase I, assuming step-like deformation and 4 mm indentation depth.

As it is shown in the figures, the stiffness characteristics of the artificial tissue samples are close to linear and there the relaxation phenomenon is negligible. However, Fig. 6.4 shows that the breast and liver samples have a significant decrease in the reaction force

TABLE 6.1

PARAMETER ESTIMATION RESULTS FROM FORCE RELAXATION AND CONSTANT COMPRESSION RATE TESTS DURING PHASE I.

Specimen	K_0 [N/m]	K_1 [N/m]	K_2 [N/m]	b_1 [Ns/m]	b_2 [Ns/m]	κ_0 [m ⁻¹]	κ_1 [m ⁻¹]	κ_2 [m ⁻¹]
A	1093.1	1.0616	251.09	9209.2	190	0.0056899	531.99	0.00093
B	1002.3	1.0861	190.38	104350	145.76	3.3147e-05	22.679	3.3201e-05
C	473.13	17.062	70.787	88365	66.985	58.497	234.68	7.2614e-05
D	1.0001	1.0091	28.361	28.287	8.2608	577.97	969.71	10.898
E	1.007	86.917	184.27	5375.5	4.4498	8830.2	291.66	40.536

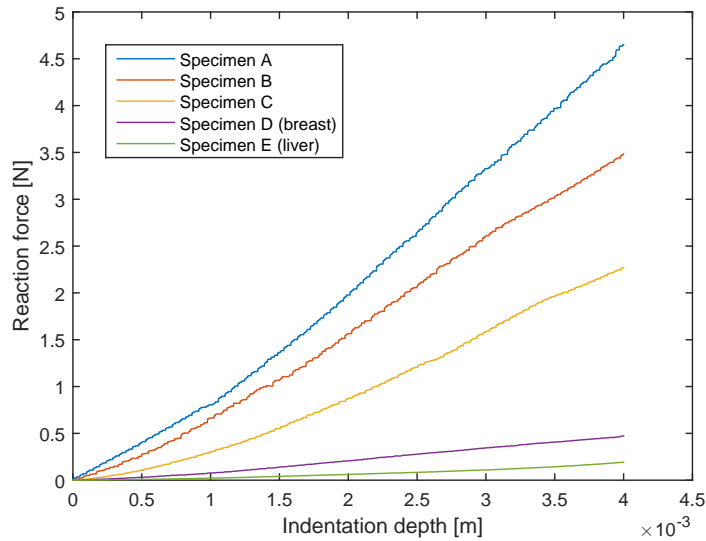


Fig. 6.5. Typical force response curves for the specimens used during Phase I, assuming constant compression rate deformation and 4 mm indentation depth.

due to tissue relaxation, as expected. Tissue parameters were acquired by curve fitting, using the MATLAB *fminsearch* function, taking the sum of the RMSE values from both experimental data sets as the cost function for each sample. The simulated response was calculated by solving Eq. (4.15) and Eq. (4.16) for the iterated parameter values for the nonlinear Wiechert model. The estimated parameters for each of the specimens, based on the results of curve fitting, are shown in Table 6.1. It is important to note that these values are only valid for this specific experimental setup, as this chapter focuses on the empirical comparison methodology of the investigated samples instead of proposing global parameters value sets for the chosen materials.

Tissue Characterization Trials

The virtual Tensor Product model of each of the specimens was created and implemented into the experimental software. The da Vinci MTM served as a haptic device, requesting force commands from either directly from the OptoForce sensor or from the virtual model (simulation). The current position and velocity of the MTM were implemented as the input of the system. A force upscaling factor of 10 was applied for helping the participants distinguishing between the models. The measured maximum reaction force applied by the da Vinci MTMs was below 50 N, which did not exceed the 63 N saturation limit. The upscaling of the 4 mm indentation was determined by the participants, restricted by the workspace of the da Vinci MTM. The scaling factor of the indentation depth upscaling was set for each volunteer independently by their choice, and typically had a scaling factor of 20–50.

10 subjects participated in the Phase I trials: 8 male and 2 female volunteers. 1 participant had hands-on surgical experience, 4 came from medical engineering background, while 1 participant had no experience in engineering practice. Participants were aged

between 21–40 years, with an average age of 25. At the beginning of each trial, the participants were asked to investigate the virtual models by compressing and releasing them, assessing the tissue properties (stiffness, relaxation, elastic behavior) verbally. Then, after getting familiar with the virtual models, the simulation was switched to the real-time palpation of the tissues. The participants could switch back from the actual palpation to the palpation of the virtual models at any time, and were asked to draw a conclusion, which virtual model (A–E) corresponds to the *ex vivo* tissue. For the palpation tests, gravity compensation of the da Vinci MTM was switched off due to known stability issues of the DVRK in the current master release of the Software Development Kit (SDK) and the orientation of the last 4 axes (tool tip orientation) was locked, allowing only z-axis motion (direction along the PSM tool shaft).

Altogether, 20 trials (10 participants for 2 tissue models) were carried out. 95% of the participants accurately paired the *ex vivo* tissue to its corresponding virtual model. One participant mistook specimen D (the chicken breast sample) for the virtual model E (liver sample), the rest of the answers were correct from all participants. Besides the correctness of the answer, some general conclusions were recorded from the participants, listed below:

- Models A and B were significantly stiffer than the rest of the virtual models and the *ex vivo* palpated samples: 85%
- The *ex vivo* samples had progressive stiffness characteristics, which disclosed models A, B and C from the comparison: 65%
- The reaction force from specimen and model E was very difficult to feel, even in the case of rapid compression: 70%
- Participants spent most of the palpation time differentiating between models C and D before drawing the final conclusion, when palpating specimen D: 75%

6.4.2 Results for Phase II: User Matches

Based on the results of Phase I, Phase II was planned, taking into account the following:

- The liver tissue sample was removed from the investigation due to its low stiffness compared to the silicone samples.
- Specimens A and B were also removed due to their significantly larger stiffness compared to the chicken breast sample.
- Specimen C was kept as a reference, and further silicone samples were created by adding more silicone oil during the preparation, until reaching physical limits (saturation of oil in the silicone).

Data Collection

During Phase II, 14 silicone artificial tissue samples were created, utilizing the same method as in Phase I. The samples were molded from Silorub ds f-TG silicone, softening was carried out with a combination of Rubosil methyl-silicone oil and Rubosil silicone grease. Binding was enhanced by using Silorub ds K RTV-2 catalyst, adding 2 ml to every 20 ml of silicone used. Samples were numbered from 1–14, created with a uniform cubic shape with the edge length of 20 mm. Baking soda was added to sample 13 to further

soften the silicone by creating artificial inclusions, and vinegar was added to sample 14, also for softening purposes. Samples were numbered from 1–14, created with a uniform cubic shape with the edge length of 20 mm. The volume ratio of the silicone, oil and grease for each of the samples is listed in Table 6.2. The *ex vivo* chicken breast sample was marked as specimen 15. All samples were covered with fresh-keeping film in order to keep the silicone oil from damaging the silicone surface of the OptoForce sensor. Typical force relaxation response curves and the results of constant compression rate indentation are shown in Fig. 6.6 and Fig. 6.7, respectively. The average force response curves used for model identification are also displayed in the Figures.

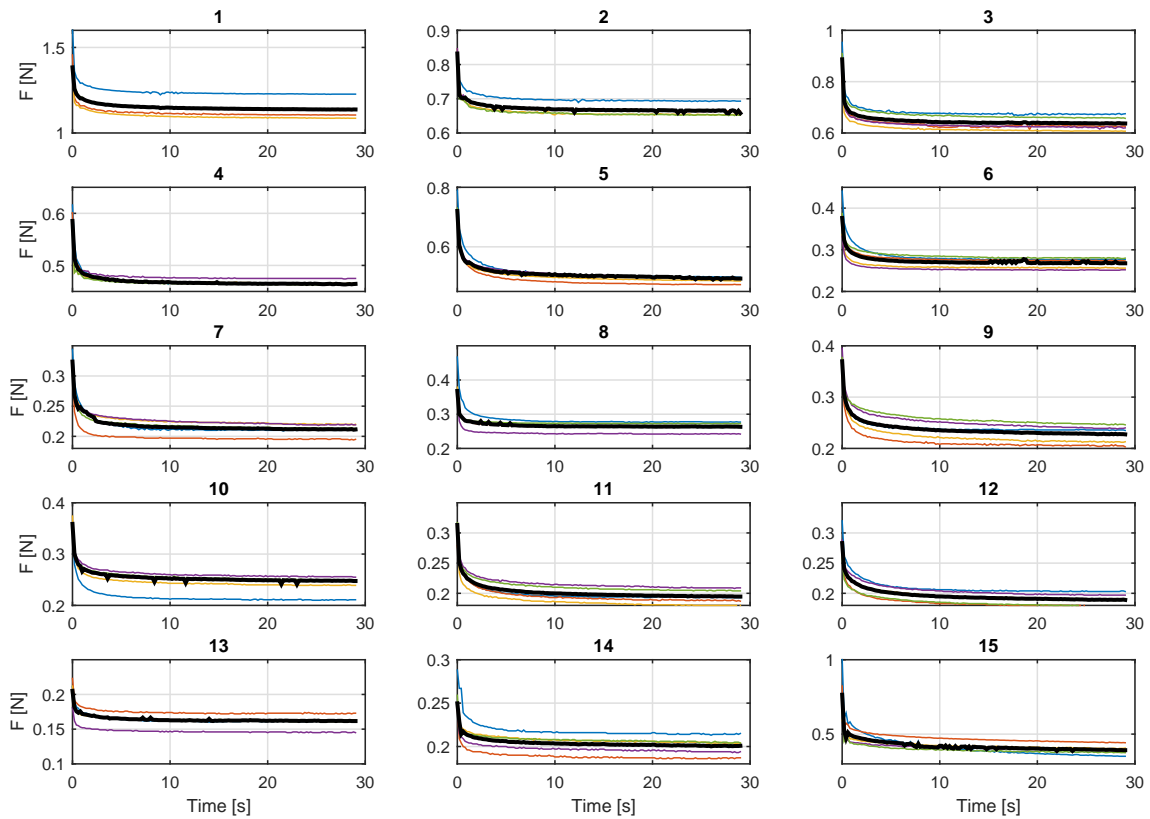


Fig. 6.6. Measured and average (black) force response curves for the specimens used during Phase II, assuming step-like deformation and 4 mm indentation depth.

TABLE 6.2

SILICONE–OIL–GREASE VOLUME RATIO USED FOR CREATING ARTIFICIAL TISSUE SAMPLES FOR PHASE II. *BAKING SODA ADDED; ** VINEGAR ADDED.

Specimen	1	2	3	4	5	6	7	8	9
silicone : oil	1:0.30	1:0.50	1:0.75	1:1	1:1.25	1:1.50	1:1.85	1:2.25	1:2.70
Specimen	10	11	12	13	14				
silicone : oil : grease	1:0.30:0.50	1:0.30:1	1:0.30:1.70	1:0.30:1.70:0.80*	1:0.30:1.70:0.80:0.80**				

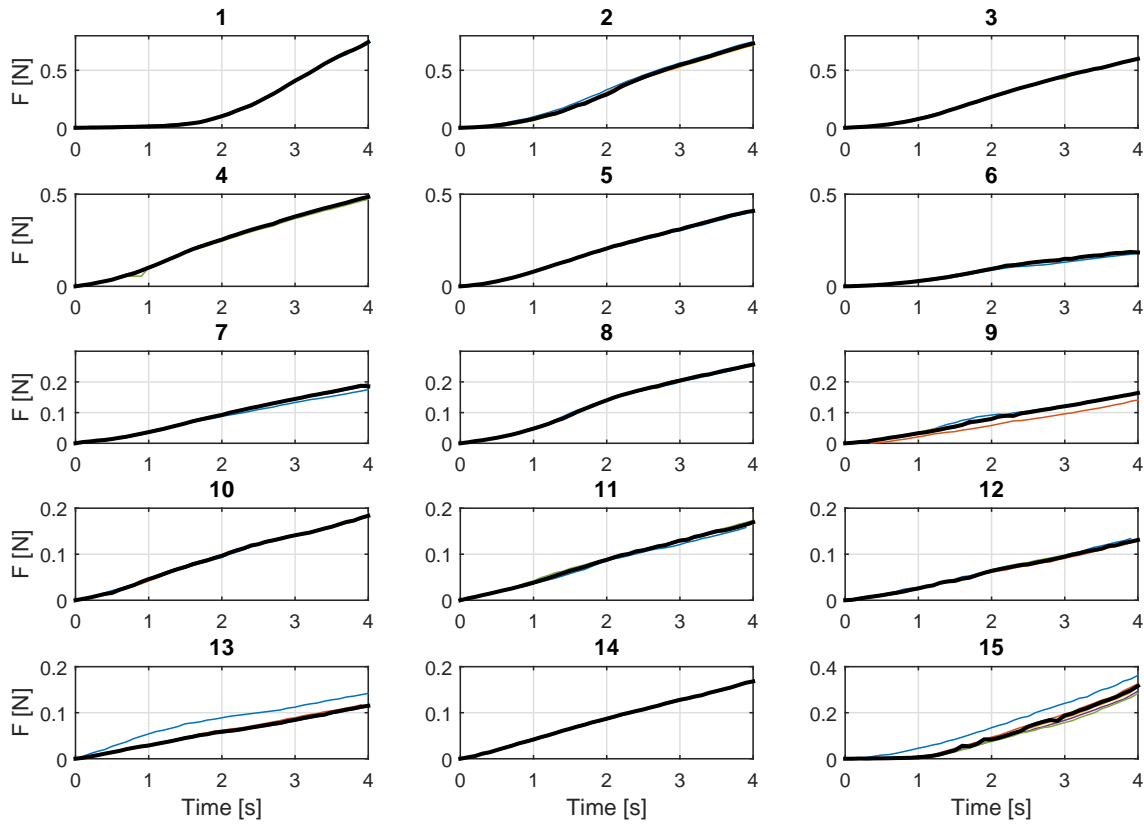


Fig. 6.7. Measured and average (black) force response curves in Phase II, assuming constant compression rate deformation and 4 mm indentation depth.

Tissue Characterization Trials

Before the tissue characterization trials, six silicone specimens were selected based on the different behavior of the created tissue samples during the data collection phase. The samples were selected from a wide range of stiffness and maximum reaction force values, taking into account that some of these samples had very similar behavior during relaxation and constant compression rate indentation tests. The virtual TP model of each of the selected samples and the *ex vivo* chicken breast sample were created similar to that of Phase I and was implemented into the software. The parameter estimation results for the selected samples from the indentation tests for Phase II are shown in Table 6.2. In order to improve haptic sensation and enhance comparability between the virtual and real specimens, the da Vinci MTML (left-side MTM) served as a haptic teleoperation device, requesting force commands directly from the OptoForce sensor, while the da Vinci MTMR (right-side MTM) reflected force values from the virtual model (simulation). The current position and velocity of the MTML and MTMR were implemented as the inputs of the real and virtual systems, respectively. For Phase II, a force upscaling factor of 20 was applied for helping the participants distinguishing between the models, and the upscaling of the 4 mm indentation at the MTMs was identically set as in Phase I. The participants were requested to aim for identical ranges for both MTMs, in order to make it easier to compare

samples. This way, simultaneously and identically moving the two MTMs, the real and virtual tools reached the tissue surface at the same z-coordinate of the MTMs.

In Phase II, 23 participants went through the trials, 19 male and 3 female participants. 3 volunteers had hands-on surgical experience, 15 came from engineering or medical engineering background, 5 of them came from other fields. The participants were aged between 21–60 years, with an average age of 30 years. At the beginning of each trials, the participants were asked to practice individually on both MTM arms in order to achieve a stable grip, doing so by resting their lower arm on the soft bar da Vinci master console. Once a stable teleoperation was achieved, a randomly chosen virtual model was fed to the MTMR, while the force signal from the OptoForce sensor was constantly fed back to the MTML from the indentation of the *ex vivo* chicken breast tissue. On request of the participants, the virtual model was switched to another one of the 7 possibilities (models of the selected 6 artificial tissues and the model of the chicken breast tissue), until they found the best match between the virtual and real tissues according their subjective haptic sensation. Gravity compensation of the da Vinci MTMs was switched off and the orientation of the last four axes were locked, as it was done in Phase I. Fig. 6.8 summarizes the answers from the participants on which virtual tissue model resembled the most on the behavior of the *ex vivo* chicken breast tissue during the palpation tests from the 23 successive trials.

6.4.3 Discussion of the Results

Results of Phase I indicated that the participants were able to distinguish between the investigated silicone samples and the *ex vivo* tissue samples in 95%, which verifies the usability of the tissue model if there is a significant difference between the mechanical properties of the samples. During Phase II, 7 of 23 participants were able to correctly match the virtual chicken breast model to the *ex vivo* tissue, while samples 8 and 10 were chosen 5 and 9 times, respectively. Based on these results, two important conclusions can be drawn:

- The soft tissue model used for representing the tissue behavior is sufficiently good for use in haptic simulators, training and general reaction force estimation. This is based on the observation that a significant percentage (30%) of participants were able to match the virtual soft tissue model to the real one.

TABLE 6.3

PARAMETER ESTIMATION RESULTS FROM FORCE RELAXATION AND CONSTANT COMPRESSION RATE TESTS DURING PHASE II.

Specimen	K_0 [N/m]	K_1 [N/m]	K_2 [N/m]	b_1 [Ns/m]	b_2 [Ns/m]	κ_0 [m ⁻¹]	κ_1 [m ⁻¹]	κ_2 [m ⁻¹]
2	115.97	2.45	5.10e-7	238.59	13.58	90.32	747.11	19.98
3	99.572	0.11764	0.101	10.001	115.64	118.85	1.56e3	115.51
5	69.62	5.58	0.10	1.07	166.37	142.92	577.81	332.75
8	63.95	0.48	3.44e-5	0.61	9.07	9.94	990.62	59.83
10	25.54	1.00e-3	1.00e-3	0.63	141.44	222.95	2.31e3	1.55
12	18.79	5.65	0.17	0.29	0.07	226.61	355.52	431.72
15 (<i>ex vivo</i>)	18.89	0.54	13.89	329.43	17.09	217.35	1.38e3	16.70

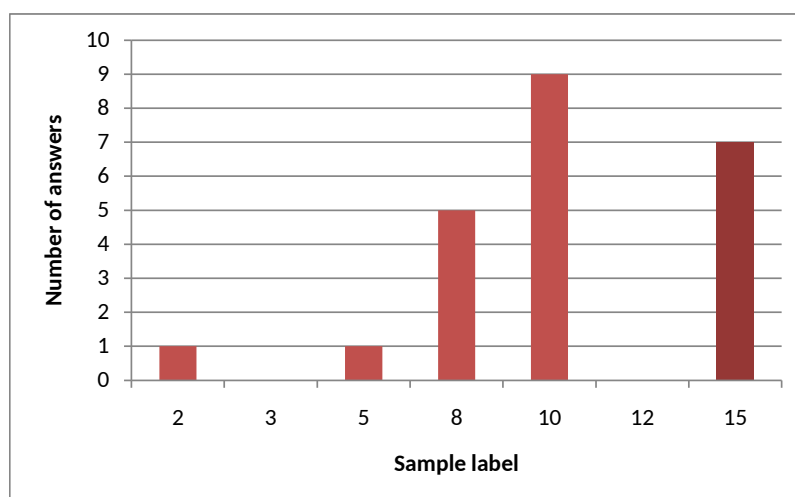


Fig. 6.8. Tissue characterization results from Phase II, summarizing the participants answers to the question: 'Which virtual tissue model's behavior resembles the most to the *ex vivo* chicken breast?' The correct answer is indicated by a different color, belonging to sample 15.

- Silicon samples 8 and 10 with the proposed composition are capable of modeling soft tissues (in this particular case, chicken breast) in artificially built surgical scenarios or physical phantoms. The conclusion is based on the observation that a large percentage (60%) of the participants were unable to distinguish between the physically palpated soft tissue sample and the virtual model of the silicon artificial tissue samples of similar mechanical properties. This similarity is based on the observation of tissue relaxation and constant compression rate tests.

6.5 Summary of the Thesis

Along with force control, the problem of haptic feedback in telesurgical systems remains an open challenge in the related cognitive or ergonomic fields of research. Current surgical teleoperation systems lack haptic feedback capabilities, limiting their usability in everyday practice. This work proposed a validation method for tissue models and their polytopic representation by creating an experimental framework using the da Vinci Research Kit. Furthermore, allowing haptic feedback from the manipulated real tissue, functionality can be extended to surgical simulation using virtual tissue models created by the proposed soft tissue modeling method.

The experimental methodology provided results, which showed that the proposed non-linear tissue model very well mimics the mechanical behavior of the *ex vivo* tissue both from qualitative and quantitative point of view. This allows one to integrate the model into virtual tissue models used in surgical simulators, where it is critical to have a realistic haptic sensation reflected to the human operator when manipulating the tissues. Results also showed that using a haptic interface, it is challenging to distinguish between artificial silicone tissues and real tissues during teleoperation, indicating that by creating a silicone sample by the methods presented in this work, surgical training can be enhanced by artificial tissue phantoms, though providing realistic haptic sensation to the trainees.

Henceforward, this chapter described a methodology for the quantitative evaluation of haptic teleoperation devices for soft tissue characterization. Utilizing a structured method for extracting mechanical properties of *ex vivo* or artificial soft tissues, the simultaneous palpation of real and virtual samples is an efficient way of assessing the capabilities of both the human operator and the teleoperation system with haptic feedback. Furthermore, when the palpation is carried out through a teleoperated instrument with force feedback, the proposed tissue model gives a realistic reflection of the dynamic behavior of the palpated samples, both quantitatively and qualitatively.

Future work focuses on the extension of the system database to different *ex vivo* tissue models, developing methods for creating artificial silicone samples based on the mechanical properties of these models and on the implementation of this approach into more complex virtual surgical scenarios.

Chapter 7

CONCLUSION

7.1 Summary of Contributions

My thesis gives an overview of the importance of tool–tissue interaction modeling in the control engineering design of modern telesurgical systems. The work relies on an extensive literature review of the existing tool–tissue interaction models, soft tissue modeling approaches and their validity range. A novel nonlinear soft tissue model was proposed and verified experimentally, motivated by the limitations of current rheological, widely used soft tissue models. Literature research has also been carried out on the existing methods for force control and haptic feedback on current surgical robotic applications, extending the scope to open-source software and hardware tools, aiding the development of these systems. In order to verify the proposed tissue model and its polytopic representation for model-based control approaches, an experimental usability testing method was proposed and carried out with the aid of human participants, addressing the practical usability of the integrated topics investigated in the thesis.

Addressing the challenges stated in *Problem 1*, explained in chapter 2, I developed and verified a novel tool–tissue interaction approach, introducing a nonlinear soft tissue model. In chapter 4, I carried out a detailed investigation of linear mass–spring–damper soft tissue models, exploring their usability for modeling soft tissue behavior during tissue palpation, based on experimental data. I showed that while the linear Wiechert model represents this behavior in tissue relaxation phase, the model fails in the prediction of reaction forces in constant compression rate phase, both qualitatively and quantitatively. Based on the measurements, I conducted on liver tissue samples at the Austrian Center for Medical Innovation and Technology, I created an 8-parameter nonlinear mass–spring–damper model, and obtained the representative tissue parameters by curve fitting to the data. It was found that in the case of uniaxial deformation, the reaction force from tissue palpation can be estimated very accurately. The model was also verified for non-uniform surface deformation scenarios, where the deformation shape was estimated empirically, showing that for deformations until 20%, the method gives a good estimation on these forces. The method was later successfully applied for different *ex vivo* and artificial tissue samples as well, in the context of parameter acquisition in chapter 6.

In the next phase of my work, I carried out an extensive literature research on the current control methods used in telesurgical applications as described in chapter 5, addressing *Problem 2*. I found that communication delay in teleoperation systems is a major

contributor to stability and accuracy degradation during these interventions, which restricts the possible use of these systems to unilateral teleoperation scenarios. However, besides opening up possibilities to bilateral approaches, the reliable execution of (semi-)automated surgical tasks requires the integration of the tissue model in the controller design. Based on the concept of Tensor Product modeling, I created the polytopic representation of the tissue model and following the guidelines of Linear Matrix Inequality approach, I tested the proposed controller against various force tracking tests. I found that due to the slow poles of the system, the conventional modeling approach fails in tracking tasks, therefore I proposed and verified a novel methodology for the representation of these models, a controller design for discretized systems, and addressed robustness in terms of parameter uncertainty and latency.

In the context of investigating the practical usability of the proposed soft tissue model, I suggested a novel methodology for its evaluation from the haptic bilateral teleoperation point of view in chapter 6, addressing *Problem 3*. Based on the methods from chapter 4, I carried out further measurements on two *ex vivo* tissue samples and 17 silicone phantoms with different mechanical properties, mimicking the behavior of the *ex vivo* pieces. I created a comparative list of the mechanical properties of these samples, based on the proposed nonlinear Wiechert model, and integrated them as virtual tissue samples to the da Vinci Surgical System. I proposed an experimental methodology, where participants with different engineering and medical background were asked to address the difference between the properties of the teleoperation-based tissue palpation and the palpation of the virtual tissues, created using the model utilizing the polytopic representation discussed in chapter 5. From the trials I concluded that the proposed nonlinear tissue model very well mimics the mechanical behavior of the *ex vivo* tissue both qualitatively and quantitatively. This allows its integration into virtual tissue models used in surgical simulators, where it is critical to have a realistic haptic sensation reflected to the human operator when manipulating the tissues. I also found that using the da Vinci MTMs as a haptic interface, it is challenging to distinguish between artificial silicone tissues and real tissues during teleoperation, indicating that by creating a silicone sample according to the guidelines presented in this work, surgical training can be accelerated and enhanced by artificial tissue phantoms, yet providing realistic haptic sensation to the trainees.

7.2 New Scientific Results

Thesis 1

I developed and verified a novel, nonlinear, 8-parameter mass–spring–damper soft tissue model. In contrast to the current models employed, the qualitative advantage of this model is that it represents the soft tissue behavior in both pure relaxation and constant deformation rate compression phases. I showed that in the case of uniaxial deformation, the reaction force from tissue palpation can be estimated with a relative error of 12%. I verified the model for non-uniform surface deformations, showing that below 20% relative deformation, the reaction forces can be estimated with a relative error of 35%.

Related publications: [TA-3, TA-6, TA-7, TA-8, TA-11, TA-13, TA-14, TA-15, TA-16].

Thesis 2

Based on the concept of Tensor Product modeling, I created the polytopic representation of the nonlinear soft tissue model, and showed that this representation described the soft tissue behavior with sufficient accuracy for controller design. Utilizing the Linear Matrix Inequality method, I designed a controller for the force control task in teleoperation systems. I found that due to the slow poles of the system, the conventional design strategies were not applicable, and I proposed a new approach for designing force feedback control with polytopic representation of the tool–tissue interaction model. I verified the designed controller for robustness in terms of parameter uncertainty and time-delay.

Related publications: [TA-4, TA-5].

Thesis 3

I designed the evaluation of tissue characterization trials, where based on the outcome of independent test subjects, I experimentally proved that the proposed nonlinear soft tissue model represents the behavior of *ex vivo* tissues both qualitatively and quantitatively. In the case of the force-feedback teleoperation system, 30% of the human operators were able to distinguish between *ex vivo* and artificial soft tissues, which verifies the realistic behavior representation of the nonlinear soft tissue model. Furthermore, 60% of human operators mistook the virtual models of artificial soft tissues for *ex vivo* models in force-feedback teleoperation scenarios, when the quantitative mechanical parameters of the virtual models were alike. This validates the use of artificial soft tissue samples in education and research.

Related publications: [TA-1, TA-2]

Other publications related to the Ph.D. thesis and the accompanying research work: [TA-9, TA-10, TA-12].

7.3 Future Work

The field of surgical robotics is rapidly changing and is under constant development. It is expected that in the next years, numerous challenges will need to be solved, with a growing need for model-based solutions. I am enthusiastic in extending the scope of my Ph.D. research to these new areas, applying the results in the clinical environment as well. At the Antal Bejczy Center for Intelligent Robotics, there are already numerous students from different academic levels, who are involved in the research topics, achieving outstanding results.

During my research, I had the opportunity to start building an international network with researchers in various fields of surgical robotics. I am convinced that these connections can lead to fruitful joint collaborations, international projects. Thanks to the unique, extensive and diverse robot infrastructure of our Center, there is a positive outlook on future cooperations with our regional partners. I would like to highlight the Austrian Center for Medical Innovation and Technology (ACMIT) in Wiener Neustadt, and the Central European Living Lab for Intelligent Robotics (CELLI), a partnership of regional higher education and research institutions. As Óbuda University is conducting an active research on the da Vinci Research Kit, we are becoming an integral part of a unique community, managed by the prestigious Johns Hopkins University, which opens up new opportunities towards international collaborations. On the other hand, the results in tissue characterization and the quantitative assessment of *ex vivo* and silicone tissue samples can initiate discussion with experts in surgical simulator and training box developers.

The results of chapter 4 showed that the proposed model can be a sophisticated tool for estimating the force response of the tissue during surgical manipulations. This allows its integration into model-based control approaches and surgical simulators for training and education. While chapter 5 and 6 discussed these possibilities in details, alternative approaches to these challenges can also rely on these results. However, there is still room for the investigation of the case of complex surface deformation scenarios, the real-time prediction of the reaction force based on on-line deformation shape measurement and the modeling of more sophisticated surgical interventions. As a long-term plan, the extension of the model to multidimensional deformation and the consideration of lateral forces during the manipulation also poses an interesting research topic, as well as its integration into coupled problems including invasive, biochemical and thermo-mechanical interactions.

As a future work, the control architecture proposed in chapter 5 can be generalized for various tissue manipulation tasks during robotic surgery. The implementation of this method into supervised teleoperation systems can enhance performance both in terms of precision and robustness, and the research can be extended for the investigation of bilateral teleoperation scenarios with haptic feedback. Therefore, the experimental validation of the control algorithm is a first step of the future work, utilizing it both in virtual and *ex vivo* surgical scenarios. This requires the model of the discrete-time PDC observer in the simulation environment, which is an ongoing research of today.

The methodology discussed in chapter 6 allows one to create a general database of different *ex vivo* tissue models and widely-used silicone materials for phantom generation and assembly. It can also aid the field of tissue engineering to provide realistic tissue samples for modeling and planning surgical interventions. Future work also aims to create a methodology for the development of artificial silicone samples, mimicking the mechan-

ical behavior of various soft tissues, based on the parameters acquired for the proposed nonlinear soft tissue model. The implementation of the approach to more complex virtual surgical scenarios is also possible, while the validation of the method using different haptic devices is also among future research topics.

The major topics discussed in this thesis work are partly utilizing the results in a hierarchical way: the proposed and verified soft tissue model is used for the model-based controller design, while the polytopic representation is utilized for the tissue characterization trials in the implementation phase. While strongly connected, these topics can be further developed independently as well. This allows one to extend the scope of research and use the results in other fields of studies outside medical technologies.

While this work tends to give a solution to the problems stated in chapter 2, naturally, new questions arose during the elaboration on the topics, along with challenges to be addressed in the field of surgical robotics. This work provides an outlook on these issues in-line, providing an extensive literature reference for those interested in them.

REFERENCES

- [1] T. Haidegger, J. Sándor, and Z. Benyó, “Surgery in space: the future of robotic telesurgery,” *Surgical Endoscopy*, vol. 25, no. 3, pp. 681–690, 2011.
- [2] M. Hoeckelman, I. Rudas, P. Fiorini, F. Kirchner, and T. Haidegger, “Current capabilities and development potential in surgical robotics,” *International Journal of Advanced Robotic Systems*, vol. 12, no. 61, pp. 1–39, 2015.
- [3] T. Haidegger, “Surgical robots: System development, assessment, and clearance,” in *Robotics: Concepts, Methodologies, Tools, and Applications*. IGI Global, 2014, pp. 1148–1187.
- [4] E. Flynn, “Telesurgery in the united states,” *Journal of Homeland Defense*, vol. 6, pp. 24–28, 2005.
- [5] C. Nguan, B. Miller, R. Patel, P. P. Luke, and C. M. Schlachta, “Pre-clinical remote telesurgery trial of a da Vinci telesurgery prototype,” *The International Journal of Medical Robotics and Computer Assisted Surgery*, vol. 4, no. 4, pp. 304–309, 2008.
- [6] H. H. King, B. Hannaford, K.-W. Kwok, G.-Z. Yang, P. Griffiths, A. Okamura, I. Farkhatdinov, J.-H. Ryu, G. Sankaranarayanan, V. Arikatla *et al.*, “Plugfest 2009: Global interoperability in telerobotics and telemedicine,” in *IEEE International Conference on Robotics and Automation (ICRA)*. IEEE, 2010, pp. 1733–1738.
- [7] N. J. Soper and G. M. Fried, “The fundamentals of laparoscopic surgery: its time has come,” *Bull Am Coll Surg*, vol. 93, no. 9, pp. 30–32, 2008.
- [8] “Application of risk management for it-networks incorporating medical devices-part 1: Roles, responsibilities and activities,” Standard, 2010.
- [9] J. Sándor, B. Lengyel, T. Haidegger, G. Saftics, G. Papp, Á. Nagy, and G. Wéber, “Minimally invasive surgical technologies: Challenges in education and training,” *Asian Journal of Endoscopic Surgery*, vol. 3, no. 3, pp. 101–108, 2010.
- [10] T. Haidegger, L. Kovács, R.-E. Precup, B. Benyó, Z. Benyó, and S. Preitl, “Simulation and control for telerobots in space medicine,” *Acta Astronautica*, vol. 81, no. 1, pp. 390–402, 2012.
- [11] N. Diolaiti, G. Niemeyer, F. Barbagli, and J. K. Salisbury, “Stability of haptic rendering: Discretization, quantization, time delay, and coulomb effects,” *IEEE Transactions on Robotics*, vol. 22, no. 2, pp. 256–268, 2006.
- [12] R. B. Gillespie and M. R. Cutkosky, “Stable user-specific haptic rendering of the virtual wall,” in *Proceedings of the ASME International Mechanical Engineering Congress and Exhibition*, vol. 58, 1996, pp. 397–406.

- [13] R.-E. Precup, T. Haidegger, S. Preitl, Z. Benyó, A. S. Paul, and L. Kovács, “Fuzzy control solution for telesurgical applications,” *Applied and Computational Mathematics*, vol. 11, no. 3, pp. 378–397, 2012.
- [14] R. Hess and A. Modjtahedzadeh, “A control theoretic model of driver steering behavior,” *IEEE Control Systems Magazine*, vol. 10, no. 5, pp. 3–8, 1990.
- [15] G. Ornstein, “The automatic analog determination of human transfer function coefficients,” *Medical Electronics and Biological Engineering*, vol. 1, no. 3, pp. 377–387, 1963.
- [16] C. C. Macadam, “Understanding and modeling the human driver,” *Vehicle System Dynamics*, vol. 40, no. 1-3, pp. 101–134, 2003.
- [17] R. G. Costello and T. J. Higgins, “An inclusive classified bibliography pertaining to modeling the human operator as an element in an automatic control system,” *IEEE Transactions on Human Factors in Electronics*, no. 4, pp. 174–181, 1966.
- [18] C. MacAdam, “Development of a driver model for near/at-limit vehicle handling,” Tech. Rep., 2001.
- [19] J. H. Chien, M. M. Tiwari, I. H. Suh, M. Mukherjee, S.-H. Park, D. Oleynikov, and K.-C. Siu, “Accuracy and speed trade-off in robot-assisted surgery,” *The International Journal of Medical Robotics and Computer Assisted Surgery*, vol. 6, no. 3, pp. 324–329, 2010.
- [20] L.-W. Sun, F. Van Meer, Y. Bailly, and C. K. Yeung, “Design and development of a da vinci surgical system simulator,” in *IEEE International Conference on Mechatronics and Automation*. IEEE, 2007, pp. 1050–1055.
- [21] A. A. Syed, X.-g. Duan, X. Kong, M. Li, Q. Huang *et al.*, “6-dof maxillofacial surgical robotic manipulator controlled by haptic device,” in *IEEE International Conference on Ubiquitous Robots and Ambient Intelligence (URAI)*. IEEE, 2012, pp. 71–74.
- [22] L. Pelyhe and P. Nagy, “Relative visibility of the diagnostic catheter,” *Acta Polytechnica Hungarica*, vol. 11, no. 10, pp. 79–95, 2014.
- [23] N. Famaey and J. V. Sloten, “Soft tissue modelling for applications in virtual surgery and surgical robotics,” *Computer methods in biomechanics and biomedical engineering*, vol. 11, no. 4, pp. 351–366, 2008.
- [24] M. Tavakoli and R. D. Howe, “Haptic effects of surgical teleoperator flexibility,” *The International Journal of Robotics Research*, vol. 28, no. 10, pp. 1289–1302, 2009.
- [25] C. Basdogan, S. De, J. Kim, M. Muniyandi, H. Kim, and M. A. Srinivasan, “Haptics in minimally invasive surgical simulation and training,” *IEEE computer graphics and applications*, vol. 24, no. 2, pp. 56–64, 2004.
- [26] Y. Bao, D. Wu, Z. Yan, and Z. Du, “A new hybrid viscoelastic soft tissue model based on meshless method for haptic surgical simulation,” *The Open Biomedical Engineering Journal*, vol. 7, pp. 116–124, 2013.

- [27] T. Yamamoto, "Applying tissue models in teleoperated robot-assisted surgery," Ph.D. thesis, The Johns Hopkins University, 2011.
- [28] T. Yamamoto, N. Abolhassani, S. Jung, A. M. Okamura, and T. N. Judkins, "Augmented reality and haptic interfaces for robot-assisted surgery," *The International Journal of Medical Robotics and Computer Assisted Surgery*, vol. 8, no. 1, pp. 45–56, 2012.
- [29] A. M. Okamura, C. Simone, and M. D. O'leary, "Force modeling for needle insertion into soft tissue," *IEEE transactions on biomedical engineering*, vol. 51, no. 10, pp. 1707–1716, 2004.
- [30] F. Leong, W.-H. Huang, and C.-K. Chui, "Modeling and analysis of coagulated liver tissue and its interaction with a scalpel blade," *Medical & Biological Engineering & Computing*, vol. 51, no. 6, pp. 687–695, 2013.
- [31] C. Liu, P. Moreira, N. Zemiti, and P. Poignet, "3d force control for robotic-assisted beating heart surgery based on viscoelastic tissue model," in *IEEE Annual International Conference of the Engineering in Medicine and Biology Society (EMBC)*. IEEE, 2011, pp. 7054–7058.
- [32] O. Goksel, S. E. Salcudean, and S. P. Dimaio, "3D simulation of needle–tissue interaction with application to prostate brachytherapy," *Computer Aided Surgery*, vol. 11, no. 6, pp. 279–288, 2006.
- [33] S. Misra, K. B. Reed, B. W. Schafer, K. Ramesh, and A. M. Okamura, "Mechanics of flexible needles robotically steered through soft tissue," *The International Journal of Robotics Research*, vol. 29, no. 13, pp. 1640–1660, 2010.
- [34] M. Mahvash and P. E. Dupont, "Mechanics of dynamic needle insertion into a biological material," *IEEE Transactions on Biomedical Engineering*, vol. 57, no. 4, pp. 934–943, 2010.
- [35] S. N. Kosari, S. Ramadurai, H. J. Chizeck, and B. Hannaford, "Robotic compression of soft tissue," in *IEEE International Conference on Robotics and Automation (ICRA)*. IEEE, 2012, pp. 4654–4659.
- [36] "Robots and robotic devices—safety requirements for industrial robots—part 2: Robot systems and integration," Standard, 2010.
- [37] A. Ellery, "Survey of past rover missions," in *Planetary Rovers*. Springer, 2016, pp. 59–69.
- [38] S. Park, Y.-C. Lee, and G.-W. Kim, "Implementation of spatial visualization for a tele-operated robot in a complex and hazardous environment," in *IEEE International Conference on Automation Science and Engineering (CASE)*. IEEE, 2014, pp. 285–289.
- [39] J. K. Chapin, K. A. Moxon, R. S. Markowitz, and M. A. Nicolelis, "Real-time control of a robot arm using simultaneously recorded neurons in the motor cortex," *Nature Neuroscience*, vol. 2, no. 7, pp. 664–670, 1999.
- [40] R. C. Luo and T. M. Chen, "Development of a multi-behavior based mobile robot for remote supervisory control through the internet," *IEEE/ASME Transactions on Mechatronics*, vol. 5, no. 4, pp. 376–385, 2000.

- [41] J. Park and O. Khatib, "A haptic teleoperation approach based on contact force control," *The International Journal of Robotics Research*, vol. 25, no. 5-6, pp. 575–591, 2006.
- [42] S. Sirouspour and A. Shahdi, "Model predictive control for transparent teleoperation under communication time delay," *IEEE Transactions on Robotics*, vol. 22, no. 6, pp. 1131–1145, 2006.
- [43] I. Lenz, R. Knepper, and A. Saxena, "Deepmpc: Learning deep latent features for model predictive control," in *Proceedings of Robotics: Science and Systems*, Rome, Italy, July 2015.
- [44] D. A. Lawrence, "Stability and transparency in bilateral teleoperation," *IEEE Transactions on Robotics and Automation*, vol. 9, no. 5, pp. 624–637, 1993.
- [45] G. J. Raju, G. C. Verghese, and T. B. Sheridan, "Design issues in 2-port network models of bilateral remote manipulation," in *IEEE International Conference on Robotics and Automation (ICRA)*. IEEE, 1989, pp. 1316–1321.
- [46] G. M. Leung, B. A. Francis, and J. Apkarian, "Bilateral controller for teleoperators with time delay via μ -synthesis," *IEEE Transactions on Robotics and Automation*, vol. 11, no. 1, pp. 105–116, 1995.
- [47] H. Kazerooni, T.-I. Tsay, and K. Hollerbach, "A controller design framework for telerobotic systems," *IEEE Transactions on Control Systems Technology*, vol. 1, no. 1, pp. 50–62, 1993.
- [48] S. Sirouspour, "Modeling and control of cooperative teleoperation systems," *IEEE Transactions on Robotics*, vol. 21, no. 6, pp. 1220–1225, 2005.
- [49] W.-H. Zhu and S. E. Salcudean, "Stability guaranteed teleoperation: an adaptive motion/force control approach," *IEEE Transactions on Automatic Control*, vol. 45, no. 11, pp. 1951–1969, 2000.
- [50] J. K. Tar, J. F. Bitó, I. J. Rudas, K. Eredics, and J. A. T. Machado, "Comparative analysis of a traditional and a novel approach to model reference adaptive control," in *IEEE International Symposium on Computational Intelligence and Informatics (CINTI)*. IEEE, 2010, pp. 93–98.
- [51] D. Lee and P. Y. Li, "Passive bilateral control and tool dynamics rendering for nonlinear mechanical teleoperators," *IEEE Transactions on Robotics*, vol. 21, no. 5, pp. 936–951, 2005.
- [52] J.-H. Ryu, D.-S. Kwon, and B. Hannaford, "Stable teleoperation with time-domain passivity control," *IEEE Transactions on Robotics and Automation*, vol. 20, no. 2, pp. 365–373, 2004.
- [53] K. Hashtrudi-Zaad and S. E. Salcudean, "Transparency in time-delayed systems and the effect of local force feedback for transparent teleoperation," *IEEE Transactions on Robotics and Automation*, vol. 18, no. 1, pp. 108–114, 2002.
- [54] T. Imaida, Y. Yokokohji, T. Doi, M. Oda, and T. Yoshikawa, "Ground-space bilateral teleoperation of ets-vii robot arm by direct bilateral coupling under 7-s time delay condition," *IEEE Transactions on Robotics and Automation*, vol. 20, no. 3, pp. 499–511, 2004.

- [55] H. Baier and G. Schmidt, "Transparency and stability of bilateral kinesthetic teleoperation with time-delayed communication," *Journal of Intelligent and Robotic Systems*, vol. 40, no. 1, pp. 1–22, 2004.
- [56] D. Sun, F. Naghdy, and H. Du, "Application of wave-variable control to bilateral teleoperation systems: A survey," *Annual Reviews in Control*, vol. 38, no. 1, pp. 12–31, 2014.
- [57] R. Ortega, J. A. L. Perez, P. J. Nicklasson, and H. Sira-Ramirez, *Passivity-based control of Euler-Lagrange systems: mechanical, electrical and electromechanical applications*. Springer Science & Business Media, 2013.
- [58] S. Lee and H. S. Lee, "Modeling, design, and evaluation of advanced teleoperator control systems with short time delay," *IEEE Transactions on Robotics and Automation*, vol. 9, no. 5, pp. 607–623, 1993.
- [59] G. Hirzinger, J. Heindl, and K. Landzettel, "Predictive and knowledge-based telerobotic control concepts," in *IEEE International Conference on Robotics and Automation (ICRA)*. IEEE, 1989, pp. 1768–1777.
- [60] P. Arcara and C. Melchiorri, "Control schemes for teleoperation with time delay: A comparative study," *Robotics and Autonomous systems*, vol. 38, no. 1, pp. 49–64, 2002.
- [61] S. Munir and W. J. Book, "Internet-based teleoperation using wave variables with prediction," *IEEE/ASME Transactions on Mechatronics*, vol. 7, no. 2, pp. 124–133, 2002.
- [62] A. C. Smith and K. Hashtrudi-Zaad, "Smith predictor type control architectures for time delayed teleoperation," *The International Journal of Robotics Research*, vol. 25, no. 8, pp. 797–818, 2006.
- [63] J. M. Azorín, O. Reinoso, R. Aracil, and M. Ferre, "Generalized control method by state convergence for teleoperation systems with time delay," *Automatica*, vol. 40, no. 9, pp. 1575–1582, 2004.
- [64] D. Hanawa and T. Yonekura, "A proposal of dead reckoning protocol in distributed virtual environment based on the Taylor expansion," in *2006 International Conference on Cyberworlds*. IEEE, 2006, pp. 107–114.
- [65] L. F. Penin and K. Matsumoto, "Teleoperation with time delay: A survey and its use in space robotics," National Aerospace Laboratory (NAL), Tech. Rep., 2002.
- [66] T. B. Sheridan, "Space teleoperation through time delay: review and prognosis," *IEEE Transactions on Robotics and Automation*, vol. 9, no. 5, pp. 592–606, 1993.
- [67] W. S. Kim, B. Hannaford, and A. Fejczy, "Force-reflection and shared compliant control in operating telemanipulators with time delay," *IEEE Transactions on Robotics and Automation*, vol. 8, no. 2, pp. 176–185, 1992.
- [68] B. Hannaford, L. Wood, D. A. McAfee, and H. Zak, "Performance evaluation of a six-axis generalized force-reflecting teleoperator," *IEEE Transactions on Systems, Man, and Cybernetics*, vol. 21, no. 3, pp. 620–633, 1991.

- [69] Z. Wang and S. Hirai, "Modeling and parameter estimation of rheological objects for simultaneous reproduction of force and deformation," in *International Conference on Applied Bionics and Biomechanics (ICABB)*, 2010, pp. 1–6.
- [70] W. Maurel, Y. Wu, D. Thalmann, and N. M. Thalmann, *Biomechanical models for soft tissue simulation*. Springer, 1998.
- [71] X. Wang, J. A. Schoen, and M. E. Rentschler, "A quantitative comparison of soft tissue compressive viscoelastic model accuracy," *Journal of the Mechanical Behavior of Biomedical Materials*, vol. 20, pp. 126–136, 2013.
- [72] C. Machiraju, A.-V. Phan, A. Pearsall, and S. Madanagopal, "Viscoelastic studies of human subscapularis tendon: relaxation test and a Wiechert model," *Computer Methods and Programs in Biomedicine*, vol. 83, no. 1, pp. 29–33, 2006.
- [73] P. Baranyi, "TP model transformation as a way to LMI-based controller design," *IEEE Transactions on Industrial Electronics*, vol. 51, no. 2, pp. 387–400, 2004.
- [74] P. Baranyi, Y. Yam, and P. Várlaki, *Tensor Product Model Transformation in Polytopic Model-Based Control*, 1st ed. Boca Raton, CRC Press, 2013.
- [75] L. De Lathauwer, B. De Moor, and J. Vandewalle, "A multilinear singular value decomposition," *SIAM journal on Matrix Analysis and Applications*, vol. 21, no. 4, pp. 1253–1278, 2000.
- [76] P. Grof and Y. Yam, "Furuta Pendulum—A Tensor Product Model-Based Design Approach Case Study," in *2015 IEEE International Conference on Systems, Man, and Cybernetics (SMC)*, 2015, pp. 2620–2625.
- [77] J. Kuti, P. Galambos, and A. Miklós, "Output Feedback Control of a Dual-Excenter Vibration Actuator via qLPV Model and TP Model Transformation: Control Design of a Dual-excenter Vibration Actuator," *Asian Journal of Control*, vol. 17, no. 2, pp. 432–442, 2015.
- [78] P. Galambos, J. Kuti, P. Baranyi, and I. J. Rudas, "Tensor Product based Convex Polytopic Modeling of Nonlinear Insulin-Glucose Dynamics," in *IEEE International Conference on Systems, Man, and Cybernetics*. Hong Kong, IEEE, 2015, pp. 2597–2602.
- [79] P. Galambos, P. Baranyi, and G. Arz, "Tensor product model transformation-based control design for force reflecting tele-grasping under time delay," *Proceedings of the Institution of Mechanical Engineers, Part C: Journal of Mechanical Engineering Science*, vol. 228, no. 4, pp. 765–777, 2014.
- [80] K. Parker, "A microchannel flow model for soft tissue elasticity," *Physics in medicine and biology*, vol. 59, no. 15, pp. 4443–4460, 2014.
- [81] J. Rosen, J. D. Brown, S. De, M. Sinanan, and B. Hannaford, "Biomechanical properties of abdominal organs in vivo and postmortem under compression loads," *Journal of Biomechanical Engineering*, vol. 130, no. 2, pp. 021 020:1–17, 2008.

- [82] N. Alkhouli, J. Mansfield, E. Green, J. Bell, B. Knight, N. Liversedge, J. C. Tham, R. Welbourn, A. C. Shore, K. Kos *et al.*, “The mechanical properties of human adipose tissues and their relationships to the structure and composition of the extracellular matrix,” *American Journal of Physiology-Endocrinology and Metabolism*, vol. 305, no. 12, pp. E1427–E1435, 2013.
- [83] K. L. Troyer, S. S. Shetye, and C. M. Puttlitz, “Experimental characterization and finite element implementation of soft tissue nonlinear viscoelasticity,” *Journal of Biomechanical Engineering*, vol. 134, no. 11, p. 114501, 2012.
- [84] M. Li, J. Konstantinova, E. L. Secco, A. Jiang, H. Liu, T. Nanayakkara, L. D. Seneviratne, P. Dasgupta, K. Althoefer, and H. A. Wurdemann, “Using visual cues to enhance haptic feedback for palpation on virtual model of soft tissue,” *Medical & Biological Engineering & Computing*, vol. 53, no. 11, pp. 1177–1186, 2015.
- [85] F. C. Leong, “Modelling and analysis of a new integrated radiofrequency ablation and division device,” Ph.D. thesis, National University of Singapore, 2009.
- [86] B. M. Pacheco, Y. Fujino, and A. Sulekh, “Estimation curve for modal damping in stay cables with viscous damper,” *Journal of Structural Engineering*, vol. 119, no. 6, pp. 1961–1979, 1993.
- [87] J. op den Buijs, H. H. Hansen, R. G. Lopata, C. L. de Korte, and S. Misra, “Predicting target displacements using ultrasound elastography and finite element modeling,” *IEEE Transactions on Biomedical Engineering*, vol. 58, no. 11, pp. 3143–3155, 2011.
- [88] T. Haidegger, L. Kovács, S. Preitl, R.-E. Precup, B. Benyó, and Z. Benyó, “Controller design solutions for long distance telesurgical applications,” *International Journal of Artificial Intelligence*, vol. 6, no. S11, pp. 48–71, 2011.
- [89] P. Kazanzides, J. Zuhars, B. Mittelstadt, and R. H. Taylor, “Force sensing and control for a surgical robot,” in *IEEE International Conference on Robotics and Automation (ICRA)*. IEEE, 1992, pp. 612–617.
- [90] M. C. Lee, C. Y. Kim, B. Yao, W. J. Peine, and Y. E. Song, “Reaction force estimation of surgical robot instrument using perturbation observer with smcspo algorithm,” in *IEEE/ASME International Conference on Advanced Intelligent Mechatronics (AIM)*. IEEE, 2010, pp. 181–186.
- [91] S. G. Yuen, D. P. Perrin, N. V. Vasilyev, P. J. Del Nido, and R. D. Howe, “Force tracking with feed-forward motion estimation for beating heart surgery,” *Robotics, IEEE Transactions on*, vol. 26, no. 5, pp. 888–896, 2010.
- [92] P. Moreira, C. Liu, N. Zemiti, and P. Poinet, “Soft tissue force control using active observers and viscoelastic interaction model,” in *IEEE International Conference on Robotics and Automation (ICRA)*. IEEE, 2012, pp. 4660–4666.
- [93] S. B. Kesner and R. D. Howe, “Robotic catheter cardiac ablation combining ultrasound guidance and force control,” *The International Journal of Robotics Research*, vol. 33, no. 4, pp. 631–644, 2014.

- [94] N. Zemiti, G. Morel, T. Ortmaier, and N. Bonnet, "Mechatronic design of a new robot for force control in minimally invasive surgery," *IEEE/ASME Transactions On Mechatronics*, vol. 12, no. 2, pp. 143–153, 2007.
- [95] P. Baranyi, Y. Yam, and P. Varlaki, "TP model transformatoin in polytopic model-based control," *Automation and Control Engineering. Taylor and Franci*, 2013.
- [96] G. F. Franklin, J. D. Powell, and M. L. Workman, *Digital control of dynamic systems*. Addison-Wesley Menlo Park, 1998, vol. 3.
- [97] E. Rahimy, J. Wilson, T. Tsao, S. Schwartz, and J. Hubschman, "Robot-assisted intraocular surgery: development of the iriss and feasibility studies in an animal model," *Eye*, vol. 27, no. 8, pp. 972–978, 2013.
- [98] Z. Petres and P. Baranyi, "Reference signal tracking control of the tora system: A case study of tp model transformation based control," *Periodica Polytechnica Electrical Engineering*, vol. 49, no. 1-2, pp. 109–122, 2006.
- [99] J. H. Lilly, "Parallel distributed control with takagi–sugeno fuzzy systems," *Fuzzy Control and Identification*, pp. 106–120.
- [100] J. Kuti, P. Galambos, and P. Baranyi, "Minimal volume simplex (mvs) approach for convex hull generation in tp model transformation," in *Intelligent Engineering Systems (INES), 2014 18th International Conference on*. IEEE, 2014, pp. 187–192.
- [101] J. Klespitz, I. J. Rudas, and L. Kovács, "Lmi-based feedback regulator design via tp transformation for fluid volume control in blood purification therapies," in *Systems, Man, and Cybernetics (SMC), 2015 IEEE International Conference on*. IEEE, 2015, pp. 2615–2619.
- [102] J. Lofberg, "Yalmip: A toolbox for modeling and optimization in matlab," in *IEEE International Symposium on Computer Aided Control Systems Design*. IEEE, 2004, pp. 284–289.
- [103] E. D. Andersen, C. Roos, and T. Terlaky, "On implementing a primal-dual interior-point method for conic quadratic optimization," *Mathematical Programming*, vol. 95, no. 2, pp. 249–277, 2003.
- [104] G. Tholey, J. P. Desai, and A. E. Castellanos, "Force feedback plays a significant role in minimally invasive surgery: results and analysis," *Annals of Surgery*, vol. 241, no. 1, pp. 102–109, 2005.
- [105] M. V. Ottermo, M. Øvstedal, T. Langø, Ø. Stavadahl, Y. Yavuz, T. A. Johansen, and R. Mårvik, "The role of tactile feedback in laparoscopic surgery," *Surgical Laparoscopy Endoscopy & Percutaneous Techniques*, vol. 16, no. 6, pp. 390–400, 2006.
- [106] M. I. Tiwana, S. J. Redmond, and N. H. Lovell, "A review of tactile sensing technologies with applications in biomedical engineering," *Sensors and Actuators A: Physical*, vol. 179, pp. 17–31, 2012.
- [107] C. E. Reiley, T. Akinbiyi, D. Burschka, D. C. Chang, A. M. Okamura, and D. D. Yuh, "Effects of visual force feedback on robot-assisted surgical task performance," *The Journal of thoracic and cardiovascular surgery*, vol. 135, no. 1, pp. 196–202, 2008.

- [108] A. M. Okamura, L. N. Verner, C. Reiley, and M. Mahvash, “Haptics for robot-assisted minimally invasive surgery,” in *Robotics Research*. Springer, 2010, pp. 361–372.
- [109] D. Morris, H. Tan, F. Barbagli, T. Chang, and K. Salisbury, “Haptic feedback enhances force skill learning,” in *Joint EuroHaptics Conference and Symposium on Haptic Interfaces for Virtual Environment and Teleoperator Systems (WHC)*. IEEE, 2007, pp. 21–26.
- [110] K. Montgomery, C. Bruyns, J. Brown, S. Sorkin, F. Mazzella, G. Thonier, A. Tellier, B. Lerman, and A. Menon, “Spring: A general framework for collaborative, real-time surgical simulation,” *Studies in health technology and informatics*, pp. 296–303, 2002.
- [111] I. Brouwer, J. Ustin, L. Bentiay, A. Dhruv, and F. Tendick, “Measuring in vivo animal soft tissue properties for haptic modeling in surgical,” in *Medicine Meets Virtual Reality*, vol. 81, 2001, p. 69.
- [112] H. Delingette, “Toward realistic soft-tissue modeling in medical simulation,” *Proceedings of the IEEE*, vol. 86, no. 3, pp. 512–523, 1998.
- [113] M. Tavakoli, A. Aziminejad, R. V. Patel, and M. Moallem, “High-fidelity bilateral teleoperation systems and the effect of multimodal haptics,” *IEEE Transactions on Systems, Man, and Cybernetics, Part B (Cybernetics)*, vol. 37, no. 6, pp. 1512–1528, 2007.
- [114] E. Samur, M. Sedef, C. Basdogan, L. Avtan, and O. Duzgun, “A robotic indenter for minimally invasive measurement and characterization of soft tissue response,” *Medical Image Analysis*, vol. 11, no. 4, pp. 361–373, 2007.
- [115] M. Beccani, C. Di Natali, L. J. Sliker, J. A. Schoen, M. E. Rentschler, and P. Valdastri, “Wireless tissue palpation for intraoperative detection of lumps in the soft tissue,” *IEEE Transactions on Biomedical Engineering*, vol. 61, no. 2, pp. 353–361, 2014.
- [116] G. Picinbono, H. Delingette, and N. Ayache, “Nonlinear and anisotropic elastic soft tissue models for medical simulation,” in *IEEE International Conference on Robotics and Automation (ICRA)*, vol. 2. IEEE, 2001, pp. 1370–1375.
- [117] A. L. Trejos, J. Jayender, M. Perri, M. D. Naish, R. V. Patel, and R. Malthaner, “Robot-assisted tactile sensing for minimally invasive tumor localization,” *The International Journal of Robotics Research*, vol. 28, no. 9, pp. 1118–1133, 2009.
- [118] C. R. Wagner and R. D. Howe, “Force feedback benefit depends on experience in multiple degree of freedom robotic surgery task,” *IEEE Transactions on Robotics*, vol. 23, no. 6, pp. 1235–1240, 2007.
- [119] V. Luboz, E. Promayon, and Y. Payan, “Linear elastic properties of the facial soft tissues using an aspiration device: Towards patient specific characterization,” *Annals of Biomedical Engineering*, vol. 42, no. 11, pp. 2369–2378, 2014.
- [120] Y. Zou, P. X. Liu, Q. Cheng, P. Lai, and C. Li, “A new deformation model of biological tissue for surgery simulation,” *IEEE Transactions on Cybernetics*, vol. PP, no. 99, pp. 1–10, 2016.

- [121] T. Horeman, S. P. Rodrigues, J. J. van den Dobbelsteen, F.-W. Jansen, and J. Dankelman, "Visual force feedback in laparoscopic training," *Surgical Endoscopy*, vol. 26, no. 1, pp. 242–248, 2012.
- [122] G. L. McCreery, A. L. Trejos, M. D. Naish, R. V. Patel, and R. A. Malthaner, "Feasibility of locating tumours in lung via kinaesthetic feedback," *The International Journal of Medical Robotics and Computer Assisted Surgery*, vol. 4, no. 1, pp. 58–68, 2008.
- [123] P. Kazanzides, Z. Chen, A. Deguet, G. S. Fischer, R. H. Taylor, and S. P. DiMaio, "An open-source research kit for the da vinci® surgical system," in *IEEE International Conference on Robotics and Automation (ICRA)*. IEEE, 2014, pp. 6434–6439.
- [124] Z. Chen, A. Deguet, R. Taylor, S. DiMaio, G. Fischer, and P. Kazanzides, "An open-source hardware and software platform for telesurgical robotics research," in *MICCAI Workshop on Systems and Architecture for Computer Assisted Interventions*, 2013, pp. 22–26.
- [125] Y. Zhang, B. Orlic, P. Visser, and J. Broenink, "Hard real-time networking on firewire," in *Real-Time Linux Workshop*, 2005, pp. 1–8.
- [126] M. Barabanov and V. Yodaiken, "Real-time linux," *Linux journal*, vol. 23, no. 4.2, pp. 1–9, 1996.
- [127] J. C. Gwilliam, Z. Pezzementi, E. Jantho, A. M. Okamura, and S. Hsiao, "Human vs. robotic tactile sensing: Detecting lumps in soft tissue," in *Haptics Symposium, 2010 IEEE*. IEEE, 2010, pp. 21–28.
- [128] A. Goodwin, K. John, and A. Marceglia, "Tactile discrimination of curvature by humans using only cutaneous information from the fingerpads," *Experimental brain research*, vol. 86, no. 3, pp. 663–672, 1991.

OWN PUBLICATIONS RELATED TO THE THESIS

- [TA-1] Á. Takács, I. J. Rudas, T. Haidegger, “The Other End of Human–Robot Interaction: Models for Safe and Efficient Tool–Tissue Interactions,” in *Human–Robot Interaction: Safety, Standardization, and Benchmarking*, 1st ed. Abingdon, United Kingdom, Taylor&Francis, 2017, to be published.
- [TA-2] Á. Takács, P. Galambos, I. J. Rudas and T. Haidegger, “A novel methodology for usability assessment of rheological soft tissue models,” in *IEEE International Symposium on Applied Machine Intelligence and Informatics (SAMi)*, Herlany, Slovakia, 2017, pp. 271–278.
- [TA-3] Á. Takács, T. Haidegger and I. J. Rudas, “Reaction Force and Surface Deformation Estimation Based on Heuristic Tissue Models,” in *IEEE International Conference on Systems, Man and Cybernetics (SMC)*, Budapest, Hungary, 2016, pp. 3888–3893.
- [TA-4] Á. Takács, J. Kuti, T. Haidegger, P. Galambos and I. J. Rudas, “Polytopic Model-Based Interaction Control for Soft Tissue Manipulation,” in *IEEE International Conference on Systems, Man and Cybernetics (SMC)*, Budapest, Hungary, 2016, pp. 3899–3905.
- [TA-5] Á. Takács, T. Haidegger, P. Galambos, J. Kuti and I. J. Rudas, “Nonlinear soft tissue mechanics based on polytopic Tensor Product modeling,” in *IEEE International Symposium on Applied Machine Intelligence and Informatics (SAMi)*, Herlany, Slovakia, 2016, pp. 211–215.
- [TA-6] Á. Takács, I. J. Rudas, and T. Haidegger, “Surface deformation and reaction force estimation of liver tissue based on a novel nonlinear mass–spring–damper viscoelastic model,” *Medical & Biological Engineering & Computing*, vol. 54, no. 10, pp. 1553–1562, 2016. IF: 1.82 (2016)
- [TA-7] Á. Takács, D. Á. Nagy, I. J. Rudas and T. Haidegger. “Origins of Surgical Robotics: From Space to the Operating Room.” *Acta Polytechnica Hungarica*, vol. 13, no. 1, pp. 13–30, 2016. IF: 0.754 (2016)
- [TA-8] Á. Takács, P. Galambos, P. Pausits, I. J. Rudas and T. Haidegger. “Nonlinear soft tissue models and force control for medical cyber-physical systems,” in *IEEE International Conference on Systems, Man, and Cybernetics (SMC)*, Hong Kong, 2015, pp. 1520–1525.

- [TA-9] Á. Takács, S. Jordán, D. Á. Nagy, P. Pausits, T. Haidegger, J. K. Tar and I. J. Rudas, “Joint platforms and community efforts in surgical robotics research,” in *International Conference on Recent Achievements in Mechatronics, Automation, Computer Sciences and Robotics*, Targu Mures, Romania, 2015. pp. 93–103.
- [TA-10] Á. Takács, S. Jordán, D. Á. Nagy, J. K. Tar, I. J. Rudas and T. Haidegger, “Surgical Robotics—Born in Space,” in *IEEE International Symposium on Applied Computational Intelligence and Informatics (SACI)*, Timisoara, Romania, 2015, pp 547–551.
- [TA-11] Á. Takács, T. Haidegger and I. Rudas, ‘Investigation of soft tissue behavior using the generalized Maxwell model,’ in *Hungarian Conference on Mechanics (MAMEK)*, Miskolc, Hungary, 2015, p. 109.
- [TA-12] Á. Takács, S. Jordán, D. Nagy, P. Pausits, T. Haidegger, J. K. Tar and I. J. Rudas, “Open-source research platforms and system integration in modern surgical robotics,” *Acta Universitatis Sapientiae Electrical and Mechanical Engineering*, vol. 14, no. 6, pp. 20–34, 2015.
- [TA-13] Á. Takács, L. Kovács, I.J. Rudas, R. E. Precup and T. Haidegger, “Models for force control in telesurgical robot systems.” *Acta Polytechnica Hungarica*, vol. 12, no. 8, pp. 95–114, 2015. IF: 0.754 (2016)
- [TA-14] Á. Takács, S. Jordán, R.-E. Precup, L. Kovács, J. Tar, I. Rudas and T. Haidegger, “Review of tool–tissue interaction models for robotic surgery applications,” in *IEEE International Symposium on Applied Machine Intelligence and Informatics (SAMI)*, Herlany, Slovakia, 2014, pp. 339–344.
- [TA-15] Á. Takács, J. K. Tar, T. Haidegger and I. J. Rudas. “Applicability of the Maxwell-Kelvin model in soft tissue parameter estimation.” in *IEEE International Symposium on Intelligent Systems and Informatics (SISY)*, Subotica, Serbia, 2014, pp. 115–119.
- [TA-16] S. Jordán, Á. Takács, I. Rudas and T. Haidegger, “Modelling and Control Framework for Robotic Telesurgery,” in *Joint Workshop on New Technologies for Computer/Robot Assisted Surgery (CRAS)*, Verona, Italy, 2013, pp. 89–92.

OWN PUBLICATIONS NOT RELATED TO THE THESIS

- [TA-I] Á. Takács, Gy. Eigner, L. Kovács, I. J. Rudas and T. Haidegger. “Teacher’s Kit: Development, Usability and Communities of Modular Robotic Kits for Classroom Education.” *IEEE Robotics and Automation Magazine*, vol. 23, no. 2, pp. 30–39, 2016. IF: 3.276 (2016)
- [TA-II] D. Á. Nagy, Á. Takács, T. Haidegger and I. J. Rudas, “The CALap System—A Low-Cost Lightweight Robotic Arm for Laparoscopic Camera Handling,” presented at the ICRA Workshop: Shared Frameworks for Medical Robotics Research, Seattle, WA, 2015.
- [TA-III] D. Á. Nagy, Á. Takács, T. Haidegger and I. J. Rudas, “Computer Assisted Laparoscopy Robot—A Low-Cost Lightweight Design,” presented at The Hamlyn Symposium on Medical Robotics, London, United Kingdom, 2015.
- [TA-IV] D. Á. Nagy, Á. Takács, Sz. Barcza, I. J. Rudas and T. Haidegger, “Design and Control of a Low-cost Robotic Camera Holder for Laparoscopy Assistance,” presented at the Joint Workshop for New Technologies in Computer: Robot Assisted Surgery (CRAS 2015), Brussels, Belgium, 2015.
- [TA-V] D. Á. Nagy, Á. Takács, Sz. Barcza, I. J. Rudas and T. Haidegger, “Design and Control of a Low-cost Robotic Camera Holder Robot for Laparoscopy Training,” *Design of Medical Devices conference, programme&abstracts*, Wiener Neustadt, Austria, 2015. pp. 17–18.
- [TA-VI] J. K. Tar, L. Kovács, Á. Takács, B. Takacs, P. Zentay, T. Haidegger, I. J. Rudas, “Novel Design of a Model Reference Adaptive Controller for Soft Tissue Operations,” in *IEEE International Conference System, Man, and Cybernetics (SMC 2014)*, San Diego, CA, 2014, pp 2446–2451.
- [TA-VII] S. Jordán, Á. Takács, J. K. Tar, I. J. Rudas and T. Haidegger, “Towards Open Source Surgical Robotics,” *Joint Workshop on New Technologies for Computer/Robot Assisted Surgery (CRAS 2014)*, Genoa, Italy, 2014, pp. 154–157.